TÉCNICO LISBOA

Development of the energy demand of drive architectures for different means of transport

Atiquzzaman Khan Ankur

Thesis to obtain the Master of Science Degree in

Energy Engineering and Management

Supervisors: Prof. Rui Manuel Gameiro de Castro

Eng. Stefan Kraus

Examination Committee

Chairperson: Prof. Jorge de Saldanha Gonçalves Matos

Supervisor: Prof. Rui Manuel Gameiro de Castro

Member of the Committee: Prof. João Paulo Neto Torres

January 2021

Acknowledgements

First and foremost, praise and thanks be to God Almighty for blessing me with the health and capacity to conduct this thesis work successfully.

I would like to express my deepest and sincerest gratitude to my research supervisor, Stefan Kraus. Stefan has taught me how to approach a project of this magnitude without getting lost, and without his constant support and supervision, I could never have completed this thesis. I would also like to thank Dr. Thomas Grube, first of all, for accepting and welcoming me into his team. But above all, for always being available with his expertise and being a safety net that always protected me whenever I slipped up. I must thank Prof. Dr. Detlef Stolten and all the members of Team Transport of IEK-3 at Forschungszentrum Jülich for their warm welcome and for making my time there a memorable one. I must also thank Forschungszentrum Jülich for providing me with all the facilities and support so that I could concentrate on my work and not have to worry about other matters.

I want to thank Prof. Rui Castro for his invaluable guidance during this entire thesis work, and especially for always being available to solve any issues I might have. Be they thesis related or to maneuver official protocols of Instituto Superior Técnico. I would also like to thank him for his time spent coordinating the signing of the complex official documents.

I want to thank Innoenergy for giving me the most beautiful experience by attending this multicultural double master's degree in energy technologies. The last two years at Karlsruhe Institute of Technology and Instituto Superior Técnico were some of the most beautiful years of my life, and I was able to grow immensely, both personally as well as professionally. I would also like to thank all the friends I have made during this journey for making the experience that much more special.

Last but definitely not least, I would like to thank my mom and sister. My mom for all the sacrifices she has had to make to educate and prepare me for my future. Her love and prayers protect me from any harm, and the morals she instilled in me is a compass always guiding me through this life. And my sister, for being the best sister and friend and always putting me straight.

Abstract

The transport sector is responsible for around a quarter of the global primary energy consumption and carbon emissions. In this thesis, a model is developed to determine the energy demand for passenger and freight transportation within Germany for different transport modes. The modes included are light-duty vehicles (LDVs), heavy-duty vehicles (HDVs), airplanes, trains, ships, and drones. The model further estimates future development until 2050. With standard driving cycles, backward-looking longitudinal vehicle models are used to determine the energy demand for all on-road vehicle modes. For the off-road vehicle modes, real-world energy demand from literature is used to build the model.

It is found that various vehicle parameters have different effects on vehicle energy demand, depending on the driving scenario. Airplanes and drones are often the most energy-intensive modes of transport. Public transportation provides the most energy-efficient means of travel in the forms of battery electric and fuel cell buses and coaches, trams, and long-distance electric trains. International shipping is the most energy-efficient means of freight transport. Electrified trains and semi-trucks are ideal for national freight transport. Electrification of drivetrains and the implementation of regenerative braking show a large potential for fuel consumption reduction, especially in urban areas. It is found that the occupancy rates for the vehicles play a critical part in determining the energy demand per passenger-kilometer, for passenger modes, and tonne-kilometer, for freight modes.

Keywords: Transport energy demand, Future trends, Longitudinal vehicle model, battery/fuel cell electric vehicle, vehicle electrification

Table of Content

List of abbreviations

Abbreviations	Meaning
ADVISOR	Advanced Vehicle Simulator
AEC	Aviation Emissions Calculator
ANL	Argonne National Laboratory
BEV	Battery electric vehicle
CAFE	Corporate Average Fuel Economy
cng	Compressed natural gas
CSC	City Suburban Cycle
d	Diesel
EC	European Commission
EEDI	Energy Efficiency Design Index
EIS	Enter Into Service
EU	European Union
Euro NCAP	European New Car Assessment Program
EV	Electric vehicles
FASTSim	Future Automotive Systems Technology Simulator

fc	Fuel cell
FCEV	Fuel cell electric vehicle
g	Gasoline or petrol
GEMIS	Global Emissions Model for integrated Systems
GHG	Greenhouse gas
GVWR	Gross Vehicle Weight Rating
HD UDDS	Heavy-Duty Urban Dynamometer Driving Schedule
HDV	Heavy-duty vehicle, vehicles weighing over 3.5 tonnes
HEV	Hybrid electric vehicle
HVAC	Heating, ventilation, and air conditioning
HwFET	Highway Fuel Economy Test
ICAO	International Civil Aviation Organization
ICE	Internal Combustion Engines
ICEV	Internal combustion engine vehicle
IEA	International Energy Association
IMO	International Maritime Organization
LCV	Light Commercial Vehicle
LDV	Light-duty vehicle
lng / LNG	Liquefied natural gas
LTO	Landing/Take-Off
mpgge	Miles per gallon gasoline equivalent
MTCO2e	Million tonnes of CO2 equivalent
NEDC	New European Driving Cycle
NRTC	Neighborhood Refuse Truck Cycle
O	Overhead (Catenary)
OC BUS	Orange County Bus
PHEV	Plug-in hybrid electric vehicle
pkm	Passenger kilo meter
PTC	Positive Temperature Coefficient
RDE	Real Driving Emissions
REEV	Range-extended electric vehicle
SA	Single-Aisle
SAF	Sustainable Aviation Fuels
SORT	Standardized On-Road Tests Cycles
STA	Small Twin-Aisle
SUV	Sport Utility Vehicle
tkm	Tonne kilo meter
UDDS	Urban Dynamometer Driving Schedule
UNECE	United Nations Economic Commission for Europe
US EPA	United States Environmental Protection Agency’s
USA	United States of America
VECTO	Vehicle Energy Consumption Calculation Tool
vkm	Vehicle kilometer
VT-CPFM	Virginia Tech Comprehensive Power-Based Fuel Consumption Model
VTOL	Vertical Take-Off and Landing
WHVC	World Harmonized Vehicle Cycle

WLTC	Worldwide Harmonized Light Vehicles Test Cycle
WLTP	Worldwide Harmonized Light Vehicles Test Procedure

List of Symbol

Symbols	Unit	Meaning
A	m^2	Area
a	m/s^2	Acceleration
c	-	Coefficient
E	MJ	Energy
F	N	Force
G	-	Gear ratio
g	m/s^2	Gravitational constant
h	s	Time step between discrete points
I	kg·m	Moment of inertia
m	kg	Mass
p	N/m^2	Pressure
P	W	Power
t	s	Time
v	m/s	Speed / velocity
α	rad	Gradient angle
η	-	Efficiency
ρ	kg/m^3	Density
δ	-	Rotational inertia factor

List of Subscripts

Subscripts	Meaning
a	Aerodynamic / air
aux	Auxiliary
c	Constant
d	Disturbance
dri	Drivetrain
e	Equivalent
f	Frontal / front
fuel	Fuel demand
g	Gravitational
m	Motive
mech	Mechanical
mot	Electric motor
n	n^{th} time step
occ	Occupant

pm	Prime mover
r	Rolling / rotational
rec	Recuperation
tot	Total
tran	Transmission system
trac	Traction
v	Vehicle
w	Wheel

List of figures

List of tables

1. Introduction

A 2019 report by the Intergovernmental Science-Policy Platform on Biodiversity and Ecosystem Services found that around 1 million plant and animal species are under threat of extinction, unprecedented in human history. This landmark report also states that greenhouse gas (GHG) emissions from human activities have directly caused a temperature rise of 1°C compared to preindustrial levels. Some projections show that in the coming decades, the global temperature rise will become the single biggest agent changing ecosystems globally [1]. In order to prevent this unfavorable prediction of the future, GHG emissions must be brought under strict control, and the transport sector is a prime candidate for the change.

When taking a sectoral view, transportation consumes almost 29% of the global primary energy and comes in second place at 24% of the total global carbon emissions, only electricity and heating having a higher emissions figure of 41%. If the transport sector were a country, it would be the country with the second-highest GHG emissions [2]. Despite some countries having reached so-called “peak car,” which entails that the number of cars in a country, or the number of cars per capita in a country, is either stagnant or decreasing [3], the number of vehicles globally is only predicted to rise in the near future. According to Sperling and Gordon (2009), there are more than one billion cars in the world today, and it is accelerating on its way to two billion, with South and East Asia fueling most of the growth, followed by Eastern Europe and South America [4].

In 2018 25% of Germany’s final energy consumption was in the transportation sector, resulting in 22.7 % of the total emissions of 696 million tonnes of CO2 equivalent (MTCO2e) [2]. Germany has set its target to reduce GHG emissions by 80% to 95%, until 2050, compared to the emissions for the year 1990. Until now, the transport sector has shown the least improvement in emissions reduction. In 1990 it generated 163 MTCO2e and 160 MTCO2e in 2014, constituting a reduction of only 1.8%. The next lowest figure is an order of magnitude higher, at 18%, representing the agricultural sector [5]. These figures show that although substantial measures must be taken in all industries to meet these targets, the transport sector’s measures must be more radical. To help understand the energy consumption and emissions in transportation, computer models are an essential tool.

1.1. Purpose of the study

This master thesis aims to develop a Python-based model for determining the vehicle-specific energy demand for both passenger and freight transport. The model can distinguish between important possible means of transportation available in Germany and the different drivetrains for each transport means. In addition, it can take into account future developments in energy demand until 2050.

The model is divided into on-road and off-road transport modes. The on-road modes include light-duty vehicles (LDV) and heavy-duty vehicles (HDVs), which are further divided into buses and trucks. The off-road modes include airplanes, drones, trains, and ships. Longitudinal vehicle models are used to determine the energy

demand for all on-road vehicle modes. Real-world energy demand from literature is used to build the models for the off-road vehicle modes.

The user can define the vehicle occupancy rate, as well as other parameters. The model considers the effects of driving conditions like ambient temperatures and driving scenarios for on-road transport modes. The model's outputs are in terms of energy per passenger-kilometer, for passenger modes, and energy per tonne-kilometer, for freight modes. Besides, the model can also calculate total vehicle energy demands.

1.2. Significance of the study

This thesis work will be part of a more extensive study that plans to answer some valuable questions for the German transport sector. These questions include: How can the climate targets in the transport sector be met? What is the impact of sector coupling on the transport sector? How do mobility trends influence possible pathways? What impact do political measures have on future developments?

The German transport sector is in the midst of a massive transformation in an attempt to meet its climate targets. In this regard, it is expected that there will be profound modal shifts in the transport sector. Furthermore, changes in vehicle drivetrain efficiency are also expected. To better understand these possible changes, a model of the energy demand of all possible transportation modes and drivetrains within Germany must be available. It is expected that more electric vehicles will be replacing traditional combustion vehicles in German streets. However, what is an electric vehicle's advantage over a conventional one in terms of energy demand? How much energy would I consume if I traveled between two cities using a coach versus a high-speed electric train? What if I chose to fly instead? What is the energy consumption of transporting equipment on a truck versus on a train? What about international freight transport on a cargo ship versus a cargo aircraft? The model developed in this master thesis will help to answer all these questions and more. This thesis will provide the energy per passenger-kilometer as well as energy per ton-kilometer (for freight transportation) for all the major modes of transport in Germany.

1.3. Structure of the thesis

In chapter 2, a discussion on the models used to determine transport energy demand in the literature is carried out. An overview of the on-road models is first given, followed by that of the off-road models found in the literature. The chapter concludes with a discussion of the difference between the model being developed in this thesis to the ones present in the literature.

Chapter 3 presents a detailed discussion of the model developed for the on-road transport energy demand. The discussion includes an overview of the backward-looking quasistatic longitudinal vehicle energy model used. The chapter also includes discussions on the auxiliary energy demand and the effects of regenerative braking.

Chapter 4 first discusses the data preparation for the LDV, buses, and trucks. It discusses the different standard driving cycles that are used in the model to determine the on-road vehicle energy demand. It then validates the

models for these modes against literature and real-world vehicle energy data. The off-road vehicle energy models are then discussed in detail.

Chapter 5 is the results and discussions. This chapter discusses different interesting results obtained from the developed model. Some of the major results include the effects of driving conditions on the energy demand of different modes and drivetrains. The effects of occupancy rates are also discussed. It analyzes the outlook to the future. The chapter concludes with an analysis of the energy demand for last-mile deliveries using different transport modes.

Finally, chapter 6 concludes the thesis with some closing remarks and takeaways from this thesis work.

2. Literature Review

In this section, some of the literature models for determining transportation energy consumption are discussed.

2.1. On-road Transport Modes

First of all, some of the models available in the literature for determining on-road vehicle fuel consumption are discussed.

Cheng et al. (2021) discuss the impact of transportation on our society's environmental, economic, and social aspects. There are two major ways of developing sustainable transportation. One considers improving the efficiency of transport modes using technology improvements in drivetrain efficiency and the use of alternative fuels and drivetrains. The second considers the development of alternative and balanced intermodal transport systems. This approach tries to facilitate the use of public transport and other alternatives to more energy-hungry transport modes. Social, demographic, and spatial attributes are found to be significant players in determining the modal choice [6].

In the literature, there are many ways of modeling the vehicle energy demand. One of the most widely used is the longitudinal vehicle energy model. In a longitudinal vehicle energy model, the vehicle's lateral and vertical dynamics are neglected with the assumption that these do not have a significant effect on the vehicle energy demand [7].

Abousleiman et al. (2015) [8], Edwardes et al. (2014) [9], Edwardes et al. (2015) [10], Meradji et al. (2016) [11], Jardin et al. (2019) [7], Wang et al. (2018) [12], Fiori et al. (2016) [13], Grube et al. (2018) [14], Xu et al. (2019) [15], Ziyadi et al. (2018) [16], Ahmad et al. (2014) [17], and Luin et al. (2019) [18], all use some form of the longitudinal vehicle energy model to determine the energy demand for a vehicle.

There are two primary forms of longitudinal vehicle energy consumption models, namely, forward-looking and backward-looking models. In a forward-looking model, the vehicle speed is controlled to match a driving cycle while the fuel energy demand is calculated. This requires the use of controllers. On the other hand, a backward-looking model is one where the model starts with the traction energy required at the wheels to follow a driving

cycle and “work backward” through the drivetrain to the engine to determine the fuel energy demand for the vehicle. Backward-looking models are usually faster than forward-looking models in their execution time. However, forward-looking models better represent actual vehicle configuration and are favored where controllers and hardware-in-the-loop are in use. To match a target duty cycle, forward models usually must use some sort of “driver model” such as a proportional–integral–derivative controller. In the industry, forward models are commonly used to classify part interactions that impact the amounts of energy consumption and vehicle efficiency. In a backward-looking model, energy consumption is determined based on the driving cycle and vehicle characteristics data. Such models can be incorporated into more complicated systems [19].

The energy model can be further subdivided into quasistatic and dynamic methods. Guzzella and Sciarretta (2007) define a quasistatic method as one where the input variables are the road gradient and the vehicle speed and acceleration. The traction energy is determined based on this information. On the other hand, a “correct” mathematical definition of the system is the basis of the dynamic method. Typically, the powertrain model is formulated using collections of ordinary differential equations in the state-space form. However, other definitions, such as partial differential equations or equations with differential and algebraic components, are possible [20].

Autonomie and advanced vehicle simulator (ADVISOR) are two of the most widely used vehicle simulators. Autonomie is developed by the Argonne National Laboratory (ANL). It is a forward-looking model. Therefore, a driving cycle is required to compute power demand from the drivetrain. ADVISOR is developed by the National Renewable Energy Laboratory. It uses a quasi-steady backward-forward approximation. Vehicle characteristics and drive cycles are the model inputs, while the outputs are vehicle energy consumption and emissions [13].

Ahmad et al. (2014) carried out modeling and validation of the longitudinal vehicle model. The longitudinal model includes different subsystems for tire, engine, automatic transmission, and braking models. The longitudinal vehicle model is then validated against an experimental vehicle with embedded sensors. The model results are compared with experimental data for sudden braking and throttle imposed motions. It is found the model results are similar to the experimental results with an acceptable level of error [17].

Meradji et al. (2016) model the drivetrain of hybrid electric vehicle (HEV) using MATLAB/Simulink. Due to the use of basic Simulink blocks, the execution time is short. In this model, the electric motor is used to place the internal combustion engine in its optimal region. Usage profiles are used as input to the model in terms of speed references and road profiles. A proportional-integral controller is used to respond to the inputs with a zero static error. A forward-looking longitudinal vehicle model is used to determine the resistance torque at the transmission. The model considers the effects of tire rolling resistance, aerodynamic drag, and gravitational force. The electric and internal combustion engines meet this resistance through the transmission system. The result gives the instantaneous power requirement of the vehicle [11].

Edwardes et al. (2014) [9] and Edwardes et al. (2015) [10] use the Virginia Tech Comprehensive Power-Based Fuel Consumption Model (VT-CPFM) to model vehicle energy demand. The VT-CPFM uses a longitudinal vehicle

model that considers the effects of aerodynamic drag, rolling resistance, inertial effects, and road gradient. Edwardes et al. (2014) model diesel and hybrid buses. The model is calibrated using publicly available bus parameters. The model results using the Orange County bus cycle dynamometer test had an average error of less than 5% [9]. Edwardes et al. (2015) model diesel buses. Park et al. (2013) validate the VT-CPFM with real-world fuel consumption measurements. The model is calibrated using the United States Environmental Protection Agency (US EPA) city and highway fuel economy ratings [10].

Wang et al. (2018) develop an algorithm to determine the energy demand of the future trip of a battery electric vehicle (BEV) to mitigate range anxiety. Information about the road topology, traffic, and weather conditions are obtained using publicly available resources. A longitudinal vehicle model is used to determine vehicle energy demand. It considers the losses in the vehicle powertrain as well as the auxiliary power demand in addition to the rolling resistance, aerodynamic drag, inertial effects, and road gradient. The predictions from the model are found to be within 5% of the actual energy demand for the trips [12].

Ziyadi et al. (2018) analyze the impact of rolling resistance on the overall vehicle energy consumption. A roughness-speed-impact model is used to determine the energy use due to vehicle-pavement interaction. The results obtained show that a unit change in the pavement's international roughness index increases the vehicle energy consumption of between 2 to 3% for an LDV. The paper concludes that the potential savings from pavement roughness can be up to 7%. It uses a longitudinal vehicle energy model to determine vehicle energy demand. The model considers the effects of road curvature in addition to rolling resistance, aerodynamic drag, inertial effects, and road gradient [16].

Gao et al. (2007) highlight the need for modeling electric vehicles and HEV [19]. Vagg et al. (2013) studied the modeling of HEV. The paper uses dynamic modeling to optimize the controller, and the disadvantages of dynamic models are discussed [21]. Gadsden et al. (2011) develop HEV's modeling to study battery systems' fault detection [22]. Hilshey et al. (2015) model the charging demand for a plug-in hybrid electric vehicle (PHEV) [23].

Abousleiman et al. (2015) [8], Fiori et al. (2016) [13], Xu et al. (2019) [15], and Luin et al. (2019) [18] analyze the energy demand for electric vehicles (EV). Abousleiman et al. (2015) use a longitudinal vehicle model and compare the results obtained with data from driving the modeled vehicle in real-world driving conditions. The longitudinal model considers the effects of rolling resistance, aerodynamic drag, inertial effects, and road gradient on the vehicle. The impacts of auxiliary loads are also considered in the form of the vehicle's heating, ventilation, and air conditioning (HVAC) power demand and power needed for battery conditioning and other drivetrain-related power [8]. Fiori et al. (2016) develop a model to estimate the instantaneous power requirements for electric vehicles using second-by-second vehicle speed, acceleration, and road grade data as input to the model. The model used is a quasi-steady backward-looking longitudinal vehicle model due to its fast simulation times [13]. Luin et al. (2019) develop a model to simulate the energy consumption of EVs. A longitudinal vehicle energy model is used to determine vehicle energy demand. The model is run on standard driving cycles [18].

Luin et al. (2019) report a mismatch between real-world energy consumption and declared figures in the literature. The results were found to be improvements over the ones noted in the literature when a power limit is applied to the regenerative braking system. The effects of traffic lights on the vehicle energy demand are also studied due to regenerative braking impacts [18]. Abousleiman et al. (2015) use a constant efficiency value to model the regenerative braking power [8]. Hayes et al. (2014) assume that if the regenerative power is less than or equal to 20 kW, all the energy is returned to the battery pack [24]. Fiori et al. (2016) also calculate the instantaneous energy regeneration from braking. It shows that EVs can regenerate higher energy in urban driving conditions than highway driving conditions [13].

Xu et al. (2019) analyze the energy consumption for EVs in a transportation network. First, the individual vehicle energy demand is determined using the Autonomie model using a longitudinal vehicle model that considers the effects of rolling resistance, aerodynamic drag, inertial effects, and road gradient. The Autonomie results are then analyzed using classification and regression tree analysis to produce energy consumption data for varied on-road operating conditions. The regional travel demand was analyzed for a large metropolitan area, assuming different electric vehicle market share scenarios. It is then used to estimate fleet energy consumption. It is found that around a 30% reduction in energy demand can be achieved with a 50% PHEV market share [15].

Jardin et al. (2019) develop a model to determine the energy demand for different passenger vehicle drivetrains. The energy demand is divided into primary and secondary energy demands. The primary energy represents the traction energy required to follow real-world driving profiles. It is determined using a backward-looking longitudinal vehicle model developed in MATLAB. The Secondary energy demand is all other forms of energy needed to run a vehicle, and the major part is due to HVAC energy demand. A thermodynamic model is developed to model the vehicle HVAC energy demand. A fixed energy demand value is used to model other auxiliary energy demands. The model is analyzed as a function of trip distance and ambient temperature. The results show that the ambient temperatures have a significant impact on vehicle energy demand. Therefore, external conditions must be considered for a holistic assessment of a vehicle's energy consumption [7].

Fiori et al. (2016) consider the effects of auxiliary systems like air conditioning and heating systems. It demonstrates that the use of HVAC systems can reduce the EV range [13]. Abousleiman et al. (2015) model the HVAC power requirement using a function that varies with the ambient temperature. This function is shown in Figure 1 [8].

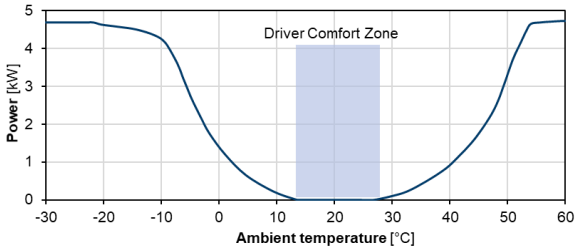

Figure 1: Cabin HVAC power consumption at different temperatures according to Abousleiman et al. (2015) [8]

Figure 1 shows that the power demand for cabin HVAC is negligible for ambient temperatures between approximately 14 and 27 °C, according to the model developed in Abousleiman et al. (2015) [8]. The power requirements sharply rise for lower or higher ambient temperatures.

Liu et al. (2018) develop a model to predict EVs' energy consumption based on observations from 68 EVs in Aichi Prefecture, Japan. This study especially takes into account the effects of ambient temperature on the energy demand for EVs. The energy model considers the energy need to overcome aerodynamic drag, rolling resistance, road gradient, inertia effects, auxiliary load, and the effects of ambient temperatures on instability in electric motor power output. The auxiliary load includes the energy required for HVAC. The vehicle's best energy efficiency is reported between ambient temperatures of 21.8 and 25.3 °C [25].

Wu et al. (2015) outline a method to measure and estimate EV energy consumption. They first present a system that can collect data for in-use vehicles. Five months of EV data were collected and used to analyze vehicle performance and driving behavior. The results show that EVs are more efficient in urban driving conditions as compared to highway conditions. Based on these results, an analytical EV power estimation model is proposed [26].

Hayes et al. (2014) use a simplified electric vehicle model using US EPA coast-down parameters to generate the vehicle loads. The vehicle load forces are modeled using an empirical quadratic formula where the coefficients are found from a coast-down test from 120km/h. The resulting model gives the force for any given vehicle speed. The results are then validated using ANL experimental test data for a specific vehicle model [24].

Some of the models from the literature are chosen for further detailed analysis. These models are discussed below.

2.1.1. Grube (2014) [27]

Grube (2014) aims to find out the potential of different vehicle drivetrains for reducing the fuel consumption of LDVs, considering different options for power consumption and supply. The MATLAB-Simulink based hybrid model, consisting of theoretical model components as well as experimentally determined operating conditions, considers vehicles with internal combustion engine vehicle (ICEV), HEV, BEV, and fuel cell electric vehicle (FCEV) drivetrains. The model analyses an extensive range of driving and auxiliary power profiles, in detail, compared to other literature. The findings are that HEVs can save 30% to 60% in fuel consumption compared to current ICEVs. This value stands at 76-89 % and 50-67% for BEVs and FCEVs, respectively. Thermoelectric generators and photovoltaic applications show a maximum of 15% in potential fuel savings [27].

Grube (2014) first identifies three forms of energy that the model must consider, which are critical for the drive, comfort, and safety of a passenger car. These are the mechanical energy for the drive, the electrical energy for vehicle electrical systems, and the thermal and mechanical energy for vehicle climate control [27]. The modeling of the above forms of energies is discussed in further detail below.

As for the drive's mechanical energy, Grube (2014) first determines the most important parameters of the vehicle to be the empty vehicle mass, frontal area, the aerodynamic drag coefficient, and rolling resistance coefficient. The rolling resistance coefficient is taken to be a function of the vehicle speed alone. Following this, Grube uses a longitudinal model of the vehicle to determine the axle torque of the driven axle [27].

The vehicle speed and acceleration values are inputs to the model and are based on driving cycle information. The study considers 25 such driving cycles. The aerodynamic drag coefficient values are also used as inputs to the model from manufacturer reported values [27].

The tire slip limits the torque transfer from the wheel to the road surface. The maximum circumferential force transferred to the road surface is next calculated using the maximum coefficient of adhesion and the axle load. The static axle load is first determined to be able to calculate the front axle load [27].

The aerodynamic lift coefficient is used to calculate the lift force due to air resistance at the front axle. The value of air density is taken at 15°C and 100kPa atmospheric pressure, to be 1.184kg/m^3 [27].

The equivalent mass of the vehicle is then calculated, taking into consideration the various rotating masses. The gear ratios of the final drive and gearbox, the moments of inertia of the drive parts, internal combustion engine, and the wheels, including the brake discs, are used for this calculation [27].

Thus, the rotational inertia factor varies depending on the specific gear ratio used. In this case, the gear to be used for any particular time is also determined by the model. Finally, the rotational inertia factor can be found [27].

As for the vehicle electrical energy demand, Grube (2014) states that there is a trend towards increasing electrical power demand in modern cars. This has led to solutions that include dual-battery and dual-voltage systems for meeting the electrical energy demands. In a conventional ICEV, a three-phase current generator is used to produce this electrical energy by using a part of the engine's mechanical energy. In this thesis, the electrical systems for ICEVs are modeled using a single, 14V system, and dual-voltage systems are used for other drivetrains like HEVs, FCEVs, and BEVs. For the latter, the high-voltage system powers the air-conditioning equipment, and other low-power auxiliary power demands are met with the low-voltage electrical system. A DC/DC converter connects the low and high- voltage systems [27].

The high-voltage network also provides traction power for the vehicle. The DC/DC converters are modeled along with characteristic curves to determine the efficiencies. The vehicle's electrical power demand is represented as a function of time, which is generated by combining the power requirements and duty cycles of all on-board power consumers. Integrating the power demand over time gives the electrical energy demand for the vehicle [27].

A detailed discussion of the model used in Grube (2014) [27] to calculate the thermal and mechanical energy for vehicle climate control can be found in Appendix A.

The energy models are used to form the final model, which is shown as a flowchart in Figure 2.

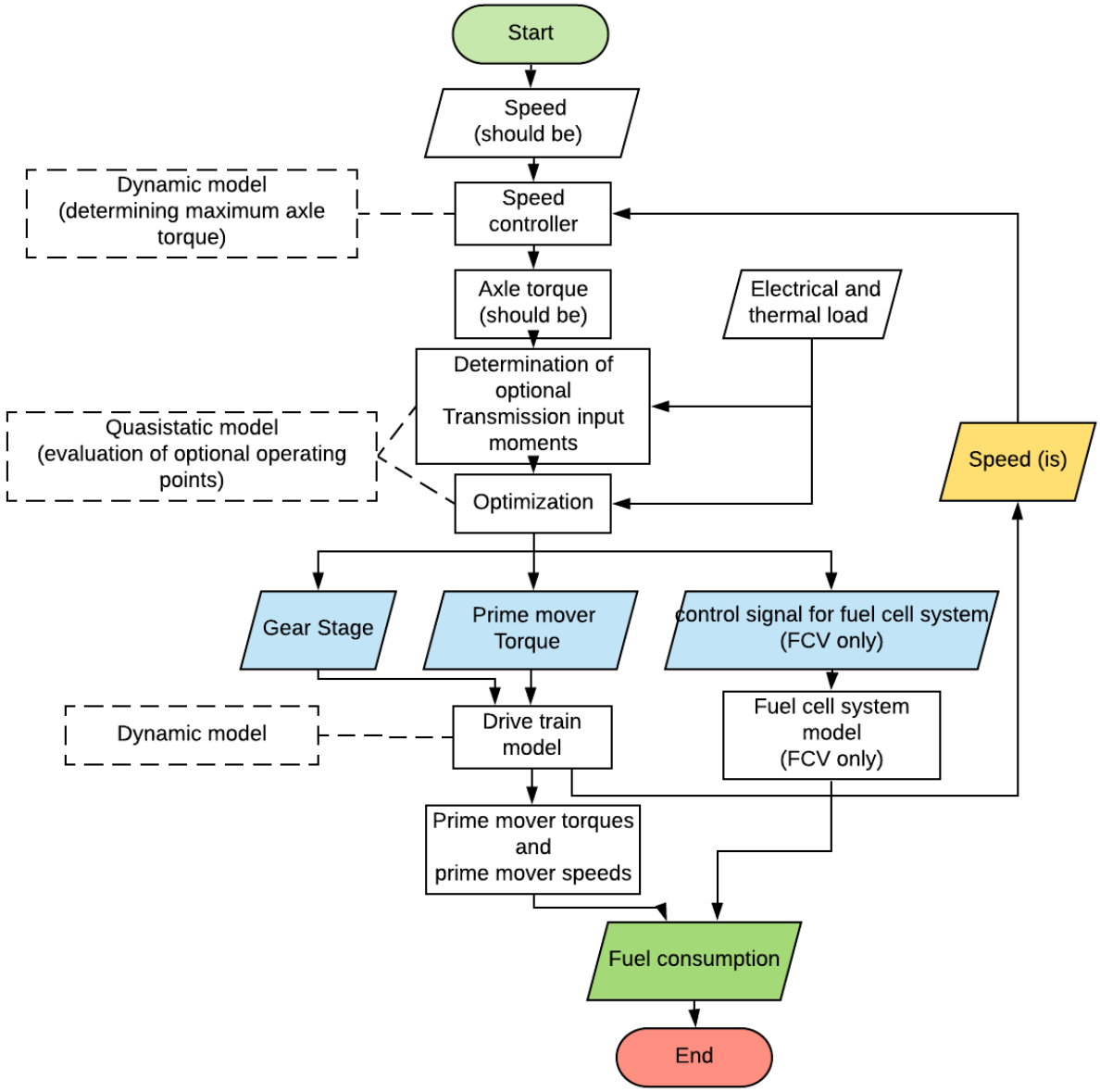

Figure 2: Flowchart showing an overview of the model (Adapted from [27]*)*

This flowchart shows an overview of the model's main processes to determine the fuel consumption of a vehicle. After the model is initiated, the required speed is read from the driving cycle information. This value is compared with the vehicle's current speed by the speed controller, which then sends the required axle torque value. The model then determines the optimal transmission moments, determining the prime mover torque and gear ratios used in the longitudinal vehicle model after the optimization process. The model outputs the prime mover torque and speed values, which, when compared with engine data, gives the fuel consumption data for the vehicle [27].

In summary, Grube (2014) has outlined the consumption reduction potentials for passenger cars with combustion engines, parallel hybrid cars, and electric cars with fuel cells and with batteries. Grube has done so

with sufficient emphasis on the effects of the selected driving profiles, as well as the use of auxiliary consumers in the vehicle [27].

2.1.2. Transitions to alternative vehicles and fuels (2013) [28]

Transitions to alternative vehicles and fuels by the National Research Council of the United States is an important report that analyzes the potentials of reducing fossil fuel consumption and GHG emissions up to the year 2050. In this regard, it compares the current scenario with the estimated future cost and performance of LDV and fuel technologies to find best-case scenarios and predict hurdles in its implementation [28].

The report has a two-step process to determine the vehicle-specific energy consumption. In the first step, the tractive force is determined for the given vehicle parameters using the Corporate Average Fuel Economy (CAFE) driving cycles. The CAFE testing procedure consists of two different driving cycles, one representing city driving; Urban Dynamometer Driving Schedule (UDDS), and the other representing highway driving; Highway Fuel Economy Test (HwFET) [28].

The second step involves working backward from the tractive energy required at the wheel, through the transmission, gearbox, until the prime mover to determine the energy input to the vehicle, in terms of the fuel, for ICEV and HEV, and electrical for PHEV and BEV. The results are presented in miles per gallon gasoline equivalent (mpgge) [28].

To determine the tractive energy requirements, firstly, the vehicle is considered without the drivetrain. A longitudinal vehicle model is built, neglecting the effects of the gradient, wind loading, and other disturbances. In this model, only the impacts of aerodynamic drag, rolling resistance, and vehicle motive force are taken into account. Using these parameters, the net force required to move the vehicle is calculated. The rolling resistance and aerodynamic drag are assumed to be functions of the vehicle speed. The frontal area is taken as 80-85% of the product of the width and height of an LDV. The value for the aerodynamic drag coefficients generally falls between 0.25 and 0.45 [28].

The motive force required to accelerate the vehicle according to the driving cycle specification is next determined. First, the rotational mass of each of the wheels is calculated to calculate the vehicle's equivalent mass. Finally, the tractive energy is calculated by integrating the force along the distance traveled [28].

The model also considers different driving conditions. As the model analyzes one second of the driving cycle at a time, it also puts the various forces into each of these driving conditions. Therefore, the final result sums up the energy inputs and outputs (braking energy) and the individual components for each (rolling resistance, aerodynamic drag, and motive force). In doing so, the fraction of the motive energy dissipated through braking can be found. Thus this can be used to estimate the benefits of implementing regenerative braking [28].

After the tractive energy is found, the model works backward, from the wheel, through the transmissions, gearbox, and the engine, to find the energy that must be input to the engine. This is done by considering the efficiencies of all the different parts of the drivetrain and the ancillary energy requirements [28].

In summary, this study only uses the CAFE driving cycles to determine vehicle energy requirements. Furthermore, it does not mention details about the modeling of auxiliary power requirements for the vehicle. This study's overarching goal is to analyze the current and future performance and costs for the different vehicle types [28].

2.1.3. FASTSim (2015) [29]

The Future Automotive Systems Technology Simulator (FASTSim) is a vehicle powertrain analysis tool developed by the United States Department of Energy's Vehicle technologies office. It is developed in Excel, and Visual Basic is used to run and manage the various models. The model incorporates models to determine vehicle efficiency, performance, cost, and battery life for LDVs and HDVs and to evaluate technology improvements. It can simulate different vehicle drivetrains, including ICEV, HEV, PHEV, BEV, and FCEV [29].

FASTSim considers the effects of aerodynamic drag, rolling resistance, acceleration, gradient, regenerative braking, and the efficiencies of different drivetrain parts in its analysis to determine the vehicle-specific energy demand. It uses the UDDS and HwFET driving cycles to estimate the fuel efficiency of LDVs. Furthermore, other driving cycles are available, while importing is also an option. For HDVs, it uses the Heavy-Duty Urban Dynamometer Driving Schedule (HD UDDS) by default. However, others are available [29].

Vehicle input parameters include aerodynamic drag coefficient, frontal area, vehicle mass, cargo mass, the center of gravity, drive axle weight fraction, and the vehicle's wheelbase. These parameters are used to solve the vehicle equations for the chosen driving cycle and predict the wheels' traction power requirements [29].

The fuel converter (prime mover) is represented by four parameters: power, time to full power, base mass, and the specific mass. The prime mover is modeled as an efficiency vs. power graph. One such curve for each engine type is used for different vehicles by scaling the model with rated power, resulting in an approximation with an accuracy of up to 5%. The motor controller model is used for electric motors instead of the fuel converter model [29].

The battery and energy management models are used to take into account the workings of batteries as storage mediums, as well as their charging and discharging characteristics. A wheel model is used to determine the road load as well as the traction limits. It is defined by the wheel's inertia, rolling resistance coefficient, radius, coefficient of friction, and the number of wheels on the vehicle [29].

The model can be run by choosing the vehicle parameters from the database, or the user can also provide it. The model can run an individual drive cycle, or a large number of drive cycles can be run at once. The model can be used to compare the different drivetrains, where it runs the same driving cycle but using different drivetrains to compare the results. It can perform a parametric study where a specific parameter is varied, and the results plotted with respect to it. This can be used to study the effects of different vehicle parts on the final energy consumption [29].

FASTSim has built-in validation processes. Fifteen different metrics from the simulation can be compared with available test data. The fuel consumption data for LDV is compared with the US EPA's test data, and they are a

close match for most vehicle models. Other results that can be validated within the model include electricity consumption, acceleration, price, component mass, and battery life [29].

2.1.4. VECTO model [30]

VECTO, which stands for Vehicle Energy Consumption calculation Tool, is a simulation tool for energy demand, fuel consumption, and CO_2 emissions. The European Commission has developed it for HDVs with a gross vehicle weight above 3500kg. Starting from the beginning of 2019, VECTO became a mandatory tool for certain new trucks in the type approval certification [31].

VECTO provides many advantages over other means of testing HDV; these include cost-efficiency, high reproducibility and flexibility, and fuel consumption data for the entire vehicle. However, a disadvantage is that the tool will need to be regularly updated to account for relevant technology improvements [30].

The advantage of VECTO is that the inputs are generated from component tests. Thus, the process becomes as easy as picking and choosing relevant data to represent the modeled vehicle. The component tests include [30]:

- Constant speed tests with standard vehicle bodies to find the vehicle's aerodynamic drag coefficient.
- Drum test, according to European Commission Regulation No 1222/2009, to get rolling resistances for different tire types.
- Engine testbed according to the United Nations Economic Commission for Europe (UNECE) Regulation 49 to get the engine fuel-map and load-map.
- Transmission and gear losses are found either by complete measurements, measuring idle losses and calculating torque dependencies, or just using default values.

Next, the auxiliary power demand has to be input into the VECTO model. The auxiliary power depends on the technology and driving cycle. Technology dependent generic data are available within the model. The auxiliary units that VECTO considers are engine cooling pump, steering pump, electric system, pneumatic system, air-conditioning system, and power take-off [30].

The VECTO tool takes in these data values as Extensible Markup Language files, which are then used to generate the specified vehicle's longitudinal dynamics model depending on the vehicle group. For trucks, VECTO classifies the vehicle into vehicle groups based on the axle configuration, chassis configuration, and permissible maximum laden mass [30].

The VECTO model then uses different mission profiles (driving cycles) to calculate vehicle energy demands. However, unlike in the other models discussed previously, the mission profiles in VECTO are target-speed cycles, where the model sets the vehicle the target to reach the specified speeds. The modeled vehicle then reaches these targets as soon as possible, depending on the vehicle's power availabilities. Multiple different mission profiles are available, both for trucks as well as for buses and coaches, to simulate the different driving scenarios the vehicle can face within European driving conditions [30].

2.2. Off-road Transport Modes

In this section, some of the literature models for determining off-road vehicle fuel consumption are discussed. Off-road transport modes include airplanes, drones, trains, and ships.

Between 1990 and 2018, international aviation had the highest relative increase, compared to other transportation modes, in energy consumption within the EU. With an increase of 124.6% in this period [32]. In Germany, aviation is responsible for 15% of all transport-related CO2 emissions for 2014, which is the second-highest after road vehicles [33]. Therefore, airplane fuel energy demand must be taken into account in any transport sector's holistic model.

Burzlaff (2017) develops a model to determine the fuel consumption of airplanes. The model can determine type-specific fuel consumption using publicly available airplane information [34]. Park et al. (2014) model the airplane fuel burn for different aircraft models globally. The paper finds that flight lengths between 1500 and 2000 nautical miles are the most fuel-efficient flights [35].

Peeters et al. (2005) assess the change in commercial airplanes' fuel efficiency from the 1930s to 2000s. It is found that the last piston-powered airplanes were as efficient as the latest commercial airplanes. There was a sudden increase in fuel consumption when the piston-powered airplanes were replaced by jet-powered airplanes [36]. Kharina et al. (2015) discuss the fuel efficiency trends for airplanes between 1960 and 2014 [37].

Chao et al. (2014) develop a model to determine the cost of cargo transportation by airplanes. It is found that the fuel cost is a major determining factor for the total cargo cost [38].

Senzig et al. (2009) develop a model to determine airplane fuel consumption in the terminal area. It uses data from a major airplane manufacturer as well as publicly available data from the Federal Aviation Administration. Compared with airline operational data, the model accurately predicts the terminal area fuel consumption [39].

Xu (2017) models the energy demand of different sized freight drones [40]. Bauhaus Luftfahrt reports the energy demand for passenger drones [41].

The energy demand for railways needs to be further studied in order to save energy due to environmental concerns and high energy costs [42].

Salvador et al. (2018) develop a dynamic model to estimate the energy consumption of diesel trains. Comparison of the model results against real operational data shows an error rate of below 9% [43].

Wang et al. (2017) build a model to determine the energy consumption of electric trains. The model is calibrated using data from Oregon, United States, and validated using data available from the National Transit Database. The model results are sufficiently accurate. The model shows that the use of regenerative braking can save around 20% of energy consumption. The model can take into account the effects of train models, route, and operational parameters [44].

Zhang et al. (2019) model the traction energy of trains to determine their optimal scheduling. The model optimizes the arrival and departure times for intermediate stations to minimize the train's overall energy consumption [42].

Zhou et al. (2019) simulate the energy consumption of high-speed electric trains. The simulation considers the effects of initial battery power, constant speed, and operation mode on traction energy consumption, auxiliary energy consumption, and train operation time. The simulation is based on the trains Urgent Operation Assistant System [45].

Zhao et al. (2016) reviews a model developed to predict the energy consumption for air conditioning in trains. The model can be used in high-speed trains air conditioning energy demand analysis [46].

The shipping industry is responsible for transporting the vast majority of global trade [47]. Jeon et al. (2018) predict the fuel consumption of ships. Modern ships collect a vast amount of data. This paper proposes the use of artificial neural networks to analyze the big data and predict the fuel demand for the ship. The paper reports this method to be more accurate and efficient than polynomial regression and support vector machine [48].

Kee et al. (2018) model the fuel consumption of ships using statistical methods. Fuel consumption in shipping is one of the major contributors to environmental degradation. Multiple linear regression method is used to determine the fuel efficiency profiles. A system is proposed to help vessel operators monitor and operate the vessels at fuel-efficient speeds. The model has the potential to save up to 37.1% in vessel fuel demand [47].

Yang et al. (2019) model the fuel consumption for ships using a genetic algorithm-based grey-box model. This model's advantage over other grey-box models is that it can better account for oblique weather directions. The proposed model's efficacy is demonstrated using the data from a crude oil tanker over a seven-year operational period [49].

One of the main differences between the model being developed in this thesis with the ones mentioned above is the number of different transport modes in the model. Germany's different transport modes must be modeled to get an overview of the German transport network's energy demand. The models mentioned above only simulate specific transport modes. The model developed in this thesis considers LDVs, HDVs (buses and trucks), aviation modes (including conventional fixed-wing planes and electric drones), trains, and ships. These modes are further subdivided into passenger and freight modes. Another difference with the literature is that the developed model can analyze the effects of different occupancy rates. The energy requirements to transport each passenger, or a tonne of cargo, can then be analyzed.

3. Methodology

This section discusses the physics behind the implemented model used to determine the on-road vehicle's mechanical energy demand, followed by a discussion of the effects of regenerative braking systems and the model used to determine the final fuel energy demand of the vehicle.

The physics behind the simulation being used for on-road vehicles are extensively discussed, as it will also be the most detailed part of the final model. This is done because German road transportation is responsible for approximately 90% of its entire transport sector energy demand, with just cars and light trucks accounting for 63.0% for the year 2017 [50].

The model is based on the book titled Vehicle Propulsions Systems by Guzzella and Sciarretta (2007). The drivetrain of a vehicle converts the stored energy in the fuel to mechanical energy of the vehicle. The mechanical energy is temporarily stored in mainly two forms: the vehicle's kinetic and potential energies. This mechanical energy is used to overcome the driving resistances. There are three main types of driving resistances [20]

1. Aerodynamic friction
2. Rolling friction
3. Energy dissipated in the brakes

These resistances can be represented in a differential form as;

$$m_{e,v}\frac{d}{dt}v(t) = F_{trac}(t) - \left(F_a(t) + F_r(t) + F_g(t) + F_d(t)\right) \qquad 3.1$$

Where

F_a = aerodynamic friction

F_r = rolling friction

F_g = gravitational force for non-horizontal roads

F_d = disturbance forces

F_{trac} = traction force at the wheel

$m_{e,v}$ = equivalent mass of the vehicle and occupants

v = speed of the vehicle

This model is referred to as the longitudinal vehicle model because it only considers the vehicle dynamics in the vehicle's longitudinal axis. It does not consider the lateral forces on the vehicle.

Equation 3.1 gives a general overview of energy pathways in a vehicle. F_d represents any external forces acting on the vehicle. F_{trac} is the force being generated at the wheel to propel the vehicle. Aerodynamic friction, rolling resistance, gravitational forces, and the equivalent mass of the vehicle are further discussed below.

3.1. Aerodynamic friction

Two different processes cause the aerodynamic drag on a vehicle. One is the viscous drag of the air on the vehicle surface, and the other is the difference in pressure between the front and rear of the vehicle due to flow separation [20].

One of the most widely used and reliable methods to determine the aerodynamic drag of a vehicle is the wind tunnel test. This method is both time and resource-intensive, although it is still used for crucial applications. The development of numerical methods for aerodynamic drag has meant that, in many situations, the aerodynamic drag of the vehicle can be found to a good approximation without the need for practical experiments. Coast-down tests are also used as a less financially intensive practical means to find the aerodynamic drag of vehicles [51].

Different parts of the vehicle cause this aerodynamic drag. The vehicle's body generates most of it (65%), followed by wheel housing at 20%, other external features like side-mirrors cause another 10%, and engine ventilation causes the remaining 5% [52].

For a simple aerodynamic drag model, the vehicle can be assumed to be a prismatic object. In such a case, the aerodynamic friction F_a can be represented as a function of the vehicle speed v [20]

$$F_a(v) = \frac{1}{2} \cdot \rho_a \cdot A_f \cdot c_a \cdot v^2 \qquad 3.2$$

where ρ_a is the density of the air, A_f is the frontal area of the prismatic body, and c_a is the aerodynamic drag coefficient.

The vehicle's frontal area and the aerodynamic drag coefficient values for a vehicle can usually be found in the vehicle specifications. However, more general values can be found for each vehicle class in the literature. Kühlwein (2016) presents the average of these values for different vehicle classes, Table 1. These values were taken from the average European Union (EU) fleet in 2013 [53].

Table 1: Frontal area and aerodynamic drag coefficient for different vehicle classes [53]

Vehicle Class	Mini cars	Small cars	Medium cars	Large cars	Executive cars	Sport utility cars
Frontal area (m2)	2.09	2.11	2.28	2.24	2.40	2.5
Aerodynamic drag coefficient (-)	0.33	0.32	0.30	0.29	0.29	0.35

In practice, the vehicle moving through the air will also generate a vertical lift force (or downforce). This vertical force has the effect of decreasing (or increasing) the apparent vehicle weight. This effect will be neglected in this study.

3.2. Rolling friction

The effects of rolling resistance will be discussed in this section. Rolling resistance is the force opposing the motion of a rolling body on a surface. This arises mainly due to the inelastic effects, where part of the energy used in the deformation of the wheel, and the road surface, is not recovered when the contact is removed. The rolling resistance by itself can account for between 20% and 30% of a vehicle's fuel consumption [54].

A simplified equation for the rolling resistance F_r is [20]

$$F_r = c_r \cdot m_v \cdot g \cdot \cos(\alpha) \qquad 3.3$$

where c_r is the rolling resistance coefficient, m_v is the mass of the vehicle along with passengers and cargo, g is the gravitational acceleration, and α is the gradient of the road. Although for practical application, $\cos(\alpha)$ can be taken as 1.

The rolling resistance coefficient depends on many different variables. The most important of these include the vehicle's speed, the tire pressure, and the road surface conditions [20]. Other variables include the temperature, the material of the tire, the tread pattern, as well as the contact patch shape, among others [54].

Rolling resistance can be found by experiment. A vehicle can be towed at different velocities in order to determine the rolling resistance [55]. It can also be found using the coast down test. Although, in both of these tests, special measures must be taken to eliminate the effects of aerodynamic drag and only consider rolling resistance [51].

Different experimental formulas are found in the literature, which can be used to estimate the rolling resistance coefficient of an LDV on a dry road. If the tire pressure is known, c_r can be found as [56]

$$c_r = 0.005 + \left(\frac{1}{p}\right) \cdot (0.01 + 0.0095 \cdot (\frac{v}{100})^2) \qquad 3.4$$

where p is the tire pressure in bar, and v is the vehicle speed in km/h

For a more straightforward approach, given that the vehicle speed remains within a moderate range, Guzzella and Sciaretta (2007) recommend using a constant value for the rolling resistance coefficient [20]. Kühlwein (2016) presents some constant values for the rolling resistance coefficient for different vehicle classes, Table 2. These values were taken from the average EU fleet in 2013 [53].

Table 2: Rolling resistance coefficient for different vehicle classes [53]

Vehicle Class	Mini cars	Small cars	Medium cars	Large cars	Executive cars	Sport utility cars
Rolling resistance coefficient	0.01167	0.01171	0.01123	0.01139	0.01163	0.01224

Since the tire pressure is not known for the different vehicles being modeled, the rolling resistance is assumed to be dependent on the vehicles' speed alone in this thesis. Thus, the rolling resistance coefficient is only a function of the vehicle speed. Grube (2013) uses such an equation in his dissertation [27].

$$c_r = 0.0088 + 0.0017 \cdot \frac{v}{100} + 0.00028 \cdot \left(\frac{v}{100}\right)^4 \qquad 3.5$$

where v is the vehicle speed in km/h. Equation 3.5 will be used to find the rolling resistances for all LDVs in the model.

3.3. Gravitational force

The gravitational force F_g the vehicle experiences when traveling up an inclined road is discussed here. It is related to the vehicle gaining or losing potential energy. It is a conservative force and can be calculated as [20]

$$F_g(\alpha) = m_v \cdot g \cdot \sin(\alpha) \qquad 3.6$$

For small values of α, which is the case for most road conditions, $\sin(\alpha) \approx \alpha$.

3.4. Equivalent mass of the vehicle

m_{ev} represents the mass of the vehicle, and occupants, along with the rotational inertia of all the rotating masses. The main rotating masses in the vehicle include all the rotating masses within the engine, the transmission shaft, and the wheel assembly. These generate d'Alembert forces, which the traction force has to overcome [20]. The vehicle's equivalent mass can be calculated by different procedures depending on the detail required and the facilities available.

Dedicated systems at test facilities can be used for experimentally determining the equivalent mass of actual production vehicles. It would be the most expensive option available. On the other hand, if enough information is known about the materials and designs of a vehicle, computer models can be used to find out the equivalent mass, as in the case of computer-aided designs [57].

Guzzellla and Sciaretta (2007) recommend a simple mathematical model to find the equivalent mass of the rotational parts of a vehicle $m_{v,r}$, which should be added to the vehicle and occupant mass to get the vehicle equivalent mass [20].

$$m_{v,r} = \frac{1}{r_w^2} \cdot I_w + \frac{G^2}{r_w^2} \cdot I_{pm} \quad 3.7$$

where r_w is the wheel radius, I_w is the moment inertia of the wheel assembly and other rotating components on the wheel side of the gearbox, G is the total transmission ratio and I_{pm} is the total moment of inertia of the rotating parts of the engine (prime mover) side of the gearbox.

Since the total transmission ratio will depend on the gear being used at any instant, this model will give different results depending on the vehicle's speed. Therefore, the equivalent vehicle mass will change with vehicle speed.

If the inertias of the rotating masses are not known, an estimate of the vehicle equivalent mass $m_{e,v}$ can be found by multiplying the vehicle mass m_v with the rotational inertia factor δ and adding the occupant mass m_{occ}. The rotational inertia factor is only a function of the total transmission ratio [57].

$$m_{e,v} = m_v \cdot \delta + m_{occ} \quad 3.8$$

$$\delta = 1 + 0.04 + 0.0025 \cdot G^2 \quad 3.9$$

This equation works because the mass of the drivetrain and the wheel increases with an increase in the mass of the vehicle.

The simplest approximation is to take an average value of the rotational inertia factor for a vehicle and apply it for all speed regions. This can be used if the total transmission ratio is also unknown. The rotational inertia factors for some production vehicles are given in Table 3, below [28]

Table 3: Rotational mass factors for specific vehicle models [28]

Vehicle Model	Toyota Yaris	Toyota Camry	Chrysler 300	Saturn Vue	Grand Caravan	Ford F-150
Rotational mass factor	1.024	1.021	1.018	1.018	1.017	1.010

For this model, an average rotational inertia factor of 1.02 is assumed for all LDV and HDV vehicles. It must be taken into account that this factor must be multiplied by the vehicle mass only, not including the cargo and passenger mass (occupant mass).

Multiplying the equivalent vehicle mass with the vehicle acceleration gives the force required for the vehicle's acceleration, which is also known as the motive force [28].

3.5. Traction Force

Traction force is the force that the wheel has to exert on the road to propel the vehicle against the resisting forces. In this thesis, an assumption is made that there is no slip between the tire and the road. In this simplified

model, the effect of the longitudinal slip, the difference between the actual velocity of the vehicle and the equivalent rotational velocity of the driving wheels, can be disregarded [58]. Because of this simplification, the torque provided by the driveshaft to the wheel is completely transferred to the road as the traction force.

Therefore, to find the traction force, the driving mode must first be determined. There are three possible driving conditions [20].

1. Traction mode: where the engine is doing work in moving the vehicle,
2. Braking mode: where the brakes are dissipating energy to slow down the vehicle
3. Coasting mode: where neither is the engine doing work on the vehicle, nor brakes dissipating energy from the vehicle, but the vehicle is moving under its own stored mechanical energy

To determine the driving modes, first, the vehicle's coasting velocity must be calculated, which can be done by using equation 3.1. The disturbance force is removed, assuming that no external forces are acting on the vehicle. Next, the traction force is removed as for a vehicle to be in coasting mode, the traction force must be zero. The models discussed previously for aerodynamic friction (equation 3.2), rolling friction (equation 3.3), and gravitational force (equation 3.6) are used. It results in the following equation for the coasting velocity [20]

$$\frac{d}{dt}v_c(t) = \frac{-1}{2 \cdot m_{e,v}} \cdot \rho_a \cdot A_f \cdot c_a \cdot v_c^2(t) - g \cdot c_r - g \cdot \alpha \qquad 3.10$$

Which can be represented as

$$\frac{d}{dt}v_c(t) = -A \cdot v_c^2(t) - B \qquad 3.11$$

The above equation can be easily solved using a numerical method. In this case, the forward Euler method is used [59].

$$v_c(t = t_{n+1}) = v_c(t = t_n) + (t_n - t_{n-1}) \cdot (-A \cdot v_c^2(t = t_n) - B) \qquad 3.12$$

where t_n is the time at the nth time-step, and coasting velocity after the nth time-step is given by $v_c(t = t_n)$. The starting velocity is $v_c(t = 0)$.

By comparing the result of this equation with the actual vehicle velocity $v(t)$ from the driving cycle, the driving mode can be determined [20].

A vehicle is in traction mode if $v(t) > v_c(t)$, in braking mode if $v_c(t) > v(t)$, and in coasting mode if $v_c(t) = v(t)$, for a finite time interval.

According to this model, the vehicle speed and the road gradient must be predetermined to find the traction force at the wheel. To have a predetermined speed, standard driving cycles are used as inputs to the model. These driving cycles will be discussed in detail in section 4.1.1 (page 26).

3.6. Mechanical energy demand

After choosing a driving cycle, the next step involves finding the mechanical energy demand of the vehicle. The vehicle's mechanical energy demand is the energy that the vehicle needs to follow the chosen driving cycle. The key parameter used in this calculation is the mean tractive force, $\bar{F}_{trac}$. The mean tractive force is defined as

$$\bar{F}_{trac} = \frac{1}{x_{tot}} \cdot \int_{t \in trac} F(t) \cdot v(t) dt \qquad 3.13$$

where $trac$ is the time intervals where $F_{trac} > 0$, in other words, those parts of the cycle when the vehicle is in traction mode, and x_{tot} is the total distance traveled during the cycle and can be calculated as follows

$$x_{tot} = \int_0^{t_{max}} v(t) dt \qquad 3.14$$

The parts of the driving cycle when the vehicle is in braking mode ($F_t < 0$), the vehicle does not require any mechanical energy from the drivetrain. The energy necessary for aerodynamic and rolling resistances is covered by the decrease of the vehicle's mechanical energy. Further decrease of the mechanical energy is brought about by the vehicle's braking system, where the energy is either dissipated as heat or converted to other forms of energy if the vehicle is equipped with an energy recuperation device.

In the case where the vehicle is in coasting mode ($F_{trac} = 0$), the energy necessary for aerodynamic and rolling resistances is precisely matched with the vehicle's mechanical energy decrease. Thus again, the vehicle does not require any additional energy from the drivetrain.

In solving equation 3.13, it must be noted that the driving cycle data is available in discrete form. Thus, the integral must be calculated in a discretized form in time. The speed for a given interval is approximated as

$$v(t) = \bar{v}_i \qquad 3.15$$

Acceleration is approximated using a central difference scheme as [60]

$$a(t) = \bar{a}_i = \frac{v_{i+1} - v_{i-1}}{t_{i+1} - t_{i-1}} \qquad 3.16$$

An approximation of the tractive force can be calculated using the formula

$$\bar{F}_{trac} \approx \frac{1}{x_{tot}} \cdot \sum_{i \in trac} \bar{F}_{trac,i} \cdot \bar{v}_i \cdot h \qquad 3.17$$

where h is the time interval between the discrete datapoints ($h = t_{i+1} - t_i$), and the summation is only carried out in the intervals where the vehicle is in traction mode.

3.7. Effects of regenerative braking

The two different scenarios for the brake energy recuperation will be discussed here. The scenarios are no recuperation and 100% recuperation.

If the vehicle is not fitted with a braking energy recuperation device, equation 3.1 is applicable. Thus, there are four significant contributions to the traction force

$$\bar{F}_{trac} = \bar{F}_{trac,a} + \bar{F}_{trac,r} + \bar{F}_{trac,m} + \bar{F}_{trac,g} \qquad 3.18$$

Guzzella and Sciaretta (2007) ignore gravity's effects in further calculations because most of the standard driving cycles are designed with the assumption of a flat road, so there is no need to consider gravitational effects. However, gravitational effects will be considered in this model to give the model more versatility.

The forces caused by aerodynamic drag, rolling resistance, acceleration resistance, and gravity are defined as

$$\bar{F}_{trac,a} \approx \frac{1}{x_{tot}} \cdot \frac{1}{2} \cdot \rho_a \cdot A_F \cdot c_a \cdot \sum_{i \in trac} \bar{v}_i^3 \cdot h \qquad 3.19$$

$$\bar{F}_{trac,r} \approx \frac{1}{x_{tot}} \cdot m_v \cdot g \cdot c_r \cdot \sum_{i \in trac} \bar{v}_i \cdot h \qquad 3.20$$

$$\bar{F}_{trac,m} \approx \frac{1}{x_{tot}} \cdot m_v \cdot \sum_{i \in trac} \bar{a}_i \cdot \bar{v}_i \cdot h \qquad 3.21$$

$$\bar{F}_{trac,g} \approx \frac{1}{x_{tot}} \cdot m_v \cdot g \cdot \alpha \cdot \sum_{i \in trac} \bar{v}_i \cdot h \qquad 3.22$$

The value of the mean tractive force can be determined by solving the above equations.

For a vehicle with perfect recuperation efficiency, there are only three significant contributions to the traction force

$$\bar{F}_{trac} = \bar{F}_{trac,a} + \bar{F}_{trac,r} + \bar{F}_{trac,g} \qquad 3.23$$

This is because any energy spent accelerating the vehicle is wholly recuperated during the braking phases by the recuperation device. Therefore, the energy consumed in the acceleration phase is ignored.

However, since all the energy during the braking phase is recuperated, the energy to overcome aerodynamic drag and rolling resistance cannot be provided by the reduction in kinetic energy and gravitational potential energy. Therefore, the summation for the aerodynamic drag and rolling resistance must be carried out over the

entire driving cycle and not just the traction regions. The summation for the gravitation effects must also be carried out for the duration of the driving cycle. The equations used for the perfect recuperation scenario is as follows

$$\bar{F}_{trac,a} \approx \frac{1}{x_{tot}} \cdot \frac{1}{2} \cdot \rho_a \cdot A_F \cdot c_a \cdot \sum_{i=1}^{n} \bar{v}_i^3 \cdot h \quad 3.24$$

$$\bar{F}_{trac,r} \approx \frac{1}{x_{tot}} \cdot m_v \cdot g \cdot c_r \cdot \sum_{i=1}^{n} \bar{v}_i \cdot h \quad 3.25$$

$$\bar{F}_{trac,g} \approx \frac{1}{x_{tot}} \cdot m_v \cdot g \cdot \alpha \cdot \sum_{i=1}^{n} \bar{v}_i \cdot h \quad 3.26$$

Once again, the mean tractive force is equal to the average energy consumed per distance traveled.

It should be noted that the perfect recuperation device, which is assumed in the latter scenario, is 100% efficient, and it does not add any extra weight to the total weight of the vehicle. Since 100% efficiency is not feasible in a real-world scenario. Therefore, based on the vehicle's recuperation efficiency, the model will interpolate the actual energy demand between the "No Recuperation" and "Perfect Recuperation" energy demands. The equation used for this interpolation is

$$\bar{F}_{trac}(\eta_{rec} = rec) = \bar{F}_{trac}(\eta_{rec} = 100\%) + (1 - rec) \cdot (\bar{F}_{trac}(\eta_{rec} = 0\%) - \bar{F}_{trac}(\eta_{rec} = 100\%)) \quad 3.27$$

where η_{rec} is the recuperation efficiency, rec is the actual recuperation efficiency of the vehicle as a fraction, $\eta_{rec} = 0\%$ is the “No Recuperation” scenario, $\eta_{rec} = 100\%$ is the "Perfect Recuperation" scenario, and $\eta_{rec} = rec$ is the scenario for the given recuperation efficiency.

Interestingly, even in the scenario with no recuperation, the vehicle still uses some of the energy during braking to cover the aerodynamic drag and rolling resistance, so in effect, "recuperating" the energy. This is better illustrated by plotting the qualitative energy demands with zero and perfect recuperation efficiencies. The vehicle is assumed to be on a flat road to simplify the discussion. Thus, the gravitation effects are neglected.

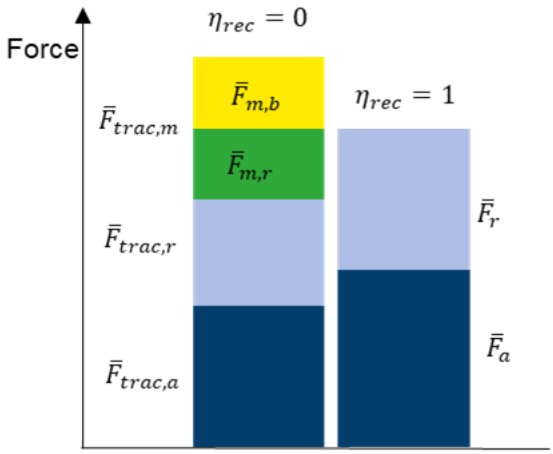

Figure 3: Qualitative mean tractive force that the engine must supply for a vehicle with zero and perfect recuperation

In Figure 3, $\bar{F}_{trac,X}$ represents the mean tractive force for the vehicle with no recuperation to overcome "X" resistance, and $\bar{F}_X$ represents the mean tractive force for the vehicle with perfect recuperation to overcome "X" resistance.

As can be seen from Figure 3, the total mean tractive force demand for perfect recuperation is larger than just the addition of the $\bar{F}_{trac,a}$ and $\bar{F}_{trac,r}$. A part of the $\bar{F}_{trac,m}$ must also be added to get to this value, here represented by $\bar{F}_{m,r}$. $\bar{F}_{m,r}$ represents the part of the kinetic energy of the vehicle used to overcome resistive forces during braking or coasting modes. Therefore, in effect, the vehicle with no recuperation is also recuperating some of its kinetic energy. $\bar{F}_{m,b}$ represents the part of the energy wasted as heat during braking.

Finally, the mechanical energy demand E_{mech} for the vehicle is calculated using the mean tractive force. The mean tractive force is equal to the average energy consumed per distance traveled. When the mechanical energy demand is expressed in units of MJ/100km, the relationship between the quantities is

$$E_{mech} = \frac{\bar{F}_{trac}}{10} \qquad 3.28$$

After calculating the vehicle's mechanical energy demand, the next major energy demand must be taken into account. These include the powers needed for the vehicle's HVAC system, electronic systems used for passenger comfort and entertainment, driving controls, and other essential parts of the vehicle. These systems are combined into one in this model and is referred to as auxiliary power P_{aux} demand. The auxiliary power demand is used as an input to the model. The auxiliary energy E_{aux} demand is then calculated as follows

$$E_{aux} = \sum_{i=1}^{n} P_{aux} \cdot h \qquad 3.29$$

Therefore, the energy provided by the drivetrain is the summation of the mechanical energy and auxiliary energy demand of the vehicle. The drivetrain efficiency can then be taken into account to find the final fuel energy E_{fuel} demand for the vehicle. However, it must be taken into account that the mechanical energy flows through the whole drivetrain, whereas the auxiliary energy does not go through the entire drivetrain. Thus the efficiencies of the different parts of the drivetrains must be taken into account for the different drivetrains. For a vehicle with an internal combustion engine, the auxiliary energy demand depends on the efficiency of the entire drivetrain η_{dri} except for the transmission system efficiency η_{tra}, which includes the transmission shaft, gearbox, and differential efficiencies. Therefore, the fuel energy demand can be calculated as

$$E_{fuel} = \frac{E_{mech}}{\eta_{dri}} + \frac{E_{aux} \cdot \eta_{tra}}{\eta_{dri}} \qquad 3.30$$

Whereas for a vehicle with an electric drivetrain, the fuel energy is calculated as

$$E_{fuel} = \frac{E_{mech}}{\eta_{dri}} + \frac{E_{aux} \cdot \eta_{tra} \cdot \eta_{mot}}{\eta_{dri}} \qquad 3.31$$

where η_{mot} is the efficiency of the electric motor.

In the cases where the vehicle has two different energy storages or motors, the mechanical and auxiliary energy demands are shared based on the driving share ratios. The final fuel energy demands are then calculated separately for individual storage and motor. Finally, the overall fuel energy demand is calculated by summing the individual fuel energy demands.

Figure 4 shows the structure of the model developed to determine the energy demand for the on-road transport modes.

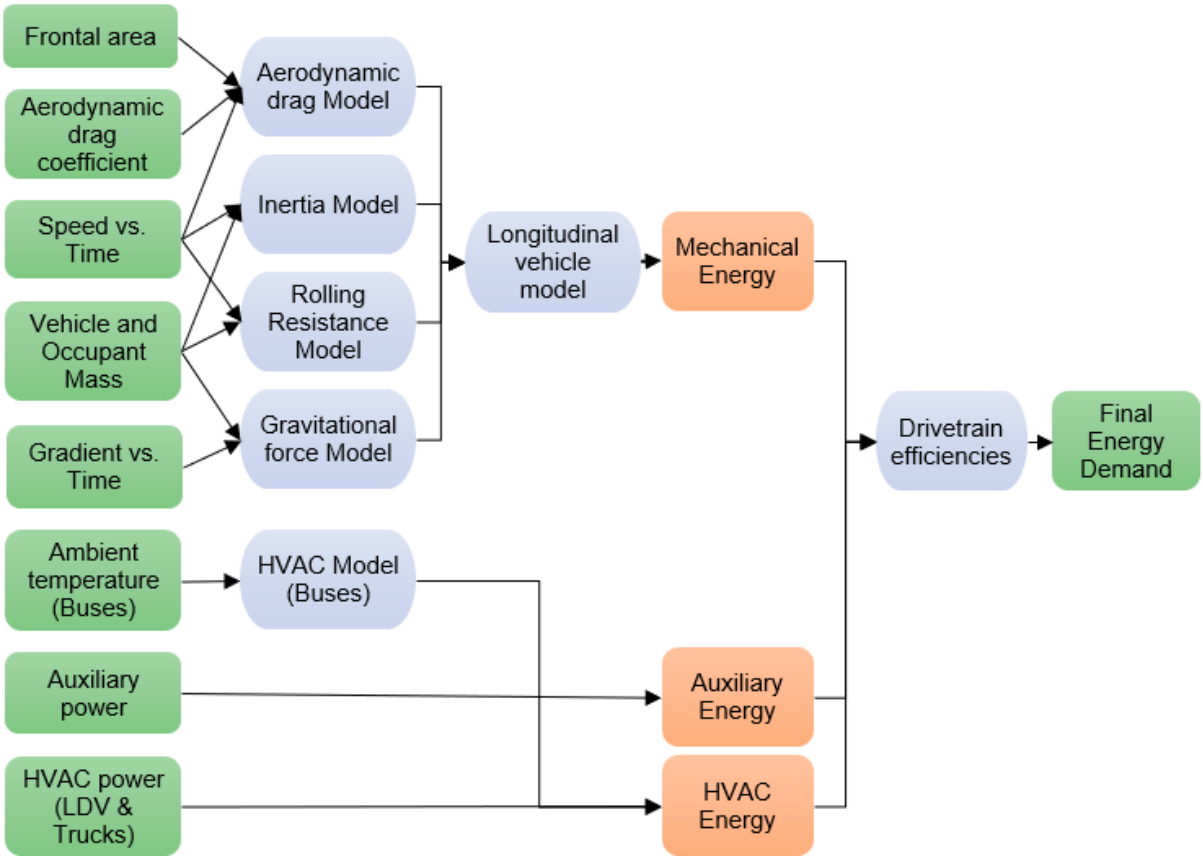

Figure 4: Structure of the model for the on-road transport mode energy demand

4. Data Preparation and Validation

4.1. On-road Transport Modes

In this section, the data used to build the on-road vehicle models is discussed in detail.

4.1.1. Standard driving cycles

Different pollutants emitted by vehicles on the road are regulated by the European Commission (EC). All new LDV and HDV engines must undergo type approval emissions tests to be sold within the EU. LDVs are tested on chassis dynamometers, and HDV engines are tested on engine testbeds. During a chassis dynamometer test, the vehicle wheels are placed on rollers that simulate friction losses and aerodynamic drag. The exhaust gases are then measured while the vehicle follows a driving cycle [61].

Since vehicle exhaust depends on many different conditions, the tests must be carried out in reproducible laboratory conditions, which try to produce real-world results. One of these factors is the driving cycle, which is a fixed sequence of vehicle operations that try to mimic real-world vehicle operation. A speed versus time profile is an essential part of this driving cycle. Since the vehicle parameters affect the emissions, different vehicle type-specific driving cycles have been developed, such as for cars, trucks, buses, delivery trucks, and motorcycles [61].

These same driving cycles also give the vehicle-specific energy consumption values, which is the most overriding parameter for this thesis.

Besides the laboratory tests performed using the standard driving cycles, EU regulations require all LDVs to undergo real-world driving tests. As of September 2017, the EU's Real Driving Emissions (RDE) regulations require all vehicles to be driven on public roads to measure pollutant emissions under actual driving conditions. The emissions are measured using a portable emissions measuring system attached to the vehicle [62]. The RDE measurements are taken under different driving conditions, including low and high altitudes, year-round temperatures, additional vehicle payload, up- and down-hill driving, urban roads, rural roads, and motorways [63]. Failing the RDE testing results in the vehicle not being allowed to be put on the market [62].

Different government bodies, as well as educational and research institutes, have developed varied driving cycles for specific applications. Some of the driving cycles used in this thesis are discussed next.

Worldwide Harmonized Light Vehicles Test Cycle (WLTC)

WLTC is a chassis dynamometer test developed by the UNECE as part of the Worldwide harmonized Light vehicles Test Procedures (WLTP). It is being used to replace the New European Driving Cycle (NEDC), which was previously used for type approval testing of LDV in the EU. It is developed to give better laboratory estimates for real-world vehicle emissions and fuel consumption. WLTC aims to be a global standard; thus, it is also being adapted to countries outside of the EU [64].

There are different versions of the WLTC based on the manufacturer's specified maximum speed and the power to mass ratio of the tested vehicle. WLTC Class 3 is representative of vehicles driven in Europe and Japan. Class 3 is further subdivided into two, 3a and 3b, based on the vehicle's maximum speed. In this thesis, primarily, the WLTC Class 3b, which is meant for LDVs with a maximum speed above 120km/h, will be used. WLTC class 3a, designed for vehicles with a maximum speed below 120km/h, is discussed in Appendix A. WLTC class 2, developed for vehicles with lower power to mass ratios, is also addressed in Appendix A [64]. All these driving cycles are available options in the model.

The WLTC class 3b is divided into four distinct driving scenarios; Low, Medium, High, and Extra-High speed regions, representing Urban, Suburban, Rural, and Highway scenarios, respectively. Figure 5 shows the driving cycle [64].

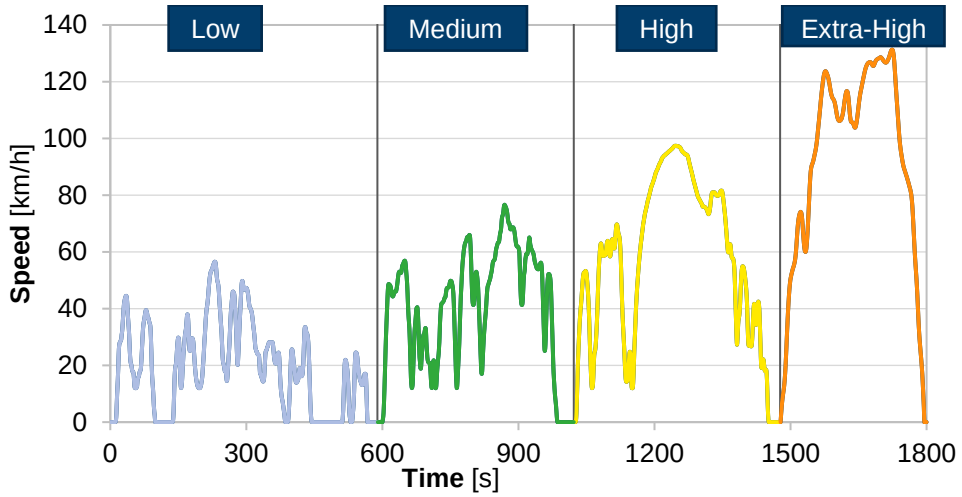

Figure 5: WLTC class 3b with different driving scenarios (Adapted from [64]*)*

As can be seen from Figure 5, the driving cycle has distinct driving characteristics for the four different driving scenarios. The Low (Urban) scenario has low speeds and frequent stops representing the stop-and-go traffic in urban centers. The extra-high (Highway) scenario has high speeds, characteristic of European highways.

Table 4 shows more detailed information about the WLTC Class 3b driving cycle [64].

Table 4: WLTC class 3b parameters [64]

	Duration (s)	Stop duration (s)	Distance (m)	Max. Speed (km/h)	Avg. Speed without stops (km/h)	Avg. Speed with stops (km/h)	Min. Acceleration (m/s^2)	Max. Acceleration (m/s^2)
Low	589	156	3095	56.5	25.7	18.9	-1.47	1.47
Medium	433	48	4756	76.6	44.5	39.5	-1.49	1.57
High	455	31	7162	97.4	60.8	56.7	-1.49	1.58
Extra-high	323	7	8254	131.3	94.0	92.0	-1.21	1.03
Total	1800	242	23266					

Table 4 shows important parameters that define the low, medium, high, and extra-high driving scenarios. The most descriptive parameter is the average speed without stops, which is the average speed when the vehicle is in motion. This parameter gives a general idea of the vehicle's speeds during the specific driving scenario. Although the time spent in the extra-high scenario is lower than that spent in the low scenario, the vehicle has to travel further in the extra-high scenario. The maximum speed of the vehicle is 131.3 km/h.

WLTC class 3b is used by default to model the energy demand of all LDVs.

World Harmonized Vehicle Cycle (WHVC)

The WHVC is a chassis dynamometer test developed by UNECE as part of the world-wide harmonized heavy-duty certification (WHDC) procedure. This chassis dynamometer test was developed with extensive data taken from

commercial HDV use in the EU, the United States of America (USA), Japan, and Australia. Therefore, although the WHVC is not officially used for HDV certification (HDV certification is done with the engine dynamometer test), it will be used for HDV consumption evaluation in this model. Figure 6, below, shows the WHVC [65], [66].

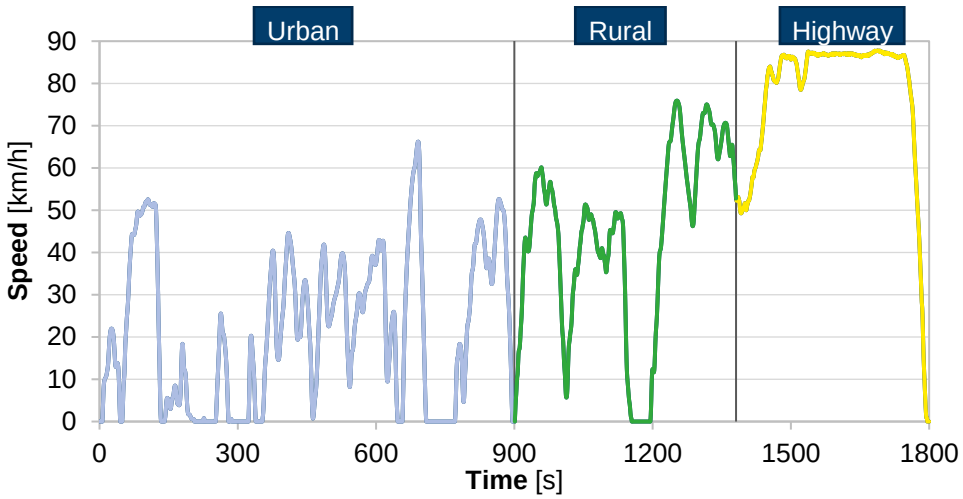

Figure 6: WHVC with different driving scenarios (Adapted from [65]*)*

As can be seen from Figure 6, the driving cycle has distinct driving characteristics for the three different driving scenarios. The Urban scenario has low speeds and frequent stops representing the stop-and-go traffic in urban centers. Highway scenario has speeds reaching almost 90km/h, the speed limit for HDV in most European countries. Table 5, below, shows more detailed information about the WHVC driving cycle.

Table 5: WHVC parameters [65]

	Duration (s)	Stop duration (s)	Distance (m)	Max. Speed (km/h)	Avg. Speed without stops (km/h)	Avg. Speed with stops (km/h)
Low	900	199	5315	66.2	27.3	21.3
Medium	481	42	5826	75.9	47.8	43.6
High	419	5	9026	87.8	77.6	76.7
Total	1800	246	20167			

The WHVC driving cycle is used by default for all trucks. Small and medium trucks are modeled using the Urban and Rural parts, while semi-trucks only use the highway part of the WHVC. Coaches also use the highway part of the WHVC by default. Large trucks use the entire driving cycle.

All the other driving cycles used in the model are described in Appendix B.

4.1.2. Light-duty vehicles

In this section, the data used to build and run the model for LDVs is discussed. LDVs in the model are subdivided into five categories, referred to as modes within the model. The five modes are small car, medium car, large car, sport utility vehicle (SUV), and light commercial vehicle (LCV).

The different modes are identified based on their European New Car Assessment Programme (Euro NCAP) classification. Euro NCAP is a European car safety assessment program [67]. The different LDV modes are also defined in the EC regulation number 4064/89 [68]. The different modes, as well as their Euro NCAP and EC classification, are shown in Table 6 below.

Table 6: LDV modes used in the model (Based on [67]*,* [68]*)*

Mode	EC	Euro NCAP
Small Car	A and B	Supermini
Medium Car	C	Small family car
Large Car	D	Large family car
SUV	J	Small Off-Road / Large Off-Road
LCV	M	Small MPV / Business Van

After the classification of the modes, an analysis of the vehicles in the market belonging to the different modes is carried out. The top 30 best-selling vehicles in Germany for the year 2019 are considered. The cars belonging to modes described in Table 6 (except LCV), along with the number of vehicles sold, are shown in Table 19, in Appendix C [69].

Out of the top 30 most sold cars in Germany, there are not many examples of LCVs. Therefore, to have a larger variation of LCV models, Europe wide sales values are considered. It is found that Ford Transit is by far the most prevalent LCV vehicle model within the EU-28. The other important LCV models include the Mercedes Sprinter, Fiat Ducato, Renault Kangoo, Citroen Berlingo, VW Transporter, Peugeot Partner, Renault Master, Renault Trafic, and VW Caddy [70].

The top-selling vehicle models and the top-selling LCVs are researched to find their aerodynamic drag coefficients c_a and frontal areas A_f. These data are collected from various sources like manufacturers' websites and online car dealers. The values obtained for the different vehicles in each mode are then averaged to find a single value for each mode. The average values are assumed to be for the year 2020. Since the model should be able to calculate data up to 2050, future development in vehicle aerodynamic properties must be considered. Islam et al. (2020) predict the percentage drag coefficient reduction based on high and low technology improvements until 2050 [71]. An average of low and high technology improvements is taken for the model. The frontal area is assumed to be constant throughout the years. The average mode-specific values for each decade until 2050 are shown in Table 7.

Table 7: Aerodynamic parameters for the average vehicle in each mode

Mode	A_f (m^2)	c_a (-)			
		2020	2030	2040	2050
Small Car	2.16	0.309	0.286	0.245	0.239
Medium Car	2.25	0.271	0.251	0.215	0.210
Large Car	2.21	0.262	0.242	0.208	0.203
SUV	2.45	0.327	0.302	0.259	0.253
LCV	3.17	0.349	0.322	0.276	0.270

Islam et al. (2020) also give the percentage improvement for rolling resistance based on high and low technology progression. Table 8 shows the average of these high and low improvement values of rolling resistance, taking the value in 2020 to be 100% [71].

Table 8: Rolling resistance improvement until 2050 [71]

Year	2020	2030	2040	2050
%	100	92.5	79.2	77.5

These average improvement values are used in the model to modify the rolling resistance calculated for 2020. The 2020 rolling resistance is calculated using equation 3.5 from Grube (2014) [27].

Cox (2018) reports the median value for auxiliary power for LDV as 636 watts [72]. This value is assumed for all LDVs. No future trends are assumed, as the variables are too many. Improvement in vehicle HVAC systems and better insulation will likely decrease auxiliary power demand in the future. However, more electronic devices and self-driving capabilities are likely to increase auxiliary power demands.

The drivetrain efficiencies are one of the most important parameters used in the model. The efficiencies of the major components of the drivetrain are first needed to calculate the total drivetrain efficiency.

Starting with battery efficiency, different values are reported in the literature. Three different values for the roundtrip efficiency (efficiency of charging and discharging) is found in literature; 81%, 88%, and 90% [73], [74], [75]. Taking the square root of the average of these values gives approximately 93% for the charging efficiency. Additional improvement of 1% per decade is assumed, reaching 96% by 2050.

A range of values is available for the total efficiency of the transmission system (Gearbox, propeller shaft, and differential) part of the drivetrain. Efficiency values between 86-94% [76] and 84-96% [77] are reported in literature. A single-speed transmission system's efficiency, where it can be assumed there is no gearbox, is effectively equal to the transmission system's efficiency without a gearbox, which is reported at 95% [78]. This value will be used for all the electric drivetrains where there are no gearboxes, and a 1% additional improvement is assumed per decade. The gearbox efficiency is taken at 93% [79], and future trend is assumed such that it reaches an efficiency of 95% by 2050.

Islam et al. (2020) report values of fuel cell peak efficiency of 61% for 2020, along with predictions for future development [71]. The value in 2020 is taken to be 60%, along with future developments from this literature. Electric motors' current efficiency is taken to be 85%, with future improvements causing it to rise to 93% in 2050 [80].

Next, the efficiency values of different internal combustion engines are collected. Islam et al. (2020) report values for different internal combustion engine efficiencies and improvements until 2050. A turbo internal combustion engine is assumed to be the default type for gasoline internal combustion engines (ICE-g). Diesel (ICE-d) and gasoline internal combustion engine data are taken from this source [71].

Table 9 shows the different part efficiencies discussed above.

Table 9: Current and future efficiencies for different parts of the drivetrain. For further information, please refer to the text. [71], [73] - [80]

Drivetrain parts	Efficiency (-)				Sources
	2020	2030	2040	2050	
Fuel-cell	0.60	0.62	0.64	0.66	[71]
Electric motor	0.85	0.9	0.92	0.93	[71]
Battery	0.93	0.94	0.95	0.96	[73], [74], [75]
Single speed transmission	0.95	0.96	0.97	0.98	[78]
Gearbox	0.93	0.94	0.945	0.95	[79]
ICE-g	0.29	0.34	0.37	0.39	[71]
ICE-d	0.30	0.39	0.42	0.44	[71]

Table 9 shows that diesel engines have a more significant improvement potential in the near future than gasoline engines. Batteries, gearbox, and transmission already have high efficiencies. Thus, there is not much potential for improvement.

Ahmed (2017) analyzes the fuel economy of HEV versus ICEV. The fuel economy analysis is carried out over real-world driving as well as using standard driving cycles. On average, the HEVs approximately resulted in an additional 4% better fuel efficiency [81]. Thus, the hybrid drivetrain efficiency is taken to be 4% higher than its conventional counterpart.

Table 10 shows all the different drivetrains that are applicable for LDVs.

Table 10: Drivetrain efficiencies for LDV, based on data from different sources. For further information, please refer to the text.

Drivetrain	2020	2030	2040	2050	Sources
ICEV-g	0.26	0.31	0.34	0.36	[71], [78], [79]
ICEV-d	0.27	0.36	0.39	0.40	[71], [78], [79]
HEV-g	0.30	0.35	0.38	0.40	[71], [78], [79], [81]
HEV-d	0.31	0.40	0.43	0.44	[71], [78], [79], [81]
PHEV-g	0.30	0.35	0.38	0.40	[71], [78], [79], [81]
PHEV-d	0.31	0.40	0.43	0.44	[71], [78], [79], [81]
PHEV-fc	0.47	0.52	0.56	0.59	[71], [73], [74], [75], [78]
REEV-g	0.30	0.35	0.38	0.40	[71], [78], [79], [81]
REEV-d	0.31	0.40	0.43	0.44	[71], [78], [79], [81]
REEV-fc	0.47	0.52	0.56	0.59	[71], [73], [74], [75], [78]
BEV	0.75	0.81	0.85	0.87	[71], [73], [74], [75], [78]
FCEV	0.47	0.52	0.56	0.59	[71], [73], [74], [75], [78]
ICEV-cng	0.26	0.31	0.34	0.36	[71], [78], [79]

The efficiencies of PHEV and range-extended electric vehicle REEV are taken to be the same as for their HEV counterparts. The efficiency for REEV-fc is assumed to be the same as for FCEV, and ICEV-cng the same as ICEV-g. Hybrid vehicles are divided into electric mode and conventional/fuel cell modes. This is a simplification. The electric mode's efficiency of all dual-drivetrain vehicles is assumed to be the same as for BEV.

Next, the recuperation efficiency for vehicles with an electric drivetrain is determined. Different values for the recuperation efficiencies are reported in the literature. Ott et al. (2012) report a recuperation efficiency of 63% [82]. Hu et al. (2013) analyzed buses' recuperation efficiencies and report values around 65% [83]. Xu et al. (2011), on the other hand, present the amount of energy saved between 8% to 25%. Converted to recuperation efficiency values, this gives a wide range of values between 28% and 89% [84]. In this model, the recuperation efficiency is determined based on the electric drivetrain efficiency, the drivetrain efficiency of BEV and the electric modes of dual-drivetrain vehicles. This is justified because the electric drivetrain is responsible for recuperating braking energy. The electric drivetrain efficiency values are squared to account for the fact that the energy recuperated from braking has to flow back and forth through the drivetrain. The result is multiplied by an assumed factor of 0.8 to account for the times when regenerative braking is not sufficient to slow down the vehicle, and additional mechanical braking is required. The resulting regenerative braking efficiencies are shown in Table 11 below. The values used are in the range of the above-cited literature values.

Table 11: Regenerative braking efficiency

Year	2020	2030	2040	2050
Efficiency (-)	0.45	0.55	0.62	0.69

The regenerative braking efficiencies are used for all vehicles with an electric drivetrain.

One of the most important parameters for PHEVs and REEVs is the percentage of the drive that takes place in electric mode. Accurately modeling this parameter will require detailed data on the vehicle's battery capacity and the distance driven after the last charging cycle. Since such detailed input data is not required, a more general approach is used. Trost (2016) takes such a perspective on the electric drive ratio for PHEV. He reports the electric drive percentage for vehicles with different yearly driven distances [85]. The data points from different vehicles show a significant spread indicating that other factors, such as the owner's charging behavior, play a part in determining the actual electric drive share. However, for this model, the median curve is used to determine the electric drive ratio. The median curve resembles a logistic function; thus, it is analyzed to determine the best fit logistic curve through the median curve. The logistic curve is then used to determine the electric drive ratio given the yearly driven distance. Because REEVs have significantly higher battery capacity than PHEVs, the logistic curve is modified to take this into account for REEVs. Figure 7 shows the electric drive share versus yearly driven distance for PHEV and REEV.

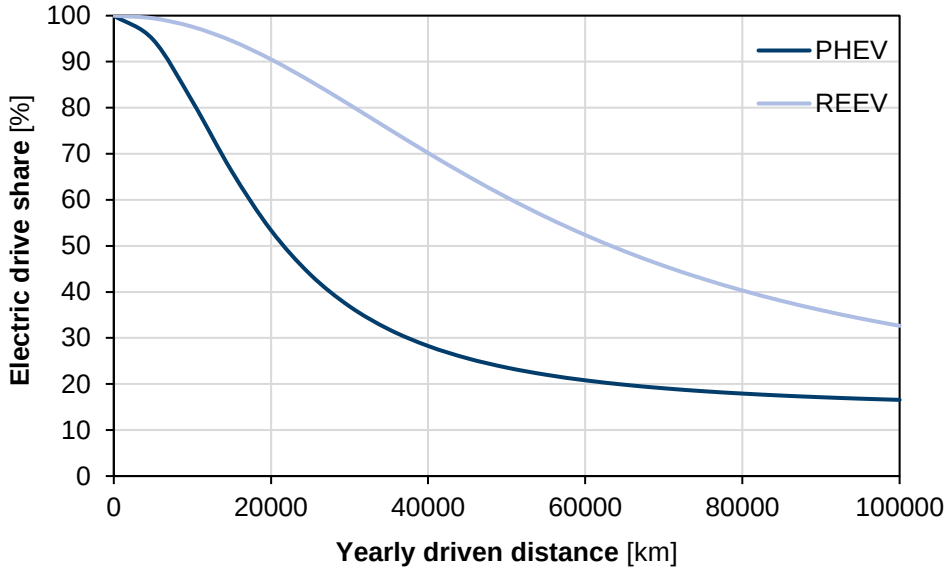

Figure 7: Electric drive ratio vs. yearly driven distance for PHEV and REEV (Based on [85]*)*

The curves in Figure 7 are also applicable for plug-in hybrid and range-extended electric drivetrain in HDVs. Nevertheless, the model can take the electric drive share as an input from the user.

Around a third of the global electric-vehicle fleet is made up of PHEVs. CO_2 emissions by PHEVs are found to be two to four times higher than those found during type-approval tests. The main reason for this is that the average real-world electric driving share for PHEVs are much lower than those assumed during the type-approval tests. Germany's average electric share for private PHEVs is 43% and 18% for company PHEVs. Decreasing the power of the combustion engine and increasing the all-electric range lead to higher electric driving shares. Increasing the all-electric range by 10km reduces CO_2 emissions by 8%-14% [86].

The average occupancy for all LDVs is taken to be 1.3 passengers per vehicle, which is the average German value [87].

The density of air ρ_a is taken as 1.225 kg/m^3, assuming a temperature of 15°C and standard atmospheric pressure [88]. This is used for all LDV and HDV modes.

According to the European Union Aviation Safety Agency, the European average passenger weight is taken to be 83 kg, which includes the mass of a person and their luggage [89]. This is used for all LDV and HDV modes.

4.1.3. Buses

HDVs are defined as vehicles with a gross vehicle weight rating (GVWR) above 3500 kg and include all buses and trucks. Although HDVs constitute less than 5% of global road-going vehicles, they are responsible for 40% of its energy consumption [90]. Therefore, good parametrization of HDVs is essential in generating a good energy demand model for transportation.

Buses are subdivided into four modes. These are small buses, medium buses, large buses, and coaches. Firstly, data about different bus models from major manufacturers like Mercedez-Benz, MAN, Setra, and Van Hool are collected. For Small Bus, manufacturers like VW, Fiat, Ford, and Easymile are considered. The data is compiled from various sources, including manufacturers' websites and other sources. The average values for each mode's frontal areas and seating capacity are found, as shown in Table 12.

The aerodynamic drag coefficient c_a for Small Bus is calculated by taking an average of the different models. For medium and large Buses, Xu et al. (2009) report a c_a value of 0.7 [91]. Kanekar et al. (2017) analyses the possible improvements that can be made on an aerodynamically unoptimized city bus and find that the c_a value can be reduced from 0.66 to 0.46 [92]. The c_a value is assumed to be 0.65, decreasing to reaching 0.5 in 2050. Coaches generally have better aerodynamic properties because they are designed for faster travel. Thus, reducing aerodynamic drag is more important than city buses. Kim (2011) studies the effects of design improvement on the aerodynamic drag of coaches. He states that the c_a value can be decreased from 0.457 to 0.332 with design improvements [93]. The c_a value is taken as 0.45 for 2020, decreasing to 0.30 in 2050. Some coach models in the market already claim c_a as low as 0.33 [94]. The c_a values for each decade are shown in Table 12.

Table 12: Total passenger capacity, frontal area, and aerodynamic drag coefficient for buses

Mode	Total passenger capacity	A_f (m^2)	c_a (-)			
			2020	2030	2040	2050
Small Bus	15	4.00	0.36	0.33	0.30	0.28
Medium Bus	91	7.79	0.65	0.60	0.55	0.50
Large Bus	162	7.85	0.65	0.60	0.55	0.50
Coach	58	9.50	0.45	0.40	0.35	0.30

For catenary buses, the aerodynamic drag coefficient changes depending on whether or not the bus is connected to the overhead lines. A c_a value of 0.83 is taken for the part of the journey where the overhead wires are engaged and 0.66 for the rest [95]. It is assumed that the overhead cables are engaged for 80% of the journey, although this value can also be an input provided by the user. These values are also used for catenary truck modes.

The rolling resistance coefficients for buses are not calculated in the same way as for LDV. The rolling resistances are based on tire regulations instead. According to Regulation (EU) 2020/740, from 1 May 2021 onwards, the tires for all HDVs (Buses and Trucks) will need to meet specific characteristics for different fuel efficiency classes. One of these is the rolling resistance coefficient of the tires. The tires are classified into five different efficiency classes, A to E, with increasing rolling resistance coefficients. Table 13 shows the fuel efficiency classes and their respective coefficient of rolling resistances c_r for HDV tires [96].

Table 13: EU fuel efficiency classes and the coefficient of rolling resistance [96]

Fuel efficiency class	c_r
A	$c_r \leq 0.004$
B	$0.0041 \leq c_r \leq 0.005$
C	$0.0051 \leq c_r \leq 0.006$
D	$0.0061 \leq c_r \leq 0.007$
E	$c_r \geq 0.0071$

The average value for all buses' rolling resistance for 2020 is taken as the upper limit of class D tires, 0.007. It is assumed that the average rolling resistance will decrease by one efficiency class every decade, reaching 0.004 for 2050. The same values are also used in the model for the trucks.

The auxiliary power of buses can be a significant portion of the total fuel consumption. This can especially be true because of the HVAC power needed in extreme weather conditions. Cox (2018) reports an average power rating of 13.05 kW for a medium bus with, and 6.15 kW without, HVAC power demand [72]. However, since the HVAC power demand for buses is significant, it is decided to consider it in more detail. Knote et al. (2017) report that the HVAC energy consumption per distance traveled as a function of the ambient temperature for medium buses. Figure 8 shows this relation for different cruising velocities [97].

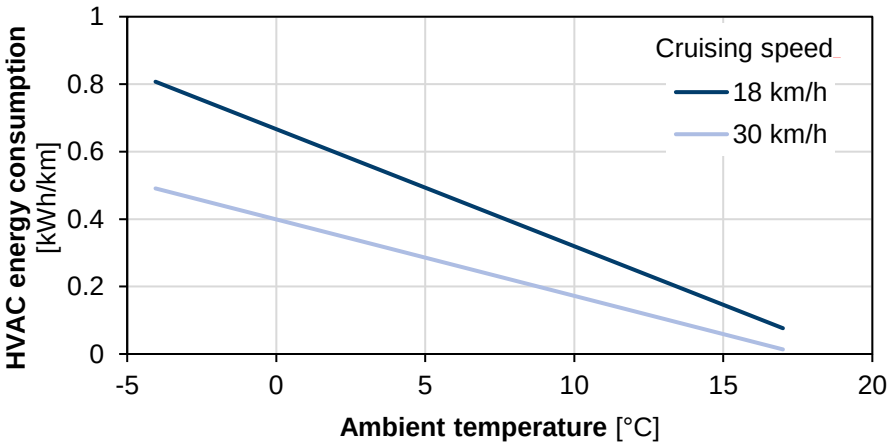

Figure 8: HVAC energy consumption as a function of ambient temperature (Adapted from [97]*)*

The HVAC energy consumption values shown in Figure 8, reported for ambient temperatures between - 4°C and 17°C, approximately, is assumed for medium buses. HVAC energy is assumed to be the same for lower ambient temperatures as the one for - 4°C and the same as for 17°C for higher temperatures. This is assuming that at

lower temperatures, the HVAC system has reached its power limitations. For higher temperatures, the HVAC system still needs to maintain ventilation functions for which the minimum energy is required. However, the model is best suited to estimate energy needs within the specified range of ambient temperatures.

The values for cruising speed of 18km/h are taken as the average for Urban driving conditions, and the 30km/h values are used for all non-urban (rural and highway) driving conditions. The values from Figure 8 are scaled to meet the HVAC power demands for the other bus modes, using the ratios of total seating capacity. Assuming that the total seating capacity is proportional to the volume of space that needs to be heated. This leads to lower energy needs for coaches compared to medium buses, despite their similarity in size; due to the lower seating density for passengers in coaches. However, coaches do not have so frequent stops; doors are not opened as often, thus lowering the HVAC power demand.

The non-HVAC related auxiliary power consumption values are reported by Cox (2018). He reports a value of 6.15 kW for medium buses [72]. The power consumption for the other modes is then evaluated using their respective curb weights ratios, assuming that the auxiliary power demands are proportional to the mass and size of the drivetrain and other equipment of the vehicle.

Since HDVs' internal combustion engines are more efficient than light-duty vehicles', different engine efficiency values must be used in the model [98]. Therefore, the engine efficiencies for the year 2020 for heavy-duty internal combustion engines are taken from Cox (2018) [72]. The efficiency of ICEV-g and ICEV-cng are assumed to be the same. The future engine efficiency improvements are based on Islam et al. (2020) [71]. The same assumptions as for LDV's are made for the rest of the drivetrains. These assumptions are valid for all HDVs. The drivetrain efficiencies for buses and trucks are shown in Table 14.

Table 14: Drivetrain efficiencies for buses and trucks based on data from different sources. For further information, please refer to the text.

Drivetrain	2020	2030	2040	2050	Sources
ICEV-g	0.27	0.32	0.36	0.38	[71], [72], [78], [79]
ICEV-d	0.29	0.38	0.41	0.43	[71], [72], [78], [79]
REEV-fc	0.47	0.52	0.56	0.59	[71], [72], [73], [74], [75], [78]
BEV	0.75	0.81	0.85	0.87	[71], [73], [74], [75], [78]
FCEV	0.47	0.52	0.56	0.59	[71], [72], [73], [74], [75], [78]
ICEV-cng	0.27	0.32	0.36	0.38	[71], [72], [78], [79]
O-HEV-d	0.33	0.42	0.45	0.47	[71], [72], [78], [79], [81]
O-BEV	0.75	0.81	0.85	0.87	[71], [73], [74], [75], [78]
O-FCEV	0.47	0.52	0.56	0.59	[71], [72], [73], [74], [75], [78]
HEV-d	0.33	0.42	0.45	0.47	[71], [72], [78], [79], [81]
PHEV-d	0.33	0.42	0.45	0.47	[71], [72], [78], [79], [81]
REEV-d	0.33	0.42	0.45	0.47	[71], [72], [78], [79], [81]

The same efficiencies for regenerative braking discussed for LDVs are also applicable for HDVs. The discussion regarding PHEV and REEV drivetrain for LDVs are still assumed to be valid for HDVs.

The default average occupancy rate for small, medium, and large buses is 19%, while coaches are higher at 57% [99].

4.1.4. Trucks

Trucks are subdivided into four different modes. These are small trucks, medium trucks, large trucks, and semi-trucks. To begin with, data on various truck models from different manufacturers are collected. These data are taken from multiple sources, including manufacturers, like VOLVO, MAN, Mitsubishi, Mercedes-Benz, SCANIA websites. These trucks are sorted into different modes based on their GVWR. The average frontal areas A_f for all the vehicles in each mode is taken as the representative value for that mode.

Aerodynamic drag coefficients are then considered. Hjelm and Bergqvist (2009) report the c_a values for semi-truck to be in the range 0.6 to 0.65 [100]. A 2012 National Research Council report states a c_a value of 0.59 according to US EPA Smartway [101]. Hariram et al. (2019) analyse different options to improve the aerodynamic characteristics of semi-trucks. They report an unoptimized vehicle to have a c_a value of 0.651 and possible improvements can reduce this to 0.457 [102]. In this study, all truck modes are assumed to have the same drag coefficients. The drag coefficient for the year 2020 is assumed to be 0.65, reaching 0.5 by 2050. The A_f and c_a for the different modes are shown in Table 15.

Auxiliary power consumption can be a significant part of the energy consumption for trucks. For trucks, the auxiliary power for non HVAC power and HVAC power are combined into one value, as is the case for LDVs. Hendricks and O'Keefe (2002) report on the auxiliary power demand of semi-trucks for local-haul, representing urban and suburban driving, and line-haul, which represents mostly highway driving. The average value for the different driving conditions is 9.425 kW [103]. A 2012 report by the National Research Council states an auxiliary power value of approximately 14.9 kW for the USA market [101]. In this model, 9.425 kW is assumed for the auxiliary power consumption of semi-trucks. The auxiliary power values for the other modes are calculated based on the ratios of their GVWR. The auxiliary power values for the different modes are shown in Table 15.

The drivetrain and recuperation efficiencies are taken to be the same as for buses, as are the electric share ratios for PHEVs and REEVs.

Table 15: Parameters for trucks

				c_a $(-)$			
Mode	GVWR (kg)	Auxiliary power (kW)	A_f (m^2)	2020	2030	2040	2050
Small truck	7500	1.77	3.90	0.65	0.6	0.55	0.5
Medium truck	12000	2.83	4.90	0.65	0.6	0.55	0.5
Large truck	26000	6.13	7.93	0.65	0.6	0.55	0.5
Semi-truck	40000	9.425	8.38	0.65	0.6	0.55	0.5

The default average occupancy rate for small and medium trucks is 32%, a large truck is 35%, and a semi-truck is 45% [99].

4.1.5. Validation

In this section, the model results are compared with data from literature and real vehicles to confirm the model's validity. One specific mode from each type of vehicle is chosen for this verification. ICEV, FCEV, and BEV drivetrains are compared with literature and actual vehicle data for the chosen modes.

Figure 9 shows the ICEV-g, FCEV, and BEV energy demands predicted by the model compared to energy demand data reported for various vehicle models by their manufacturers.

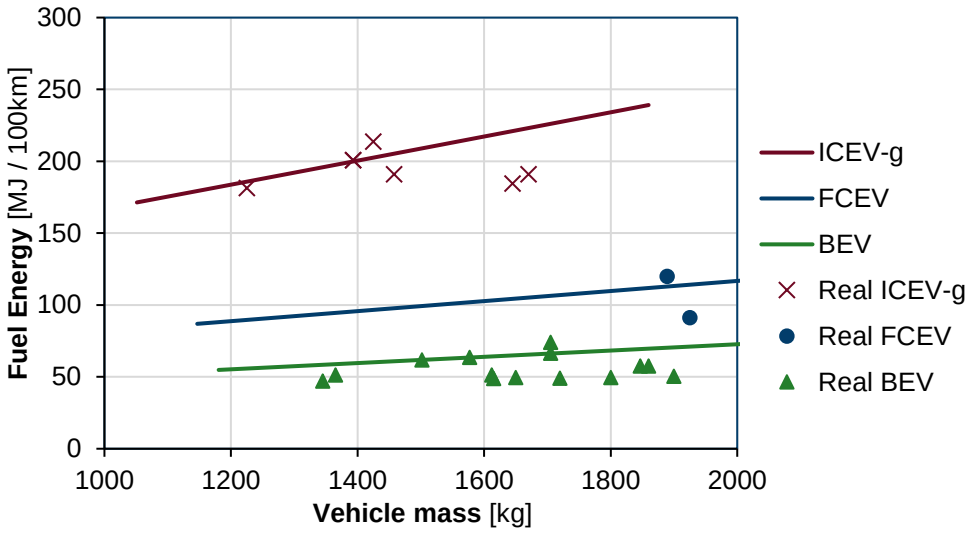

Figure 9: Comparison of real and model energy demand for medium cars for different vehicle mass. The solid lines represent model results.

As can be seen from Figure 9, the model results agree well with reported values for real vehicles in the market. The reported data are for WLTP, which does not consider HVAC's effects during the testing [104]. Therefore, the model results are little on the upper range of real-world values, but it is still within the range.

Next, the results for buses are validated using data reported for current vehicles in the literature. A medium bus is chosen to represent the bus segment due to its prominence. Figure 10 shows the model results compared with the data from the literature.

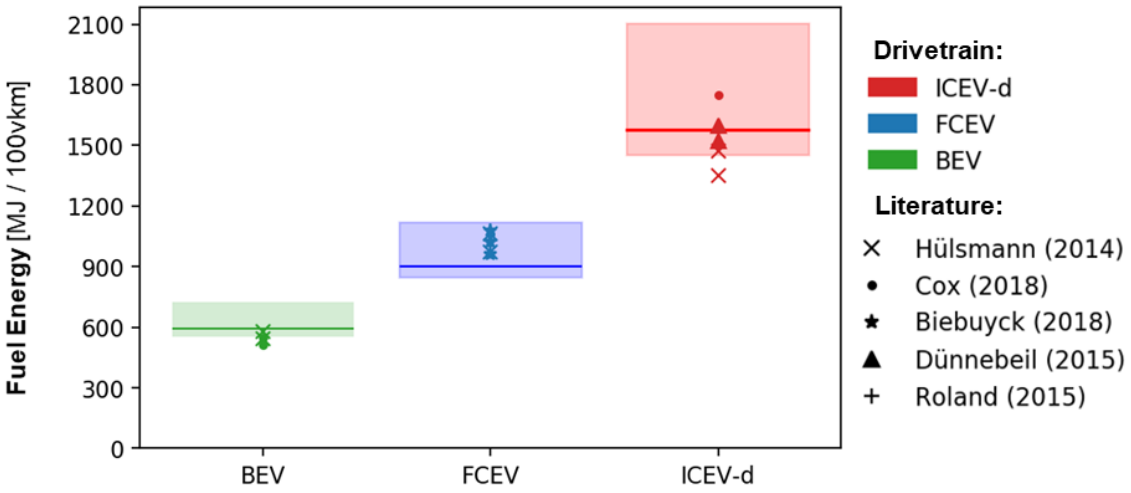

Figure 10: Model vs. Literature energy demand for medium buses [105], [72], [106]. *The solid lines represent the fuel energy demand for the average occupancy rate. The shaded area represents the energy demand for varying occupancy rates between 0% and 100%, according to the model.*

In Figure 10, ICEV-d, FCEV, and BEV drivetrains are again chosen for their importance. The range of values shown by the shaded region represents the energy demand for different occupancy rates. The lowest energy demand represents an occupancy rate of 0%, the highest represents a 100% occupancy rate, while the solid line represents the energy demand for the average occupancy rate in Germany. As can be noted, the results from the model match well with the literature values. The lower values for some of the ICEV-d buses are due to the inclusion of regenerative braking.

Finally, the model results for trucks are compared with current results from the literature. The results for ICEV-d, FCEV, and BEV drivetrain of a large truck are chosen for the validation. Figure 11 shows the model results compared with the literature data.

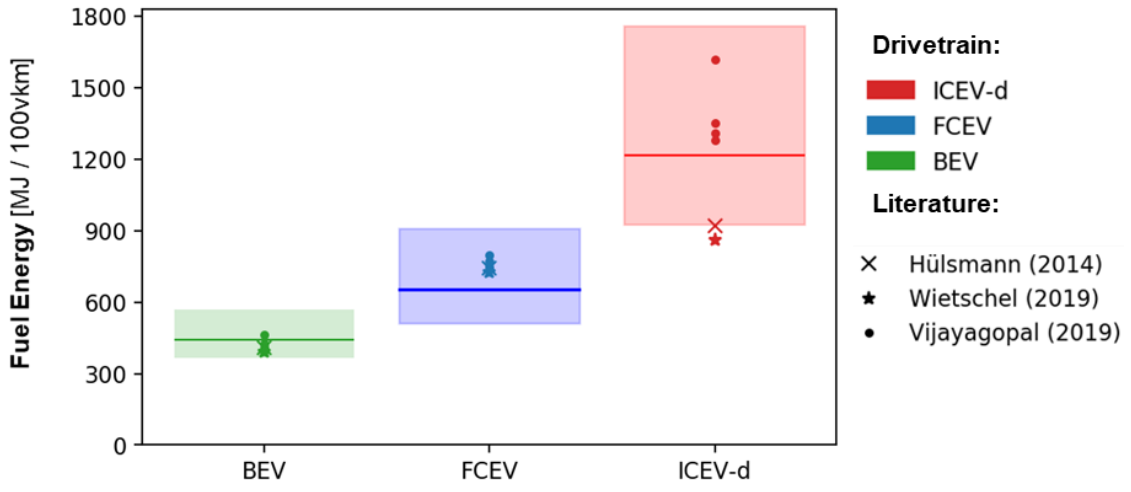

Figure 11: Model vs. Literature energy demand for large trucks [105], [107], [108]. *The solid lines represent the fuel energy demand for the average occupancy rate. The shaded area represents the energy demand for varying occupancy rates between 0% and 100%, according to the model.*

The shaded regions in Figure 11 represent the energy demands for 0% to 100% occupancy rates for the large truck. As is evident, the model results again closely resemble data from the literature. Therefore, it can be concluded that the model results are valid.

Interestingly, Figure 10 and Figure 11 show that the variation in energy demand for BEV is less than those for ICEV-d, despite having the same total cargo capacity. Two major factors cause this. First of all, BEV has a regenerative braking system, which recuperates a significant portion of the vehicle's kinetic energy. Thus, the total energy used is less dependent on the vehicle's total laden mass compared to an ICEV-d. Secondly, due to the lower drivetrain efficiencies for ICEV-d, each additional kilogram of cargo requires a higher amount of fuel energy compared to a BEV. FCEV drivetrain efficiency lies within that of ICEV-d and BEV, as does its fuel energy variation.

This validation process proves that the on-road modes' model results are valid compared to the current model and literature data.

4.2. Off-road Transport Modes

In this section, all the off-road modes are discussed, and the respective models are described.

4.2.1. Airplanes

In this section, the model for the energy demand for airplanes is discussed. Conventional fixed-wing aircraft (airplane) are usually classified according to their intended flight distance. Although different airlines and organizations use different definitions, Eurocontrol defines flights shorter than 1500km as short-haul, flights between 1500km and 4000km as medium-haul, and flights longer than 4000km as long-haul [109]. Airplanes are further classified according to the size of the fuselage into wide-body (two-aisle) and narrow-body (single-aisle) [110]

Currently, there are two types of engines commonly used in commercial aviation; turboprop and turbofan. Among these, turbofans are the most common and are used by most medium and long-haul aircraft. Turboprops are usually used by small short-haul aircraft. Although turboprops can consume up to 40% less fuel than an equivalent turbofan engine, their slower cruising speeds make them unfit for the high travel speeds expected by travelers [111].

The fuel consumption for any flight can be divided into two parts of the flight, landing/take-off (LTO) and cruise. International Civil Aviation Organization (ICAO) defines LTO as part of the flight that takes place below an altitude of 3000 feet (1000 m), which includes taxi-in and taxi-out, take-off, climb-out, approach, landing. Cruise is defined as all the activities that take place above an altitude of 3000 feet (1000 m) and includes climbing to cruise altitude, cruise, and descending from cruise altitude [35].

For airplanes, the flight distance has a significant impact on fuel energy consumption because it carries its fuel supply, which constitutes a significant proportion of the airplane's total laden mass. Long-hauls tend to have

lower seat density, as passenger comfort over longer flights requires larger seats and other amenities. Long-hauls also have higher weights due to larger passenger baggage, cargo, crew, and fuel, leading to higher fuel use. This can be seen in Figure 12, which shows the qualitative total fuel burn versus flight distance data for an exemplary commercial jet model [35]. The significant increase in fuel burn for flight distances longer than a specific range makes this plane unsuitable for the higher range both due to emissions and fuel-related expenses.

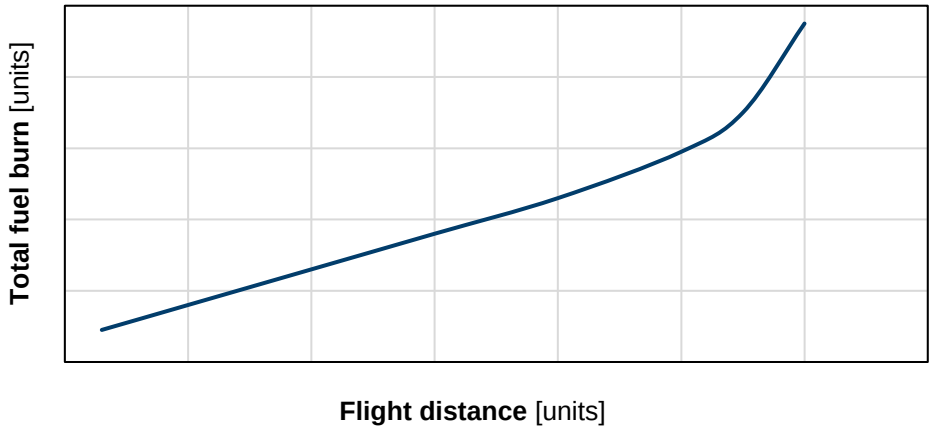

Figure 12: Total fuel burn vs. flight distance for an exemplary aircraft [35]

On the other hand, short-hauls also have high fuel use as a larger proportion of the flight is in the LTO part, which has a higher fuel burn rate. A flight distance of 1500 to 2000 nautical miles (approximately 2700 to 3700 km) is the most fuel-efficient flight distance for the average passenger airline [34]. These facts lead to a "bathtub" curve when per passenger fuel demand is plotted against the flight distance, as done in Figure 13 [34].

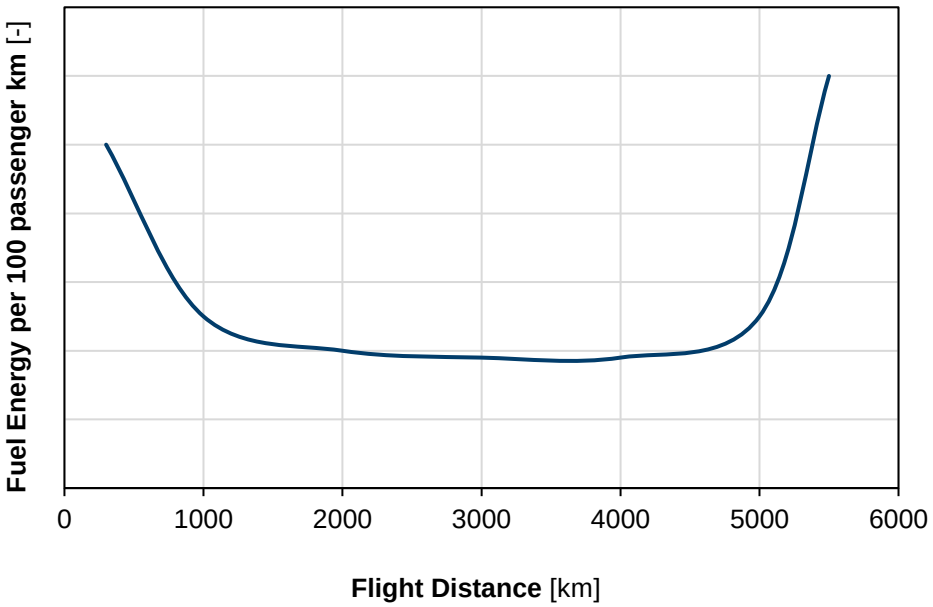

Figure 13: An exemplary "bathtub" curve showing aircraft fuel consumption vs. flight distance [34]

Figure 13 shows the qualitative “bathtub” plot of an exemplary passenger aircraft. Depending on the aircraft model and its intended designed range, the plot will have different values, but the shape remains similar to that of a bathtub.

Although air cargo constitutes only a small fraction of the total freight transport market, by weight [112], it is responsible for 35% of global trade by value [113], making it a vital freight transport mode. For perishable and other time-sensitive international cargo, there is no alternative for air cargo. This has recently been exemplified by the rise in demand for medical supplies and personal protection equipment in the wake of the COVID-19 pandemic [113].

The International Air Transport Association reports that, as of April 2020, the global air cargo demand fell by 27.7% while the capacity fell by 42%, compared to 2019. This is mainly due to the COVID-19 pandemic related sharp decline in passenger airlines, which also carry cargo as belly cargo. Thus, global belly cargo capacity declined drastically [114]. This massive imbalance of demand and supply has sent airlines scrambling to meet the demand. Passenger airlines are converting passenger airplanes to carry cargo while air cargo carriers are taking idled airplanes from storage to meet the demand [113]. Therefore, the model must include the energy demand for the critical mode of air cargo.

Due to the complex physics of aircraft flight, a detailed physics model similar to the one used for on-road vehicles is not possible. Therefore, a different approach is considered for the aviation fuel demand model.

Firstly the German aviation industry must be better understood. German aviation is the second largest in Europe, by the number of seats available [115]. Analyzing the market shares of the different players in the German aviation industry shows that Lufthansa German Airlines has the largest market share. Lufthansa, along with its subsidiary low-cost airlines under the umbrella of Lufthansa Group, had 87.1 % of the German aviation market as of 2018 [116].

Therefore, the next step involved analyzing the fleet composition of passenger aircraft in Lufthansa Group, which includes Lufthansa German Airlines and regional airlines, SWISS, Edelweiss, Austrian Airlines, Eurowings, Brussels Airlines, and Germanwings [117]. As of the end of the year 2019, the passenger aircraft fleet of Lufthansa Group included 744 aircraft. The aircraft models in the fleet of Lufthansa Group are shown in Table 20, in Appendix C [117].

The fleet composition for the entire Lufthansa Group is considered to increase the variation of the aircraft models considered in the aviation fuel demand model. In addition to the aircraft models mentioned above, other widely-used models in the industry are also considered to increase the fuel demand results' robustness.

The Aviation Emissions Calculator (AEC) accompanying the EMEP/EEA air pollutant emission inventory guidebook is next used. The AEC provides the fuel burnt and emissions data for different aircraft models and varying flight distances. The engines associated with each aircraft model in the AEC is the most common engine used for that model for the year 2015 [118].

The AEC is then used to find out the fuel burned by the selected aircraft models for different flight distances. The AEC also provides the fuel burned during the LTO separately. It provides two estimates for the LTO fuel burn, one from the ICAO and one for the average busy European airport. The ICAO values are chosen to be on the safe side, as these are slightly higher values. The LTO fuel burn is then added to the Cruise fuel burn to get the total fuel burn for the given flight distance and aircraft model. It is assumed that the aircraft is using Jet A-1 fuel [119]. The different aircraft models' average seating capacity is found from various sources, including airlines and aircraft manufacturers. These seating capacity values, along with the flight distances, are then used to calculate the fuel demand per 100 seat km. The freight capacity for the different airplane models is based on a literature review. This is used to calculate the fuel demand per tonne of cargo carried over the flight distance. The seating and freight capacity for individual airplane models are shown in Table 21 in Appendix C. Figure 14 shows the total seating and cargo capacity as a function of the flight distance used in the model.

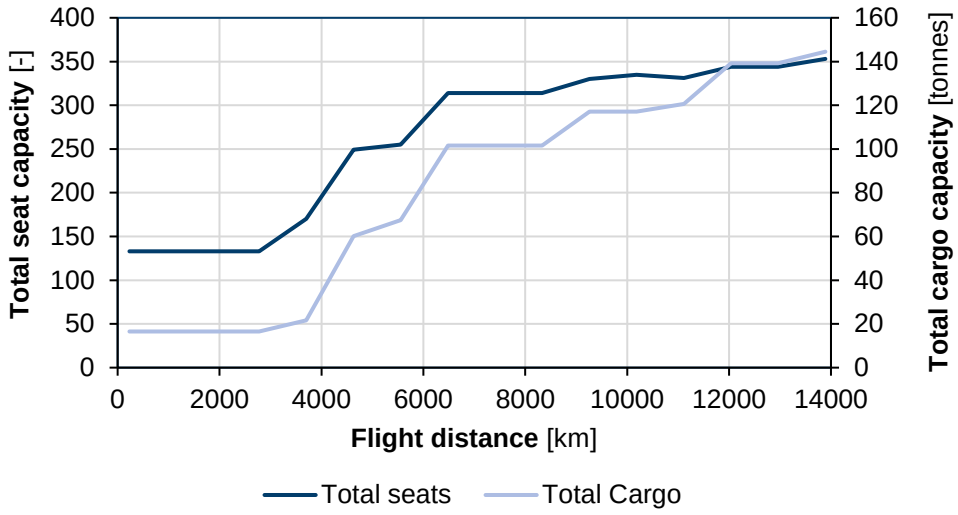

Figure 14: Seating and Cargo capacity as a function of flight distance. The seating and cargo capacity for individual airplane models are shown in Table 21, Appendix C.

For each discrete flight distance, multiple possible aircraft models are chosen. The average fuel consumption of these aircraft models is then assigned to that flight distance. Rolling averages are used to remove sudden changes in values arising from the use of discrete data points from the AEC. Because the fleet data is taken for the end of the year 2019, the calculated data can be assumed for 2020. The fuel energy demand per 100 seat km as a function of the flight distance is shown in Figure 15.

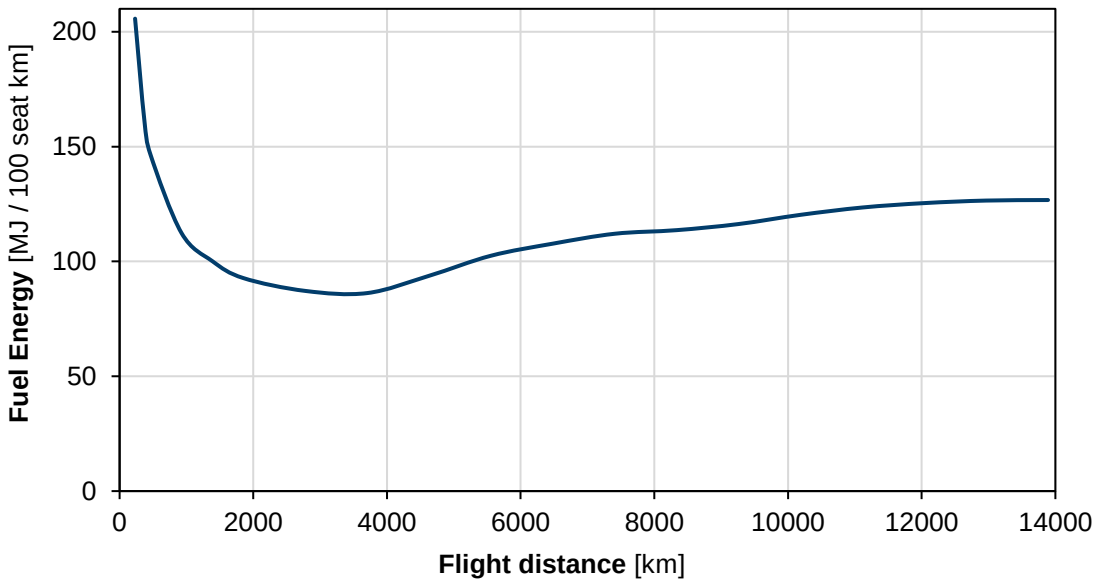

Figure 15: Fuel energy demand per 100 seat km as a function of the flight distance. The fuel energy and flight distance for individual airplane models is based on AEC [118]

Since the model needs to predict energy demand up to 2050, future aviation fuel efficiency improvement must be taken into account. Kharina and Rutherford (2015) report on the fuel efficiency trends in an International Council on Clean Transportation white paper. This report predicts the future energy efficiency improvements up to the year 2045, based on historical data. Analyzing the future trend, it can be seen that the energy efficiency improvement per decade is approximately 10%, from 2010 to 2040 [37]. The same 10% improvement is used to extrapolate the data up to the year 2050. Thus, in the aviation energy model, a 10% efficiency improvement per decade is assumed from 2020 to 2050. The fuel energy demand values are then available for each decade from 2020 to 2050 and for discrete flight distances. The model then uses bilinear interpolation to calculate the fuel energy demand for the given year and flight distance.

Figure 16 shows the change in airplane fuel consumption values from 1960 to 2045. The average value for 1968 is set to 100. The real-world values for single-aisle (SA) and small twin-aisle (STA) are shown along with their average trendline [37].

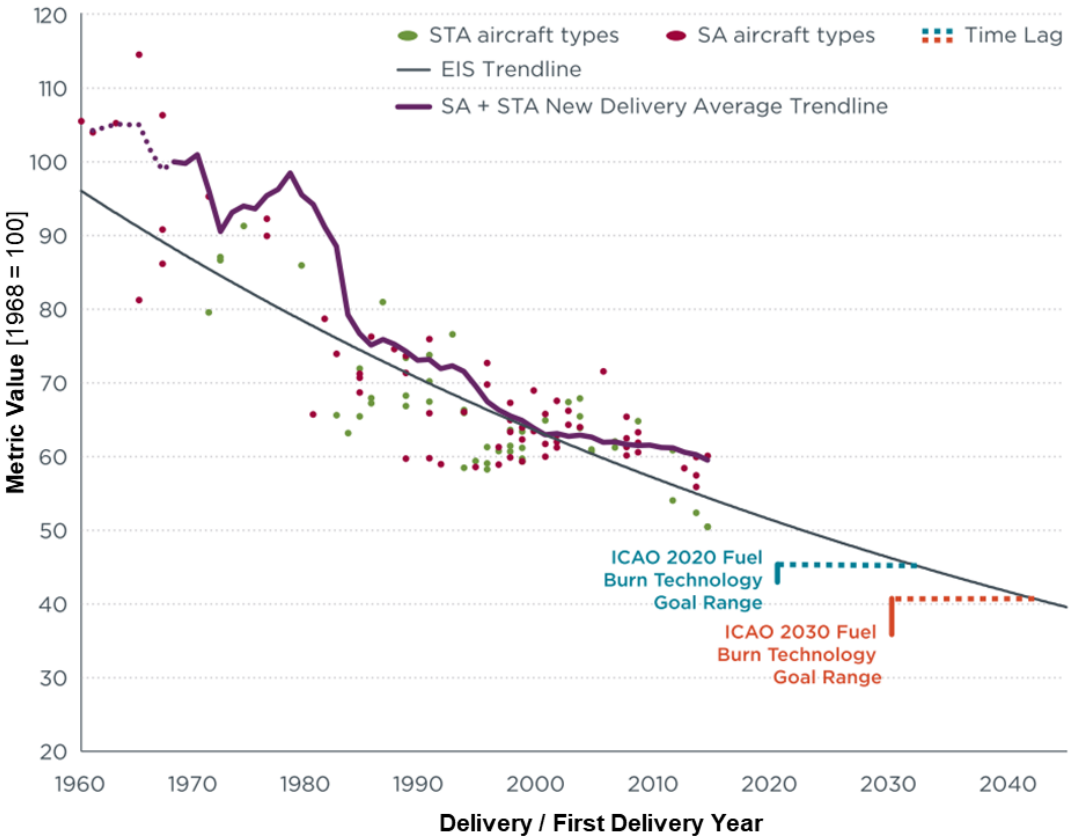

Figure 16: New single-aisle and small twin-aisle jet aircraft metric value vs. ICAO fuel burn technology goals [37]

Figure 16 also shows the trendline of the different airplane models based on the year they enter into service (EIS). It shows that there is a time lag between the goals set by ICAO and the trends in energy demand for real airplane models.

The 10% energy efficiency improvement can be justified using various arguments. A 2019 European Environment Agency report on aviation states that energy consumption per passenger kilometer has decreased by 19% between the years 2005 and 2014. Furthermore, it also forecasts that energy consumption will decrease by between 43% and 46% until 2035 [120]. These values are more optimistic than the ones used in the aviation model.

Furthermore, both bottom-up and top-down effects on airlines are causing the fleetwide efficiencies to decrease. One of the major bottom-up effects is that the passengers are increasingly aware of the carbon emissions related to taking a flight over other transport modes. Increasing social media influence of climate activists is also causing people who themselves might not be too concerned about environmental issues to avoid flights if possible. There is even a term for this called “flight shaming.” This trend and the effects of new high-speed train connections have especially affected the German short-haul market [121]. On the other hand, top-down factors influencing aviation fuel efficiency include policy implementation. EUROCONTROL has set a target to be climate neutral by 2050. In this regard, it has identified five critical topics for the industry to prioritize [122]:

- support widespread use of, and smooth transition to, alternative sustainable aviation fuels (SAF)
- develop high efficiency, short-haul, large capacity aircraft
- renew the entire fleet by 2050, and only fly wholly or partially electric aircraft for short-haul and long-hauls that only use SAF
- improve the European air traffic management network and provide shorter and better routes
- facilitate electrification of short-haul aircraft by improving battery technology and hybridization

Increased use of SAF can further increase the potential fuel efficiency. In studies, SAF has shown higher energy densities than conventional jet fuel. Furthermore, SAF results in increased fuel efficiency, up to 3%, potentially improving payload conditions or extending flight range [123].

Due to the recent unprecedented drop in passenger demand around the world caused by COVID-19, airlines are being forced to ground a large portion of their fleet. In turn, this has led airlines to ground their least efficient airplanes first. Airlines across the world have also taken this opportunity to retire aging aircraft, which usually are the ones with higher fuel consumption. Lufthansa has grounded it Airbus A380s, which is one of the aircraft in its fleet with the highest fuel consumption. Airlines are also retiring other quad-engine airplanes, intending to replace them with new generation twin-engine airplanes with better fuel efficiencies [124]. These effects combined make the assumed 10% efficiency improvement per decade used in the model a conservative estimate.

The default occupancy rate for all passenger airplanes is taken as 82% [125]. The default occupancy rate for freight aircraft is assumed to be the same. The default flight distance for all national flights is taken to be 325 km [126], and that for all international flights is taken to be 2230 km [127].

4.2.2. Drones

A flying car has been the dream for science fiction enthusiasts as well as commuters stuck in Urban traffic, at the same time being the topic of nightmares for many who dared to bring one to the market. Making a fixed or folding wing vehicle both light and aerodynamic enough to fly as well as sturdy enough to take the rigors of the road has been so far impractical, to say the least. From Curtiss Autoplane to Taylor Aerocar, many have tried to bring a mass-produced flying car to market but to no avail. However, recent developments in drone technology promise to provide some of the features long promised by flying car proponents. The ability of vertical take-off and landing (VTOL) combined with quieter electric motors and autonomous flight leads to limitless potential utility [128].

Japan, home to some of the best public transportation networks in the world as well as large urban areas prone to congestions, is pioneering the adaption of passenger drones. In August 2020, Skydrive, a Toyota backed startup, conducted a public test flight of their prototype flying car. The company plans to have flying vehicles carrying passengers within the next three years [129]. Numerous reputable companies are betting on a future with electric drones carrying passengers through city skylines across the world. Aircraft giants like Airbus and

Boeing, automakers like Toyota, Hyundai, and Porsche are all working on passenger drones. Uber is planning to make electric drone ridesharing services available in 2023 [128].

The potential of drones for freight transport can not be underestimated, especially for e-tailers where drones can significantly improve the last-mile delivery costs and emissions, often a significant portion of the entire supply chain. Stolaroff et al. (2018) analyzed the potential lifecycle carbon emissions of package delivery by small drones compared to traditional means of using delivery trucks and found it lower for the drones. Furthermore, small drones fared even better in most cases than using electric trucks for delivery [130]. Amazon, being the biggest e-tailer, has invested significant resources in developing drone technology for deliveries. It was recently awarded the Federal Aviation Administration approval for its autonomous aircraft systems [131].

Morgan Stanley Research estimates that the autonomous flying aircraft's market valuation will reach $1.5 trillion by 2040. It will be due to the culmination of technology improvements in multiple different sectors, including batteries, which is often a major limiting factor in current designs [132]. Thus, although drones are not a significant consumer of energy in the current transport fleet, it is expected to be a substantial share of the future transport fleet. Therefore, the addition of an energy model for electric drones is vital to make the model future-proof.

Similar to the airplane, it is challenging to implement a physics-based model for drones due to the complexity of the model needed. Thus energy consumption data from the literature will be used to predict the energy demand for drone transportation.

Jia Xu (2017) models the energy demand of different sized freight drones. The energy demand for the small drone, the 2016 Amazon Prime Air Drone with a maximum capacity of 2.3 kg, is used to model the energy demands for last-mile delivery drones. This model is chosen because of the dominance of Amazon in the global retail e-commerce sector. Figure 17 shows the energy demand for the delivery as a function of the flight distance [40].

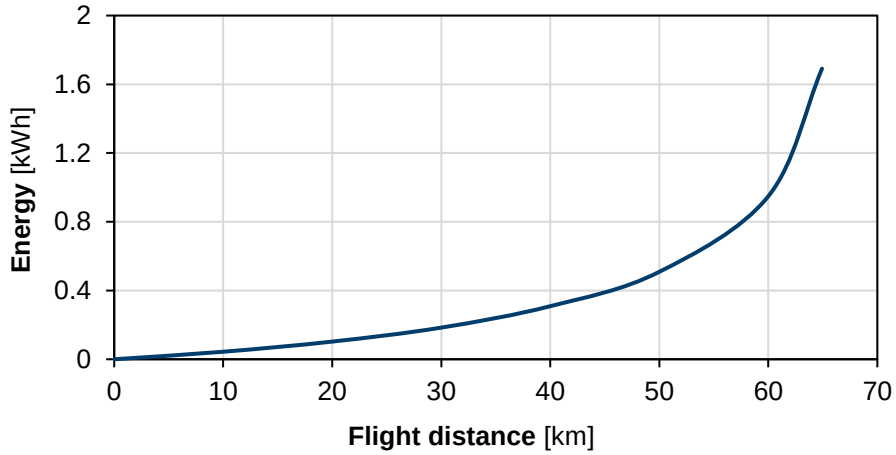

Figure 17: Freight drones energy demand for Amazon Prime Drone with a maximum capacity of 2.3kg [40]

Bauhaus Luftfahrt reports the energy demand for the two major passenger drone configurations; multicopter and lift+cruise configuration. In a multicopter configuration, large vertical axis rotors are responsible for VTOL as well as cruise flight. In a lift+cruise configuration, a set of vertically arranged rotors still provide the VTOL function; however, separate horizontal axis rotors along with fixed wings provide the lift in cruise flight. The results show that multicopter drones require less energy, although its flight range is limited compared to lift+cruise drones. In longer flights, the benefits of lift+cruise configuration are attainable in terms of lower energy demands. Figure 18 shows the energy demand per passenger-kilometer for different flight distances for drones with a maximum capacity of four passengers [41].

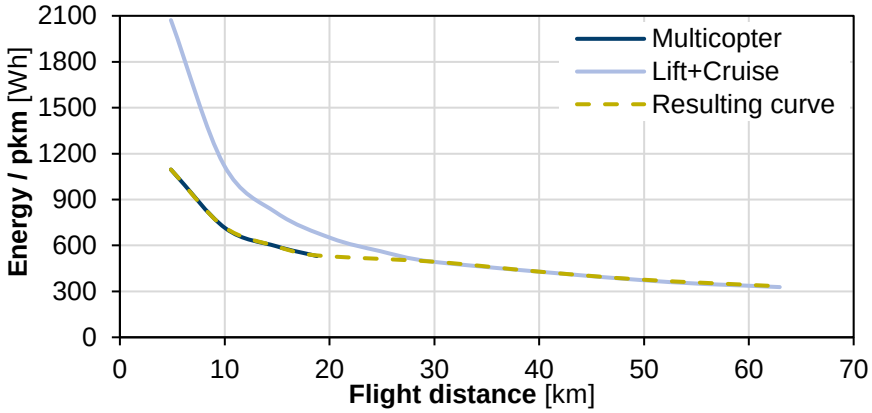

Figure 18: Passenger drones energy demand for drones with a maximum capacity of four passengers. The resulting curve is used in the model [41]

Figure 18 also shows the resulting curve used to model the energy demand for passenger drones.

It is assumed that the configuration with the lowest energy demand will be used for the given flight distance. The default occupancy rate for all drones is assumed to be the same as that for airplanes, at 82% [125].

4.2.3. Trains

Trains are an important mode of transport. Rail transportation was responsible for 4.5% of the total transport sector carbon emissions for the year 2014 in Germany [33]. It is also one of the most energy-efficient means of transport. Globally it accounts for only 3% of the total transport energy demand while providing 9% of all passenger transportation and 7% of all freight movement. International Energy Association (IEA) suggests more train travel can help meet its targets for a sustainable development scenario. Urban rail has a high capacity to move large volumes of passengers, reduce congestion, save valuable urban space, and positively affect air quality. Highspeed rail is the only possible environmentally friendly competitor for short-haul airlines. Despite the advantages, railways are not a common means of transport globally. 90% of all passenger rail activity is registered in China, the EU, Japan, India, and Russia. One of the most significant barriers for larger market penetration of rail is the large initial investment required compared to other forms of transport [133].

The important types of rail within Germany include InterCity Express, which are the fastest option for long distances and are 100% electric; InterCity, long-distance trains connecting cities; Regional Express, which

connects regional towns with local cities; Regionalbahn, which connects regional towns with more frequent stops; S-Bahn, commuter rail services for metropolitan areas; and, trams and underground commuter trains for intracity travel [134]. The railway model considers four different modes

- Trams: trams and underground intracity commuter trains
- Short-distance train: all regional trains and covers S-Bahn, Regionalbahn, and Regional Express
- Long-distance train: InterCity and InterCity Express
- Freight train: all freight trains

Different drivetrains are considered for the four modes mentioned above. All trams and long-distance trains are considered electrified and are supplied with overhead (catenary) lines. Along with using catenary lines, short-distance trains and freight trains can also be powered by diesel, compressed natural gas, or liquified natural gas engines, as well as battery and fuel-cell.

Although a detailed physics model for rail is not as challenging to implement as for a plane model, the lack of standardized driving cycles meant a different approach had to be taken. In this regard, it is decided to follow a process where data is collected from literature for the various rail types. Combined with future development scenarios, a complete passenger and freight train energy demand model until 2050 is developed.

For the trams, Kuminek (2013) reports the energy consumption values for electric catenary trams [135]. The values are assumed to be for the year 2010, and the average of the values for the different routes are taken.

Energy demands for electric and diesel short-distance trains can be found from the Global Emissions Model for integrated Systems (GEMIS) database [136]. The energy demand for ICEV-lng and ICEV-cng is assumed to be the same as that for ICEV-d like done for the other modes. The energy demand for BEV and OH-wire are assumed to be equal. Energy demand for FCEV is calculated using the data for ICEV-d along with the relevant drivetrain efficiencies reported by Klebsch et al. (2020) [137]

The data for long-distance trains is taken from Deutsche Bahn's Integrated Report [138]

The energy demands for freight trains are taken from the GEMIS database for the diesel and electric drivetrains [136]. The FCEV drivetrain data is taken from a 2018 report by the Deutsche Energie-Agentur [139].

Zimmer et al. (2016) report the future development of drivetrain efficiencies for trains, according to the Transport Emission Model. From 2010 to 2030, the drivetrain efficiency for electric drivetrains increases by 20% while diesel, and other drivetrains, show an improvement of 10%. From 2030 to 2050, all drivetrains show an improvement of 10% [140]. These assumptions are applied to all train modes. The study also provides data for the average occupancy rates and the total vehicle capacities for the different train modes [140].

The default occupancy rates for trams is 18%, short-distance trains are 21%, and that for freight trains is 38% [140]. The default occupancy rate for the long-distance trains is taken as 56%, which is the average occupancy

rate for 2018, according to Deutsche Bahn [138]. Thus the occupancy rate increases with an increase in the travel distance.

4.2.4. Ships

The importance of ships in global freight transport can not be understated. Shipping accounts for about 75% of global freight transportation, and it does so, being the most energy-efficient means of carrying cargo [141]. Inland waterway transport is responsible for 11% of Germany's cargo transportation [142].

International shipping accounted for 2% of global energy-related CO2 emissions for the year 2019. CO2 emissions from shipping have increased drastically in the last decade due to higher volumes of international shipping. Therefore, to meet the Paris Agreement, the International Maritime Organisation (IMO) has adopted a strategy to reduce GHG emissions from international shipping. The strategy, adopted in 2018, aims to reduce GHG emissions by at least 50% until 2050 and attempt to stop it altogether after that. The strategy also aims at decreasing the carbon intensity in international shipping by at least 40% by 2030 and 70% by 2050. These values are with respect to a 2008 baseline. To reach these targets, energy efficiency improvements alone will not be sufficient. Extended use of low- and zero-carbon fuels will be required [141].

One of the major steps IMO has taken is implementing regulation IMO2020. This regulation requires all ships to use fuel with a maximum Sulphur content of 0.5% as of January 2020. This is a significant step towards making the shipping industry more environmentally friendly as the previous maximum Sulphur content was 3.5% [143]. This regulation is likely to force international shipping companies to choose between using more expensive low Sulphur fuel, higher running costs, or low carbon fuels like liquefied natural gas (LNG), resulting in higher initial investment to change the engines [144].

The CO_2 emissions per energy for LNG are about 25% lower than those of diesel, combined with the fact that the engine efficiencies for LNG and diesel are almost equal, resulting in lower carbon intensity for ships using LNG [145].

The Energy Efficiency Design Index (EEDI) is the only IMO regulation that promotes greater efficiency in shipping. It warrants an annual efficiency improvement of approximately 1.5% for all new fleet from 2015 to 2025. This is lower than the historic improvement value between 2000 and 2017 of 1.6%. This regulation is meant to prevent relapse in efficiency improvements, but some organizations are asking for stricter mandates [141].

Similar to trains and aviation models, the shipping model is based on literature data. The energy demand per tonne-kilometer for international shipping is taken from IEA. Starting from 2020 values, it is assumed that the average energy efficiency improvement will be 2% until 2050. Although this value is higher than the 1.5% mandated by EEDI, it is still lower than the Sustainable Development Scenario outlined by the IEA [141]. These values are assumed for both diesel and LNG drivetrains, as the efficiency differences are negligible [145].

The energy demand for national shipping (inland waterway transport) is taken from Bründlinger et al. (2018) [139]. The default occupancy rate for national shipping is taken as 50% from Allekotte et al. (2019) [99]. Default occupancy for international shipping is assumed to be 80%.

5. Results and Discussions

The results obtained from the developed model are discussed in this section. Firstly, the effects of varying vehicle parameters are analyzed for different driving conditions in section 5.1. Next, the mechanical energy demand to overcome the resistances are analyzed for the different parts of the WLTC in section 5.2. A modal analysis is carried out for both passenger and freight transport modes in section 5.3. The modal analysis shows that aviation modes are often the most energy-hungry modes of transport.

Section 5.4 shows an analysis of the energy consumption of different drivetrains for a medium car. It shows that the electrified drivetrains often have the best energy efficiencies. Section 5.5 further investigates the effects of electrification on the energy demand of a vehicle.

Section 5.6 analyzes the effects of the driving environment on energy demand. It analyzes trucks for various uses, followed by the impact of ambient temperatures on buses' energy demand. Finally, the effects of road gradients are studied for different drivetrains in a medium car.

The outlook to the future for both passenger and freight modes is accessed in section 5.7. It also compares the results from the model with other studies. Section 5.8 analyzes the energy demand for last-mile delivery using a drone versus that using an LCV.

5.1. Basic Analysis: Parameter variation

In this section, the effects of changing certain physical parameters on the fuel energy demand of a medium car are analyzed. The parameters chosen to be varied are the vehicle's mass, aerodynamic properties, and rolling resistance. Figure 19 shows the effects of varying the parameters for an ICEV-g and a BEV medium car.

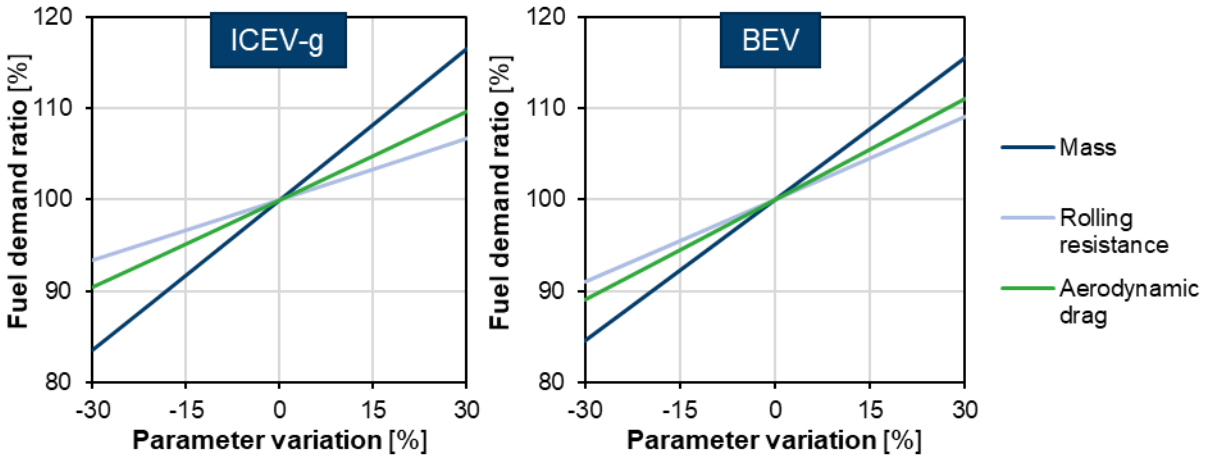

Figure 19: Effects of parameter variation on fuel demand over entire WLTC for ICEV-g (left) and BEV (right)

Figure 19 shows the impact on fuel demand for the entire WLTC driving cycle. Changing the vehicle's mass has the largest potential impact on the fuel consumption of an ICEV-g car. A 10% reduction of vehicle mass reduces the fuel demand by 5.5%. Over the entire WLTC driving cycle, the relative effects of changing the rolling resistance are the least significant. The energy demand only falls by 2.2% for a 10% reduction of the rolling resistance, while aerodynamic drag results in a saving of 3.2%.

As shown in Figure 19, the different parameters' effects are similar for a BEV as for an ICVE-g car. Here again, changing the mass has the highest effect and rolling resistance the least. However, a closer inspection shows that the relative values are different. Changing the mass, 10%, has a slightly lower impact for a BEV, 5.15 %, compared to an ICEV-g, 5.5%. This is due to the effects of regenerative braking, present in a BEV car but absent from an ICEV-g car, as regenerative braking recuperates some of the energy needed to accelerate the vehicle mass.

Furthermore, Figure 19 also shows that the effects of both changes in aerodynamic drag and rolling resistance are higher for a BEV as compared to ICEV-g. One of the reasons for this is a result of regenerative braking on a BEV. As discussed in section 3.7, the presence of regenerative braking increases the energy required to overcome aerodynamic drag and rolling resistance. Therefore, as the energy demand to overcome aerodynamic drag and rolling resistances form a larger portion of the total fuel energy demand, changing the parameters also has a relatively higher impact on the final fuel energy demand.

One interesting thing to note here is that although the aerodynamic drag can be changed by changing either the car's frontal area or its aerodynamic drag coefficient, the results are the same. A combination of the two factors can also be used without any change in the results discussed here.

Next, the effects of parameter variation on the fuel demand for different driving conditions are discussed. The analysis is carried out for a BEV medium car. The chosen driving conditions are urban driving, represented by the low region of the WLTC, and highway driving, represented by the extra high region of the WLTC. Figure 20 shows the effects of parameter variation for urban and highway driving.

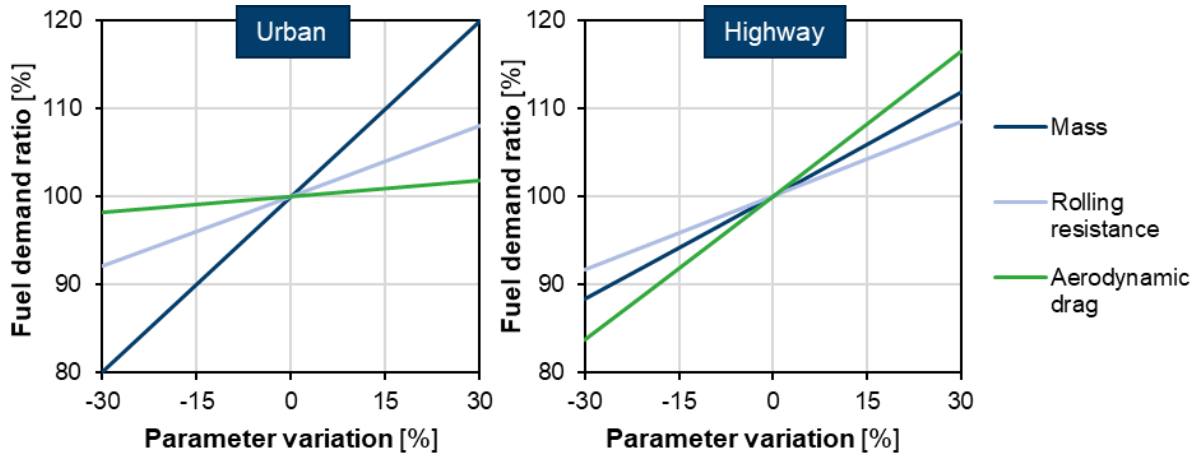

Figure 20: Effects of parameter variation on fuel demand for BEV over urban (left) and highway (right) driving scenarios

As shown in Figure 20, reducing vehicle mass has the highest effect on urban driving conditions. This is the case due to the stop-and-go driving prevalent in urban driving. This results in large energy demand to accelerate the vehicle mass. Thus reducing the vehicle mass has such a high impact on the final energy demand. If the vehicle did not have regenerative braking, the effects of changing vehicle mass on the fuel demand would be more pronounced.

Furthermore, the effects of changing the aerodynamic drag have very little impact on the final energy demand. This is because the vehicle's average speed in urban conditions is low. The aerodynamic drag force is proportional to the vehicle velocity square, equation 3.2, leading to low energy savings when the aerodynamic drag is reduced.

Figure 20 shows that changing the aerodynamic drag has the highest impact on the energy demand for highway driving conditions. This is the case because of the higher speeds in highway driving, which results in a higher proportion of the total energy demand used to overcome the aerodynamic drag. Thus improving aerodynamic drag will result in the highest savings in fuel consumption. Rolling resistance variation has the least impact on vehicle energy demand for highway driving.

5.2. Driving cycle analysis: Different parts of WLTC

This section analyzes the effects of the different parts of the WLTC on vehicle energy demand. The effects of recuperation are also considered.

To begin with, the mechanical energy demands for different parts of the WLTC are analyzed. Figure 21 shows the mechanical energy demand for the different parts of the WLTC, along with the maximum possible recuperation for a vehicle fitted with a perfect regenerative braking system. The data shown is for a BEV medium car in 2020 with default occupancy.

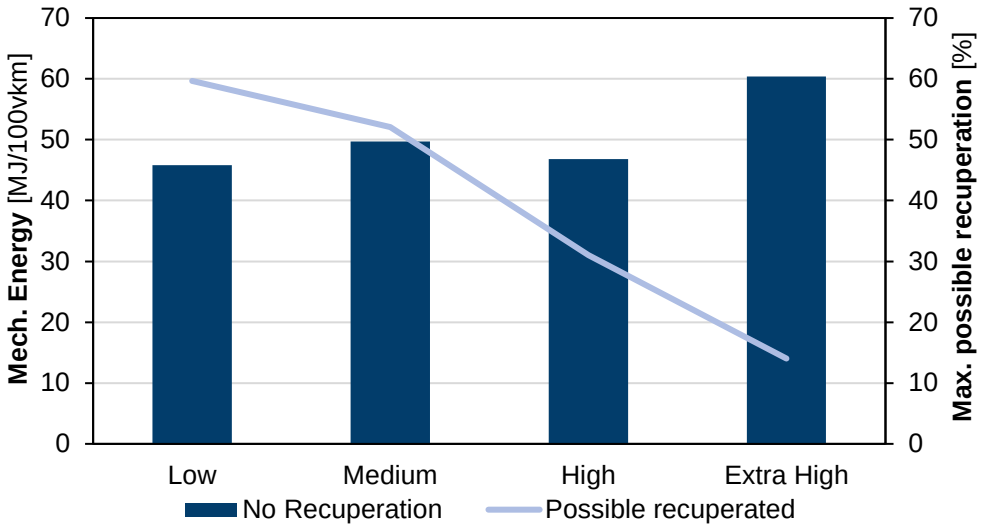

Figure 21: Mechanical energy and possible recuperation for different parts of the WLTC

Figure 21 shows that the maximum mechanical energy demand for a vehicle with no regenerative braking is in the extra high region of WLTC, representing highway driving conditions, at around 60 MJ/100vkm. The energy demands for low, medium, and high regions of WLTC are similar and fall between 45 and 50 MJ/100vkm. Looking at the maximum possible recuperation, it can be noted that highway driving provides the least opportunity for recuperation, at only 14%. Urban driving, low region, on the other hand, provides the highest possible recuperation. Almost 60% of the energy can be recuperated from urban driving using a perfect regenerative braking system. This is due to the stop-and-go traffic conditions where a large proportion of the vehicle's kinetic energy is lost due to braking for a vehicle with no recuperation. Medium and high regions also show significant energy savings when recuperation is used, at 52% and 31%, respectively.

This discussion shows that the vehicles in urban areas will get the highest benefits from a regenerative braking system. For vehicles intended mainly for highway driving, the regenerative braking system's mass and costs might need to be considered before deciding if it is justified to use one.

Next, the different types of mechanical energy demand for the different parts of the WLTC are discussed. The analysis is based on a BEV medium car in 2020 with default occupancy. The mechanical energy demand for no recuperation, 100% recuperation, and actual recuperation are discussed. Figure 22 shows the different mechanical energy demand for low, medium, high, and extra-high parts of WLTC.

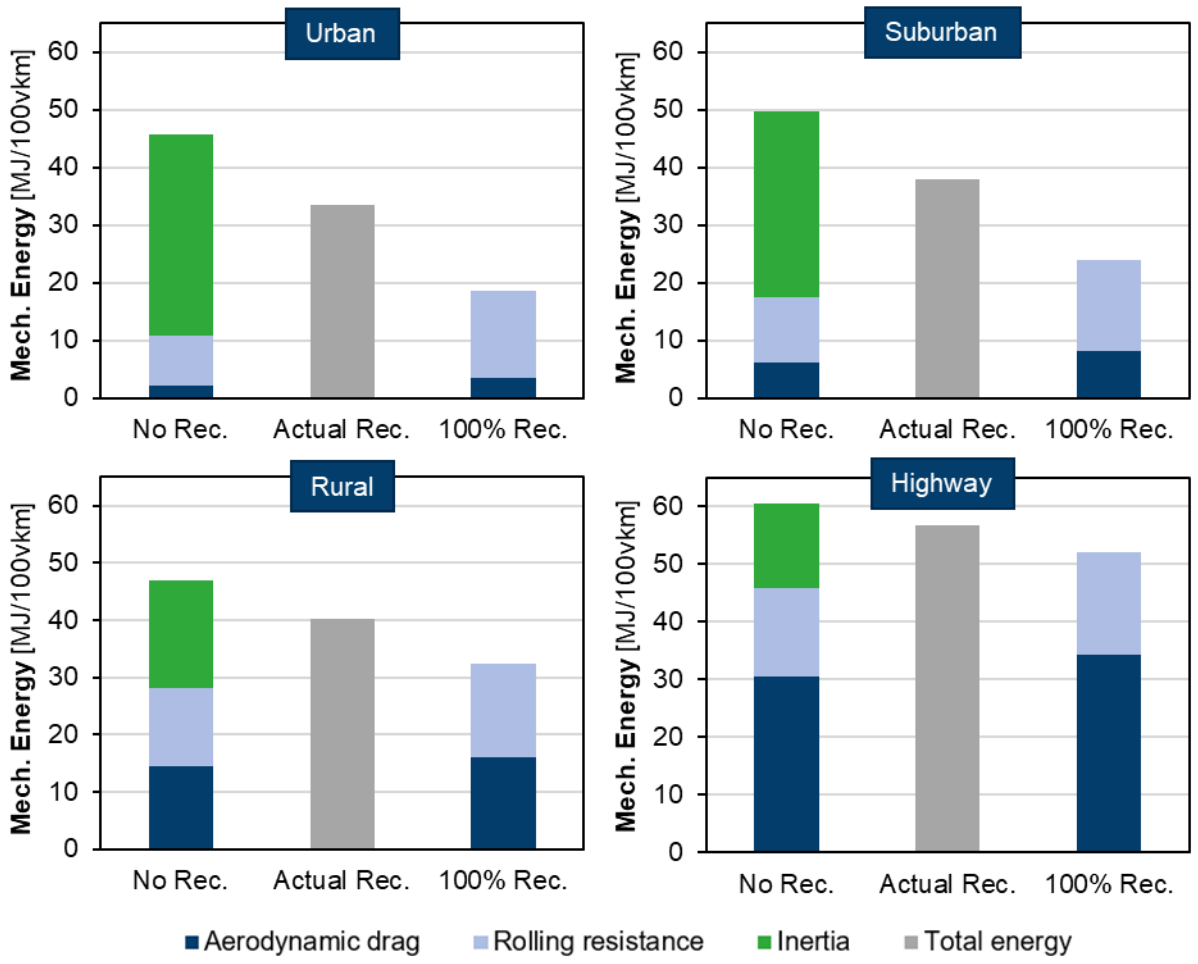

Figure 22: Mechanical energy demand for the urban region (top-left), suburban (top-right), rural (bottom-left), and highway (bottom-right) of WLTC. The actual recuperation refers to a regenerative braking system that can recuperate 45% of the total recoverable energy.

Figure 22 shows that the mechanical energy needed to overcome the aerodynamic drag increases going from low to extra-high regions, for both no recuperation and 100% recuperation scenarios. This is due to the increase in the average speed of the vehicle over the different regions. The energy needed to overcome rolling resistance also increases for both the no recuperation and 100% recuperation scenarios. However, the increase is not as significant as that for aerodynamic drag.

The energy needed to overcome inertia effects shows a large decrease going from the low region to the extra-high region for the no recuperation scenario. This is the energy that a regenerative braking system recuperates. This drastic decrease of the energy for inertial effects going from the low region, 34.9 MJ/100vkm, to the extra-high region, 14.7 MJ/100vkm, is the cause for lower maximum recuperation potential shown in Figure 21. The effects are also clear in the above figures as the total energy required for the 100% recuperation scenario increases and gets closer to the no recuperation scenario, going from the low to the extra-high regions. The middle bar represents the vehicle's actual mechanical energy demand with a realistic recuperation braking system of 45% efficiency.

To further emphasize the mechanical energy demand for the different parts of the WLTC, Figure 23 shows the different types of energy demand for all the parts of the WLTC, for no recuperation scenario, on a single figure.

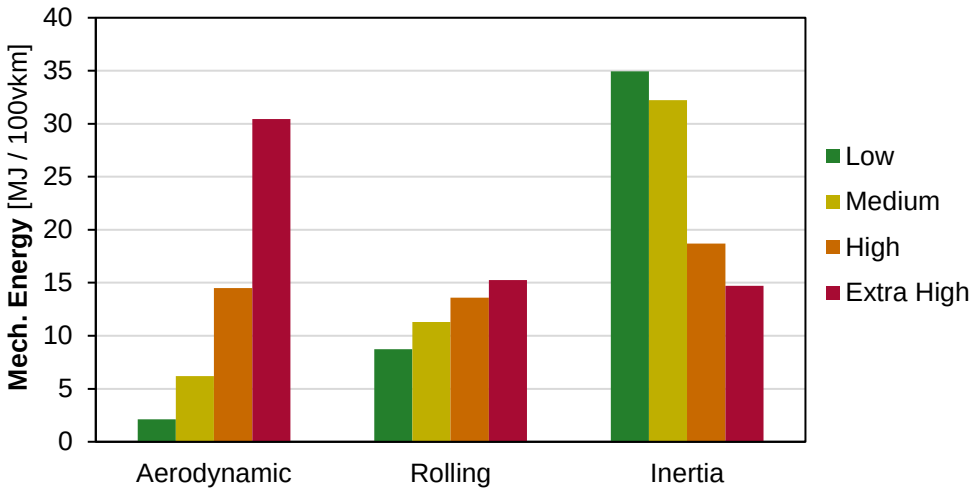

Figure 23: Mechanical energy demand of different parts of WLTC for no recuperation

Figure 23 shows that for the low region of WLTC, the energy required to overcome inertia, at around 50 MJ/100vkm, is the largest portion of the total energy. It is also the highest of the inertia energies of the different WLTC regions. The aerodynamic drag for the low region is the smallest portion of the total energy. It is also the least value of the aerodynamic drags from the different WLTC regions. The values for medium and high regions always fall in between the extremes of low and extra-high region values. The rolling resistances generally lie between their respective aerodynamic drag and inertia energies.

Figure 24 shows the same data but for the 100% recuperation scenario.

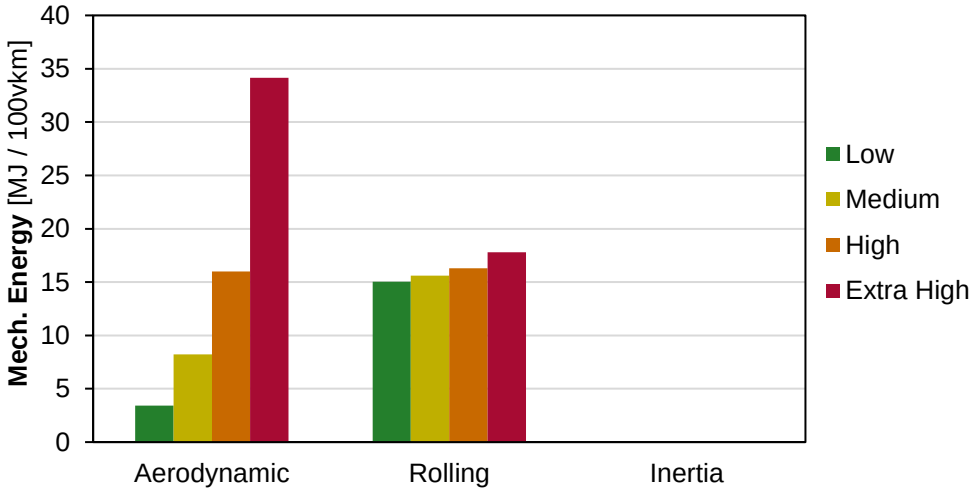

Figure 24: Mechanical energy demand of different parts of WLTC for 100% recuperation

As is evident from a comparison of Figure 23 and Figure 24, the aerodynamic drag and rolling resistance energies are higher for the 100% recuperation scenario. This effect is discussed in section 3.7. Since 100% of the inertia

energy is recuperated during the braking and cruising phases, additional energy is required to overcome the aerodynamic drag and rolling resistances during these phases. It should be noted that no energy is required to overcome the inertia effects, as a perfect regenerative braking system recuperates all the inertia energy.

It can be concluded that for vehicles intended for urban driving, regenerative braking systems are highly recommended. This is due to the high energy savings potential it brings in such driving conditions. Therefore, vehicles with an electric motor, which can be used for regeneration, are recommended for urban driving. This includes BEV, FCEV, HEV, and PHEV. For vehicles intended for highway driving, priority should be given to improving their aerodynamics, as the energy required for aerodynamic drag is the highest portion of the total energy in such conditions. Electrification is also effective in this scenario but not as much as for urban conditions.

5.3. Modal Analysis

In this section, the fuel energy demand for the different modes is discussed. The discussion is further divided into passenger and freight modes. Important drivetrains of all the different modes of transport, ICEV, FCEV, and BEV, are analyzed. ICEV-g is chosen for cars and ICEV-d for all other modes. For trains, catenary drivetrains replace BEV drivetrains.

5.3.1. Passenger modes

In this section, the fuel energy demand for the different passenger drivetrains is discussed in terms of the energy required per 100 passenger-km traveled.

Figure 25 shows the fuel demand for all short-distance passenger transport modes for varying occupancy rates. The default occupancy rates for 2020 are highlighted for each drivetrain.

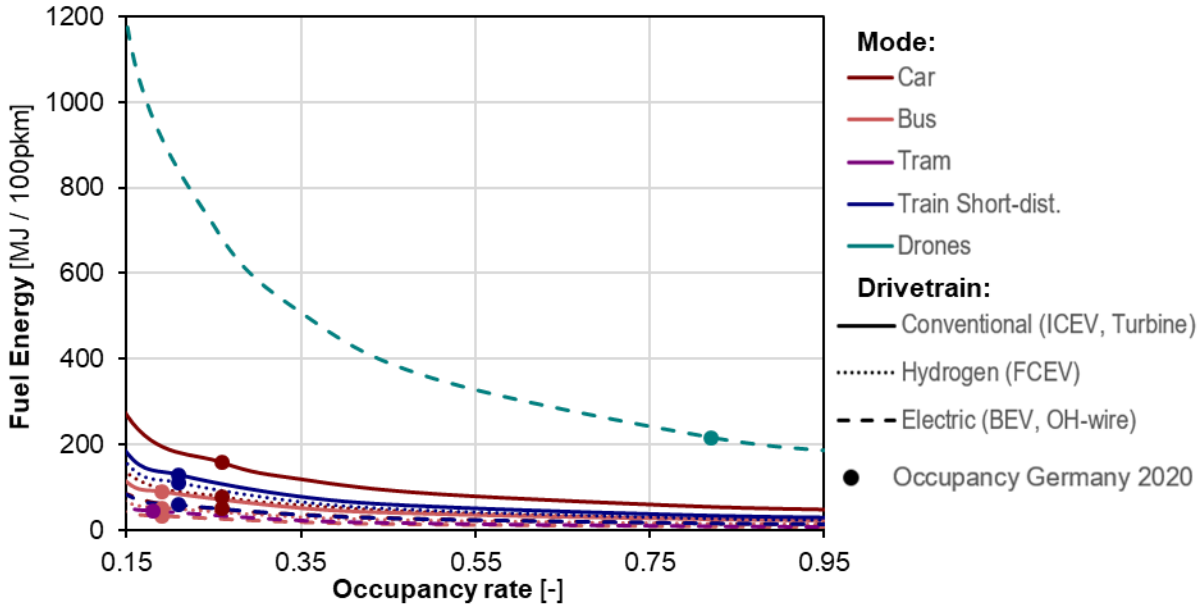

Figure 25: Fuel energy demand vs. occupancy rate for all short-distance passenger modes

As shown in Figure 25, drones have the highest energy consumption for short-distance passenger transport.

Figure 26 shows the same data in Figure 26 but zoomed in to better see the drivetrains' differences.

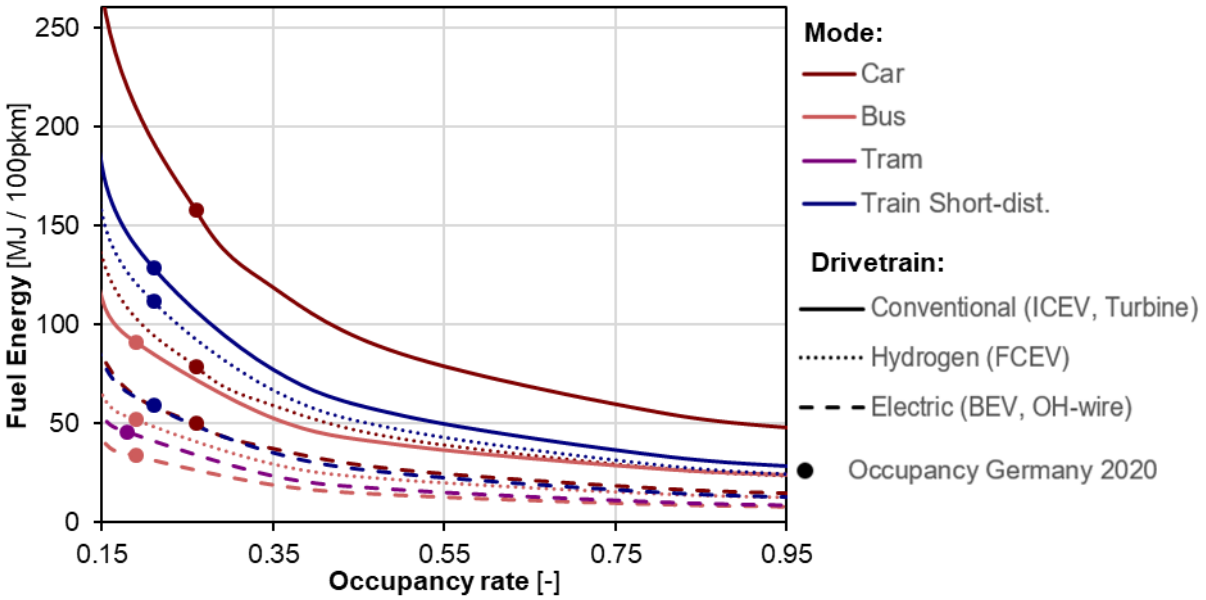

Figure 26: Fuel energy demand vs. occupancy rate for short-distance passenger modes, without drones

Figure 26 shows that, after drones, ICEV-g medium cars have the highest energy consumption for all occupancies. BEV medium buses have the lowest energy consumption for all occupancies. Trams and FCEV buses also have some of the lowest energy demands for short-distance travel. The energy needs for FCEV always lie between that of ICEV and BEV.

Overall, Figure 25 and Figure 26 clearly show the effects of occupancy rates on the fuel demand per passenger-kilometer. Most notable is the exponential rise in energy demand for low occupancy rates. This shows the importance of high occupancy rates in reducing the overall transport sector energy demand while still maintaining passenger capacity.

Figure 27 represents the fuel energy demand for the average occupancy rates of the short-distance transport modes.

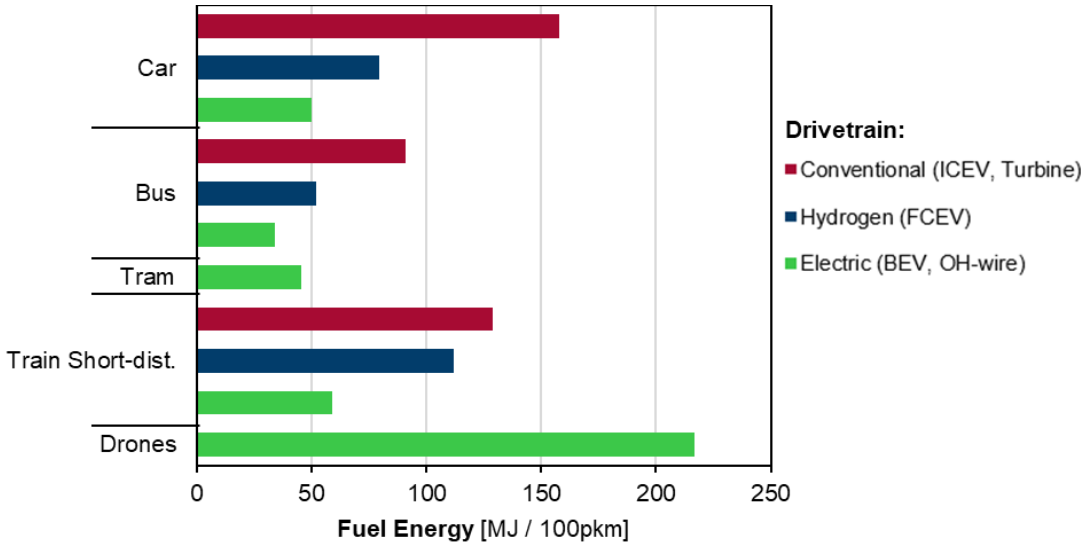

Figure 27: Fuel energy demand for average occupancy of short-distance passenger modes

Figure 27 shows the same results as discussed for the overall trend in energy demand with respect to varying occupancy rates. This is due to the similarity in the average occupancies of cars, buses, and trams, 26%, 19%, and 18%, respectively. Therefore battery-electric cars and buses, fuel cell buses, and trams, at 50, 34, 52, and 46 MJ/100pkm, respectively, are best suited for energy-efficient short-distance journeys when average occupancy rates are considered. Despite their high occupancy rates of 82%, drones still fare the worst in energy demand for short-distance travel at 217 MJ/100pkm.

Therefore, it can be concluded that for short-distance journeys, public transportation provides the most energy-efficient means of travel in the form of BEV and FCEV buses as well as trams. BEV cars also have low energy demands. Combined with the advantages of door-to-door travel, they can often be more convenient for short-distance travel.

Next, the energy demands for the long-distance passenger transport modes are analyzed. Figure 28 shows the fuel demand for all long-distance passenger transport modes for varying occupancy rates. The default occupancy rates for 2020 are highlighted for each drivetrain.

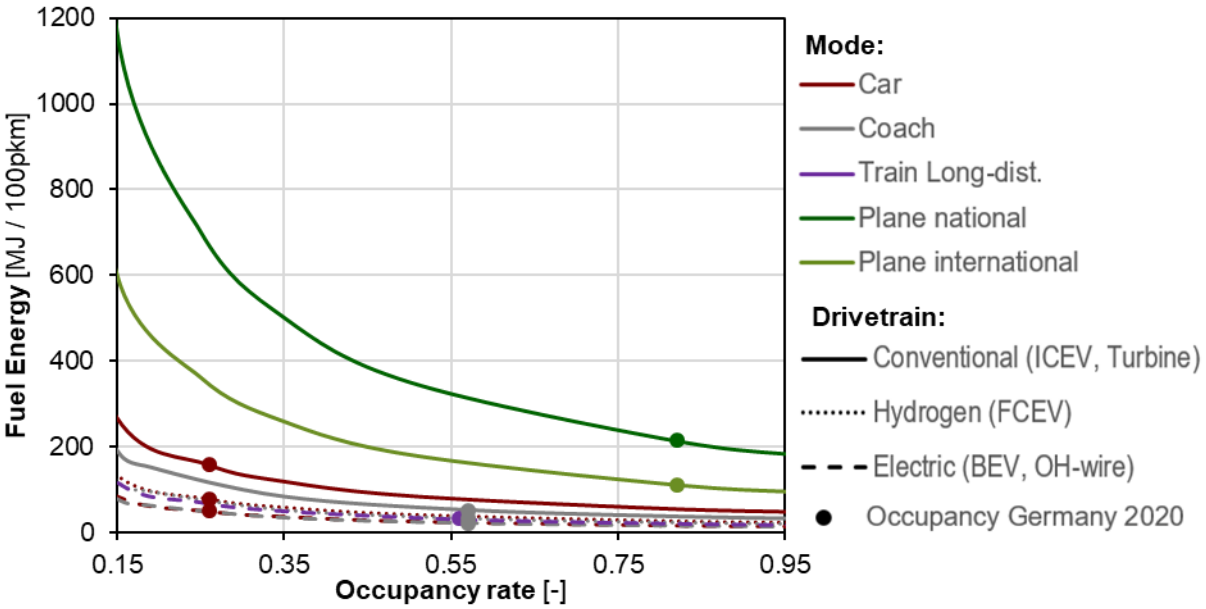

Figure 28: Fuel energy demand vs. occupancy rate for all long-distance passenger modes

Figure 28 shows that airplanes have the highest energy demand for all occupancy rates. Furthermore, national flights are more energy-intensive compared to international flights. This is due to a higher portion of the national flight being conducted within the energy-intensive LTO part of the flight. This is discussed in detail in section 4.2.1.

Figure 29 shows the same data but zoomed in to see the differences between the drivetrains better.

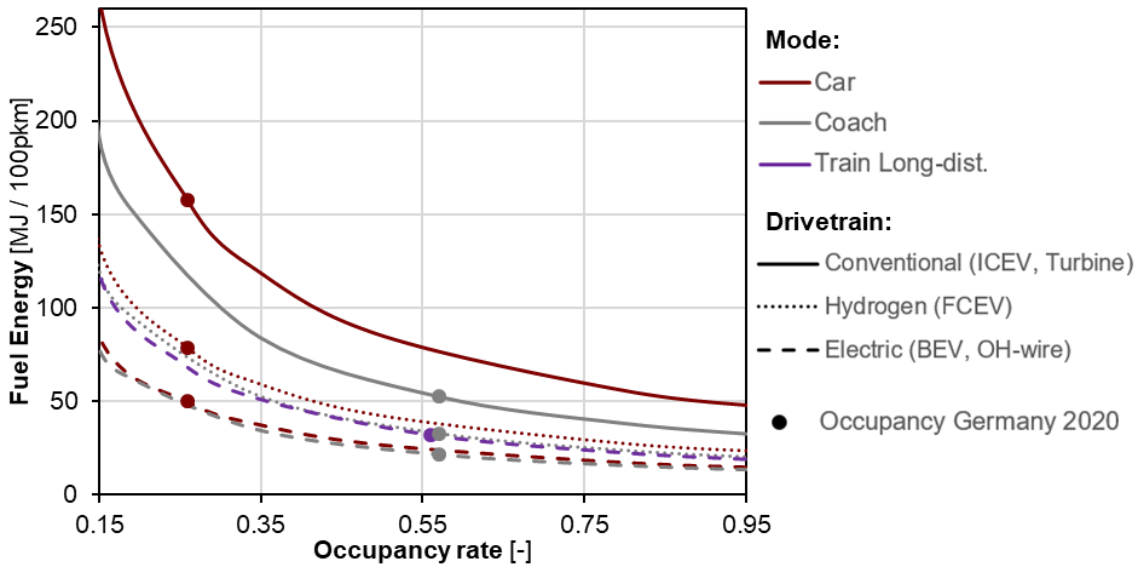

Figure 29: Fuel energy demand vs. occupancy rate for all long-distance passenger modes, without airplanes

Figure 29 shows that, after airplanes, ICEV-g medium cars have the highest energy consumption for all occupancies. BEV cars and coaches are the most energy-efficient modes of transport for long-distance travel.

Long-distance electric trains are the next best option. FCEV cars and coaches also show good energy efficiency values. It can be noted that ICVE-d coaches are a better option than ICEV-g cars at all occupancy rates.

Figure 28 and Figure 29 again point out the importance of occupancy rates on the fuel energy demand per passenger-kilometer. It is well known that taking a flight is a highly energy inefficient and carbon-intensive means of travel. However, if the choice is between a high occupancy rate international flight and a low occupancy rate ICEV-g medium car, the flight becomes the better option. Furthermore, in the current COVID-19 pandemic situation, regulations limit passenger numbers for trains and coaches to maintain social distancing. The lower occupancy rates increase these passenger modes' energy intensity and result in cars, with higher occupancy rates, becoming the better option.

Figure 30 represents the fuel energy demand for the average occupancy rates of the long-distance transport modes.

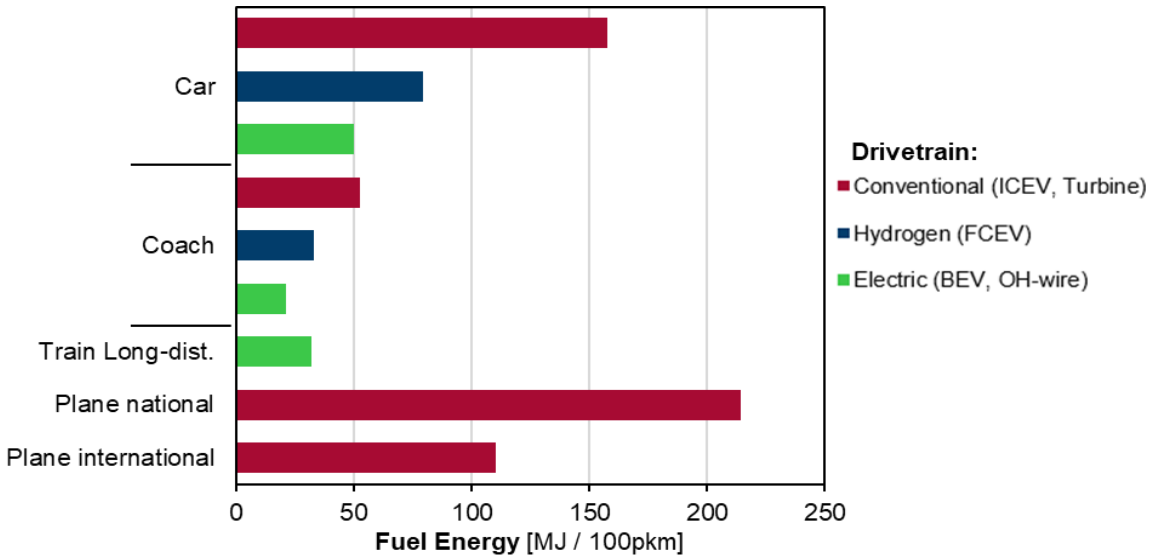

Figure 30: Fuel energy demand for average occupancy of long-distance passenger modes

Figure 30 shows that BEV coaches provide the least energy-intensive means of long-distance transport, at 21.3 MJ/100pkm, followed by long-distance electric trains, 31.8, and FCEV coaches, 32.9. A major factor in this is that the average occupancy rates for these modes are higher than those for cars. The energy demand for BEV cars, 49.9, is similar to that of ICEV-d coaches, 52.5, mainly due to the large difference in their respective occupancy rates. One interesting point to note is that for long-distance travel, airplanes consume less energy than ICEV-g cars. Again this can be attributed to the higher occupancy rates for airplanes. Although it can be noted that long-distance car travels will likely have higher occupancy rates than the average assumed in this analysis. For example, a family going on a vacation or a road trip. This will lead to lower energy demands for long-distance car journeys. National flights are by far the most energy-intensive, 215 MJ/100pkm, means of travel despite their high occupancy rates.

To sum up, it can be concluded that BEV and FCEV coach and long-distance electric trains provide the best transport modes for long-distance travel. If a BEV car has a high enough occupancy, it can also be an energy-efficient alternative to a BEV coach. National flights are the worst possible means of travel with regard to energy demand and should be discouraged for energy consumption reasons.

5.3.2. Freight modes

In this section, the fuel energy demand for the different freight drivetrains is discussed in terms of the energy required per 100 tonne-km transported.

Figure 31 shows the fuel demand for all freight transport modes for varying occupancy rates. The default occupancy rates for 2020 are highlighted for each drivetrain.

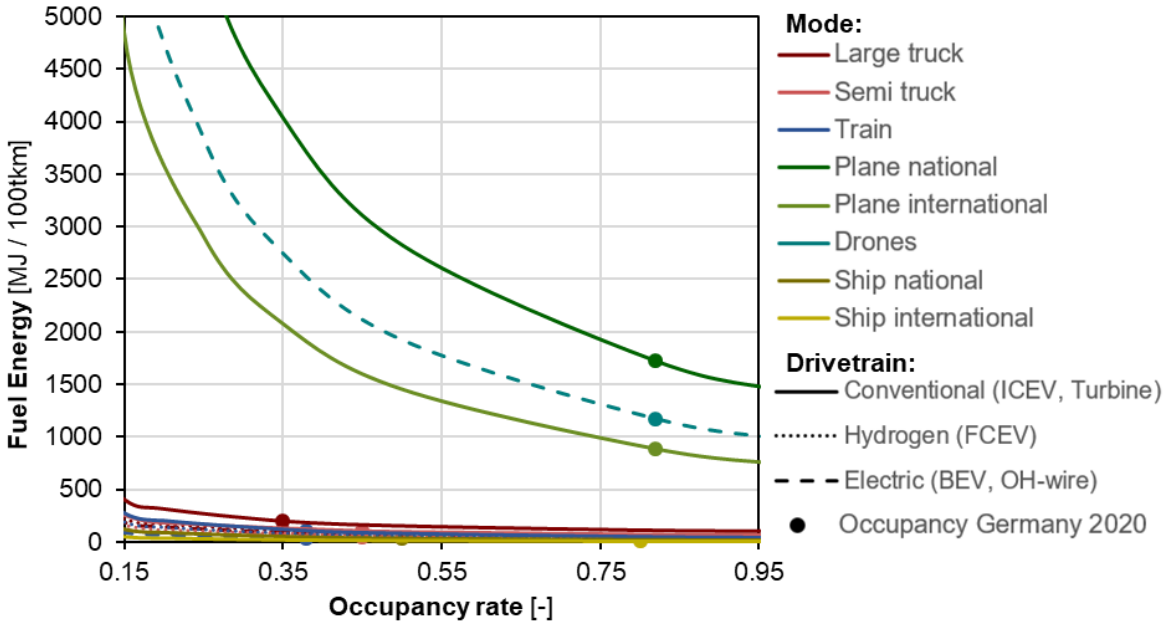

Figure 31: Fuel energy demand vs. occupancy rate for all freight modes

Figure 31 shows that the aviation modes have the worst energy consumption of all freight transport modes. Among them, national flights have the worst energy values. Drones have the second-highest energy demand, only beating out national flights. They come with the additional benefit of fulfilling door-to-door transport needs. However, it should be noted that these freight drones are built for last-mile delivery needs. Therefore they carry light packages over short distances, as compared to the other modes. Thus, other factors affecting the operational cost are often prioritized, like the time needed for loading and unloading. They also operate in densely populated areas; thus, operational safety requires additional weight for parachutes and other safety equipment. Furthermore, they operate at low speeds, which leads to higher energy consumption per distance traveled, as a large portion of the thrust is used to provide the vertical lift. These factors combined lead to high fuel energy demand when measured per tonne-kilometer.

Figure 32 shows the same data but zoomed in to see the differences between the drivetrains better.

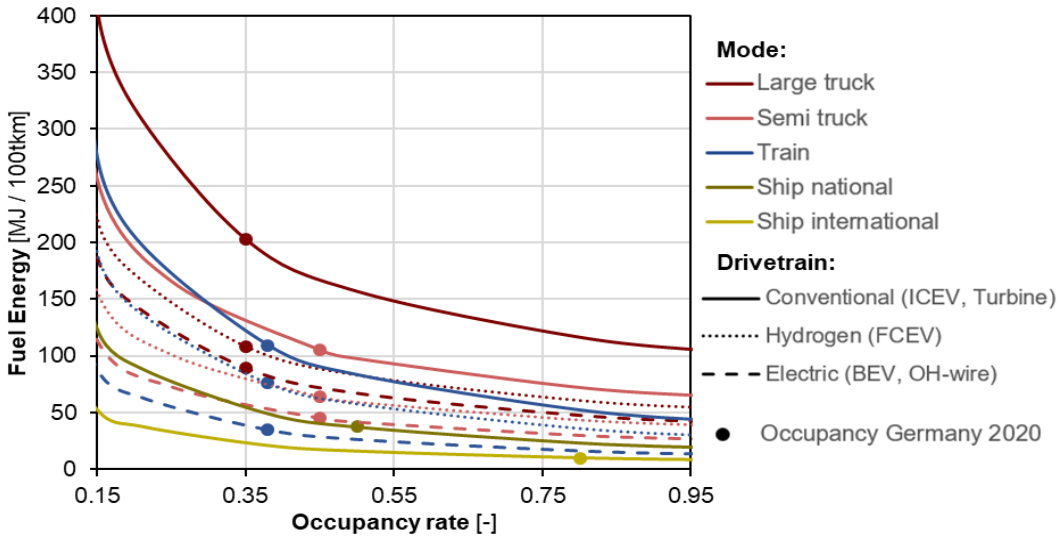

Figure 32: Fuel energy demand vs. occupancy rate for freight modes, without aviation modes

Figure 32 shows, not considering the aviation modes, ICEV-d large trucks have the worst energy consumption values. ICEV-d semi-trucks and trains are only slightly better than large trucks. International shipping has the best energy consumption for all occupancy ratings. National shipping is also one of the most energy-efficient modes, although the availability of accessible inland water bodies must be considered. Electric freight trains are the best solution for on-land freight transportation, followed by BEV semi-trucks. FCEV trains and semi-trucks also show low energy requirements.

Figure 32 shows that disregarding the aviation modes, the fuel energy depends a lot on the different modes' occupancy rates. A high occupancy rate semi-truck can be better than a low occupancy rate train. A high occupancy rate train can be better than international shipping with a low occupancy rate.

Figure 33 represents the fuel energy demand for the average occupancy rates of all non-aviation freight transport modes. The aviation modes are excluded to better distinguish between the energy demand of the other modes.

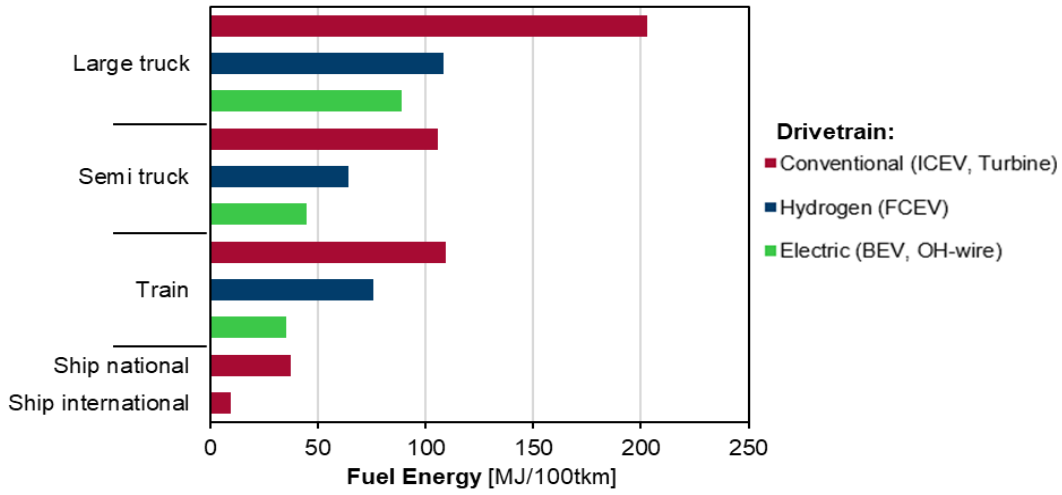

Figure 33:Fuel energy demand for average occupancy of freight modes

Figure 33 shows again that international shipping is by far the most energy-efficient means of freight transport at 9.9 MJ/100tkm. The aviation modes are the most energy-intensive modes with an order of magnitude higher energy demand than the other modes, despite their high occupancy rates. National and international planes, on average, consume 1726 MJ/100tkm and 888 MJ/100tkm, respectively. Drones consume 1174 MJ/100tkm.

Electric trains and BEV semi-trucks are the best choices for on-land freight transport at 35.2 and 45 MJ/100tkm, respectively. FCEV semi-trucks can also be a good alternative, 64 MJ/100tkm, especially considering the range limitations associated with BEV semi-trucks.

In conclusion, international shipping should be prioritized for long-distance freight transport. For short distances, electric trains and BEV and FCEV semi-trucks should be considered first.

5.4. Drivetrain Analysis

In this section, the energy demands for the different drivetrains within LDV are discussed. A medium car is used as the representative for all LDVs.

The energy demand for the different drivetrains until 2050 is shown in Figure 34.

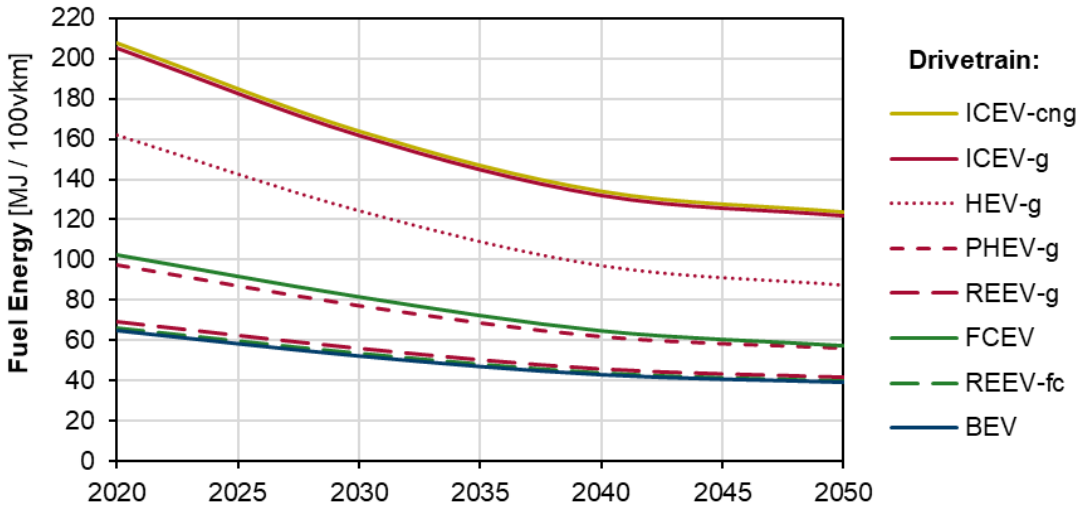

Figure 34: Energy demand for different drivetrain medium cars until 2050

Figure 34 shows that ICEVs have the worst energy demand amongst all the different drivetrains. HEV-g shows lower energy consumption values due to better drivetrain efficiencies and the use of regenerative braking. PHEV-g has lower energy consumption values due to the all-electric driving option, and REEV-g with a higher all-electric range further reduces energy demand. For PHEV-g and REEV-g, the energy demand is split into gasoline and electricity. FCEV energy demand is comparable to a PHEV-g. BEV has the best energy consumption values.

Furthermore, HEV-g shows the most significant relative improvement until 2050 of 45.7%. BEV makes the least relative improvement of 39.6%, which is still a big improvement. In terms of energy demand, ICEV-cng and ICEV-g both reduce their energy demand by roughly 80 MJ/100vkm to reach around 120 MJ/100vkm by 2050.

The effects of driving conditions are next analyzed for the different drivetrains. The effects of urban and highway driving scenarios from the WLTC are shown in Figure 35.

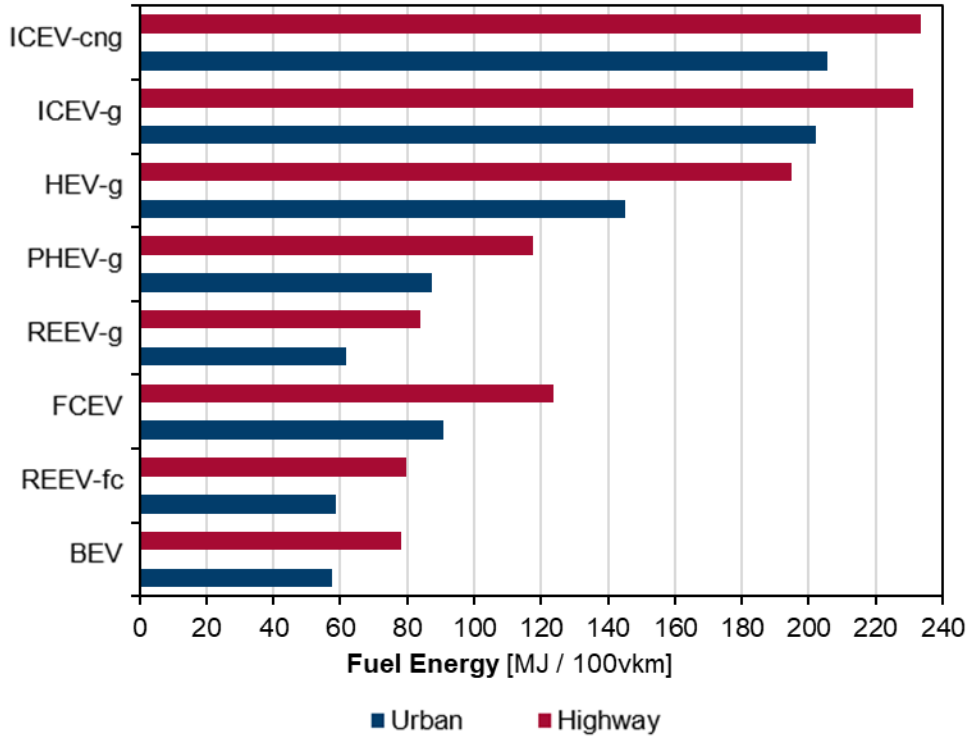

Figure 35: Energy demand for the different drivetrain medium cars in urban and highway driving scenarios.

Figure 35 shows that for all drivetrains, urban driving requires less energy than highway driving. BEV, REEV-fc, and REEV-g are consistently the best performing modes in all driving scenarios, while ICEV-cng and ICEV-g are the worst. Important to note is the relative change in energy demand between the two driving scenarios. The drivetrains with regenerative braking, which includes all drivetrains except ICEV-g and ICEV-cng, show around a 25% reduction in energy consumption when going from highway to urban driving. In contrast, drivetrains without regenerative braking show a reduction of only around 12%. This is due to the higher potential regeneration in urban driving compared to highway driving. Furthermore, the energy demand for ICEV decreases from urban to rural driving but stays the same for electrified drivetrains.

5.5. Electrification

In this section, the effects of electrification on fuel demand are considered. The effects of increasing electrification are first analyzed. Next, the effects of electrification within different car segments are discussed.

5.5.1. Electric share

Firstly the change in fuel energy demand with increased drivetrain electrification is analyzed. An HEV-g medium car is considered for a vehicle with 0% electric drive share, while a BEV represents a vehicle with a 100% electric share. A PHEV-g car is used to model electric drive shares in between. Figure 36 shows the result of this analysis.

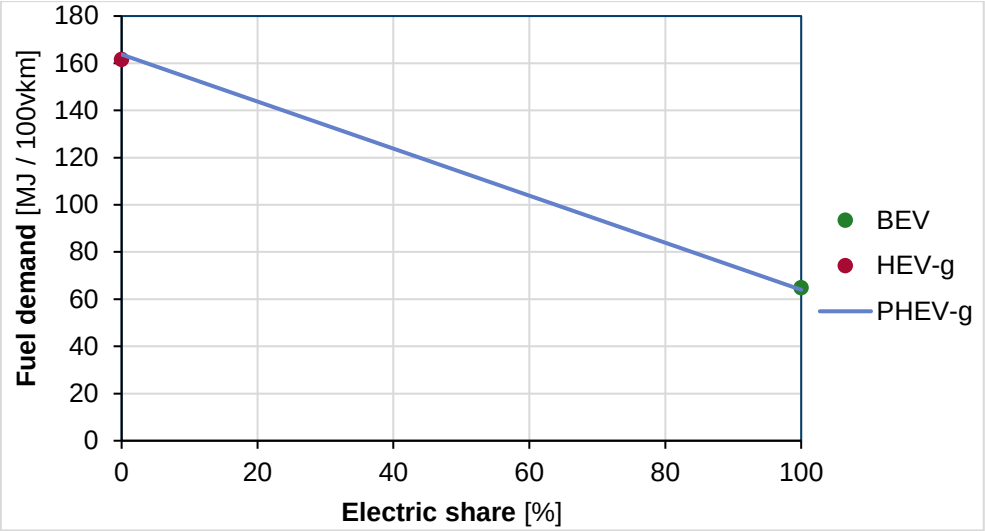

Figure 36: Fuel energy demand vs. electric share for medium car

Figure 36 shows how fuel energy demand drastically decreases with the increase in electric share. A drivetrain with a 100% electric share has almost 60% lower fuel demand than a drivetrain with a 0% electric share. The PHEV-g drivetrain shows a linear decrease in fuel demand with an increase in electric share. It is assumed that PHEV has the same configuration (battery capacity) and, therefore, the same vehicle mass. Only user behavior leads to different electric shares.

5.5.2. Electrification within car segments

The effects of electrification on a small car and SUV are analyzed. Figure 37 shows the fuel energy demand for a small car and an SUV in urban and highway driving conditions.

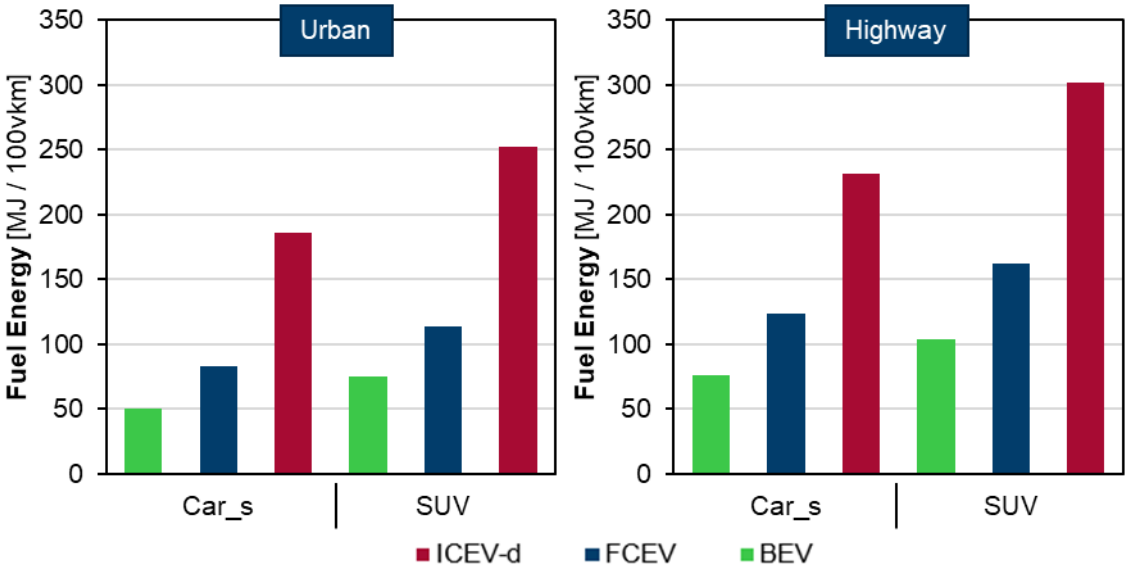

Figure 37: Fuel energy demand for small car and SUV in urban (left) and highway (right) driving scenario

Figure 37 shows that for any driving condition, the SUV consumes more energy than the small car. This is because the SUV has a higher vehicle mass, as well as a larger frontal area and air drag coefficient. For all drivetrains, small car shows a higher relative reduction in energy consumption when going from highway to urban driving. For a small car, electrification (BEV) reduces energy consumption by 73% compared to ICEV-g in urban driving, while in highway conditions, the reduction is 67%. For an SUV, electrification improves the energy demand by 70% in urban and 65% in highway conditions. Thus small car shows larger benefits from electrification in all driving conditions compared to an SUV.

5.6. Effects of Driving Environment

In this section, the effects of the driving environment on fuel energy demand are analyzed.

5.6.1. Trucks for different purposes

The energy demands for trucks used for different functions are analyzed first. A small truck used for urban cargo delivery is analyzed using the urban and rural parts of the WHVC. A large truck used for urban waste collection is analyzed using the NRTC. Finally, a semi-truck used for long-haul freight transportation is evaluated using the highway segment of the WHVC. Default occupancy rates are assumed for all modes. ICEV-d, FCEV, and BEV drivetrains are considered. Figure 38 shows the results obtained from this analysis.

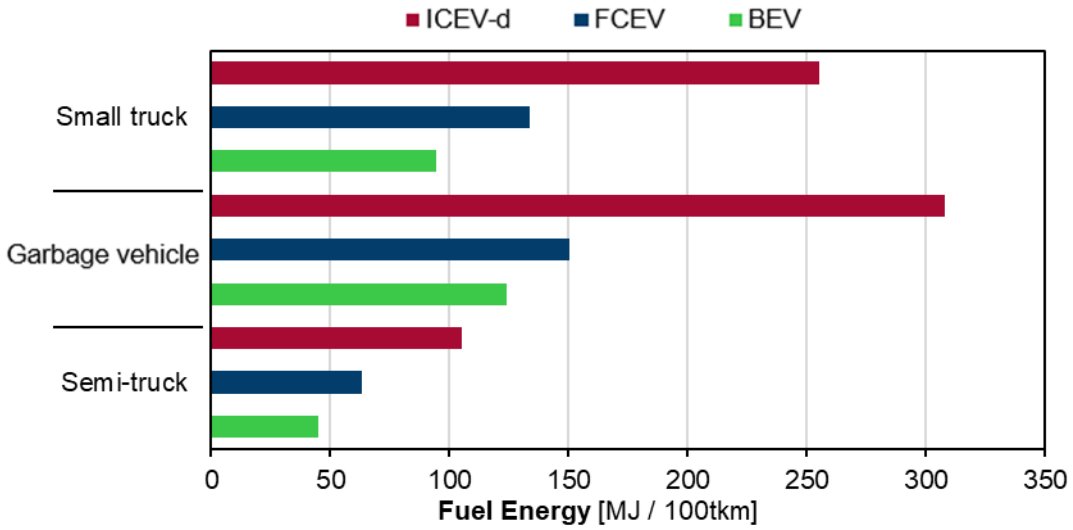

Figure 38: Fuel energy demand for a small truck (urban cargo), garbage vehicle, and semi-truck (long-haul)

Figure 38 shows that urban waste collection is the most energy-intensive while long-haul freight transport is the least energy-intensive, for all drivetrains, amongst the function analyzed. Urban cargo and waste collection benefit the most from drivetrain electrification. The energy demand drops roughly 60% for these modes when a battery-electric drivetrain is used compared to an internal combustion engine. This is due to the prevalence of stop-and-go driving conditions for these vehicles. In terms of energy needs, waste disposal benefits the most from electrification, which can be attributed to the more frequent stops in NRTC than urban and rural parts of WHVC. Long-haul cargo is the least energy-intensive means due to the lack of stops, which significantly impacts

trucks' energy demand due to their massive masses. Semi-trucks also have a higher average occupancy rate, which further reduces their energy demand per tonne-kilometer.

5.6.2. Effects of ambient temperature for buses

The impact of the ambient temperature variation on the fuel energy demand for a medium bus is analyzed next. Only the energy demand for heating and ventilation is considered. The energy demand for ICEV-d, FCEV, and BEV over a temperature range of -10 to 25 °C is shown in Figure 39.

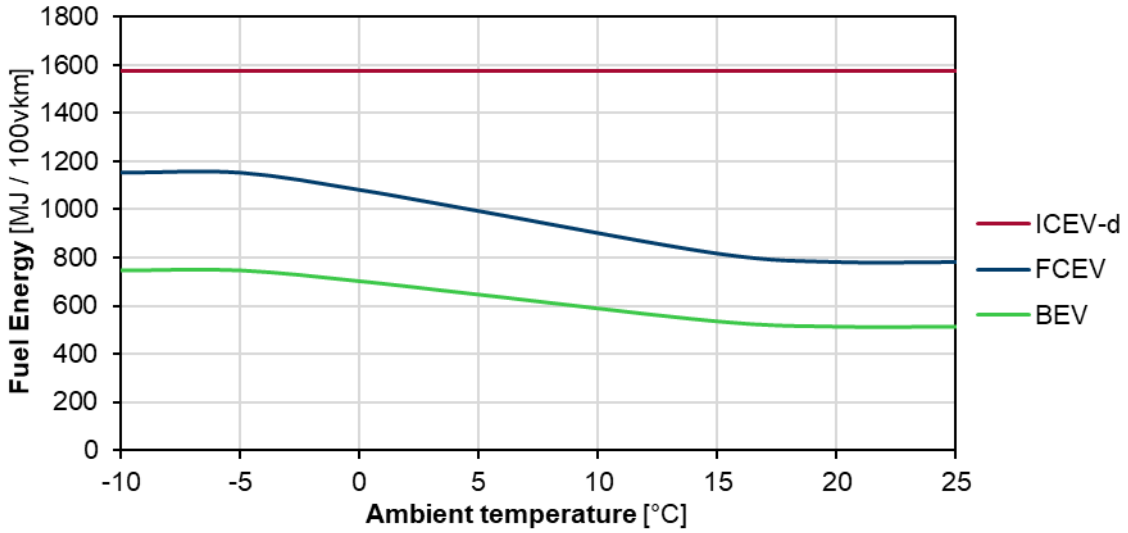

Figure 39: Fuel energy demand for medium buses for varying ambient temperature. It is assumed that the engine exhaust heat provides the entire HVAC energy demand in an ICEV-d. Refer to the text for more information.

Figure 39 shows that the energy demand for ICEV-d does not change with temperature variation. The thermal energy required to heat the passenger compartment is derived from the internal combustion engine's waste heat. For FCEV and BEV, the energy demand depends on the ambient temperatures between approximately -5 and 17°C. For higher temperatures, it is assumed that the vehicle only needs to use ventilation for passenger comfort. For lower temperatures, it is assumed that the vehicle's heating capacity is reached. Going from a temperature of 20 °C to -5 °C, the vehicle's fuel energy demand increases by almost 50%. Furthermore, lower temperatures increase the internal resistance and lower the capacity of batteries [146]. This effect is not taken into account in the developed model, so it is not shown in Figure 39. These effects combined lowers the energy consumption advantage of electrified drivetrains in cold weather conditions. Thus a higher capacity battery pack will be required to maintain the same electric driving range in such situations.

5.6.3. Effects of road gradient

The effects of the road gradient on the fuel energy demand are next analyzed. The effects are considered on ICEV-g, FCEV, and BEV medium car. The energy demand for a vehicle driven at a constant speed of 80km/h over varying gradients is analyzed. Figure 40 shows the resulting data.

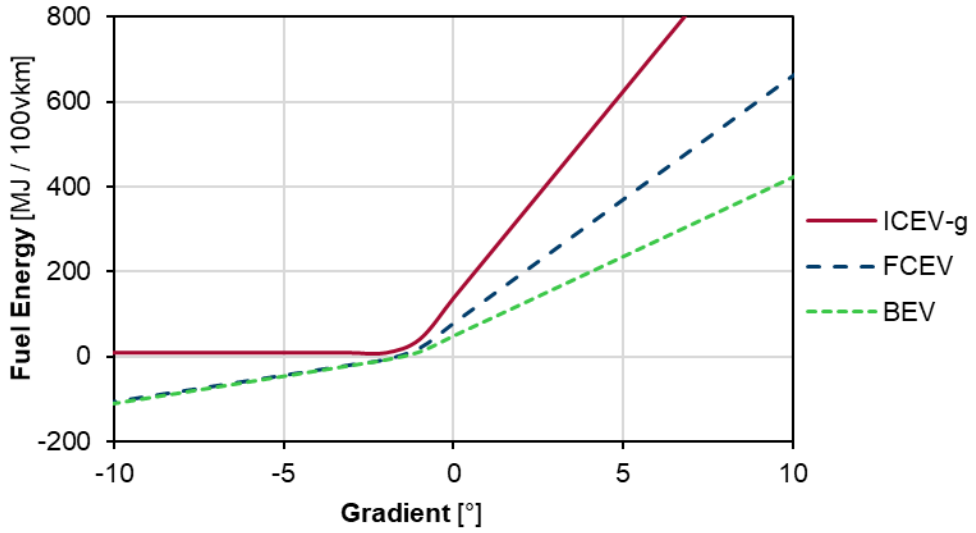

Figure 40: Fuel demand versus road gradient for a medium car at a constant speed of 80km/h. Due to the lack of a recuperation device, the ICEV-g still requires fuel energy while going down a slope.

Figure 40 shows that fuel energy demand increases for increasing the road gradient. It should be noted that the increase in energy demand is proportional to the vehicle mass, as shown in equation 3.6. This higher fuel demand is essentially used to increase the vehicle's gravitational potential energy. ICEV-g shows a steeper increase in fuel demand due to its lower drivetrain efficiency. The most interesting point to note here is the negative energy demand values, for a negative gradient, in FCEV and BEV. The negative gradient indicates that the vehicle is driving down the slope. The effects of regenerative braking in such conditions are to recuperate some of the vehicle's gravitational potential energy. This recuperated energy is used to recharge the battery and increase the vehicle range while driving down a hill. On the other hand, lacking regenerative braking, ICEV-d still consumes energy to maintain heating and other essential driving controls.

The above discussion highlights the advantage of drive electrification in hilly regions due to regenerative braking, which can recuperate gravitational potential energy in addition to the vehicle kinetic energy.

5.7. Outlook to the Future

In this section, the energy demand for different drivetrains until 2050 is analyzed. The analysis is divided into passenger and freight transport modes. Finally, the future development reported in some literature is compared with the respective modes according to the model.

5.7.1. Passenger modes

In this section, future trends in passenger transport modes are discussed. Figure 41 shows the future fuel energy requirements for short-distance passenger transport modes. It is assumed that occupancy rates do not change compared to current values.

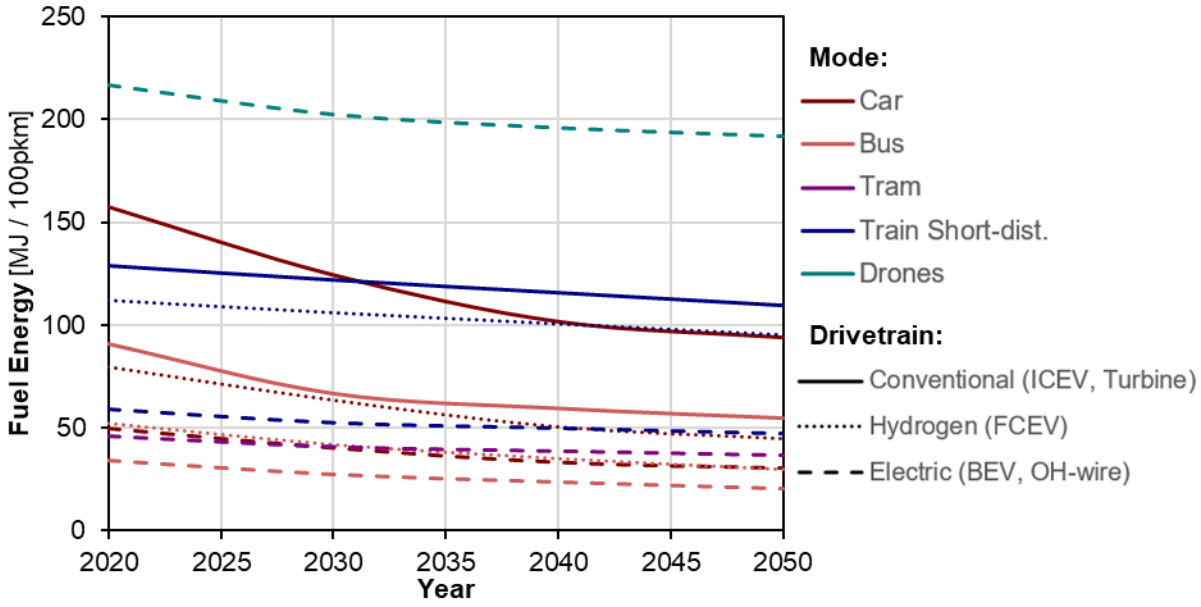

Figure 41: Future fuel energy requirements for short-distance passenger modes until 2050

Figure 42 shows the future fuel energy requirements for long-distance passenger transport modes.

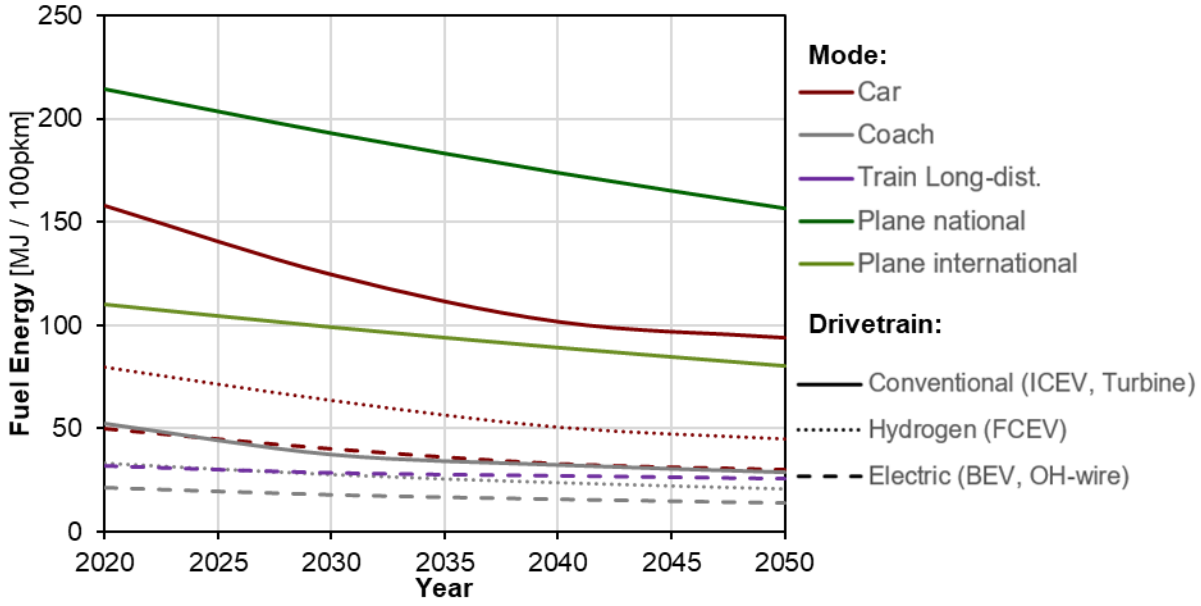

Figure 42: Future fuel energy requirements for long-distance passenger modes until 2050

Figure 41 shows that FCEV cars achieve the biggest relative improvement in fuel energy demand until 2050, with a 43.5% improvement compared to 2020 values. All the car and bus drivetrains show large improvements as well. Drones show the least improvement, with only an 11.5% reduction in fuel energy demand until 2050. For the most part, the drivetrains' order according to the energy consumption values remains constant throughout the years. Only some of the car and bus drivetrains catch up with tram and short-distance train modes.

As can be seen from Figure 42, ICEV-d coaches show the largest improvement in fuel consumption with an improvement of 45% over 2020 values. Once again, the car and coach drivetrains show the biggest improvement in energy efficiency. Long-distance trains show the least improvement at only 19.6%. Airplanes show an improvement of 27.1% over the timeframe, resulting from the compounding effects of a 10% improvement per decade. As for the short-distance modes, generally, the drivetrain's ranking related to energy stays the same throughout the years.

5.7.2. Freight modes

In this section, future trends in freight transport modes are discussed. Figure 43 shows the future fuel energy requirements for all the freight transport modes. It is assumed that occupancy rates do not change compared to current values.

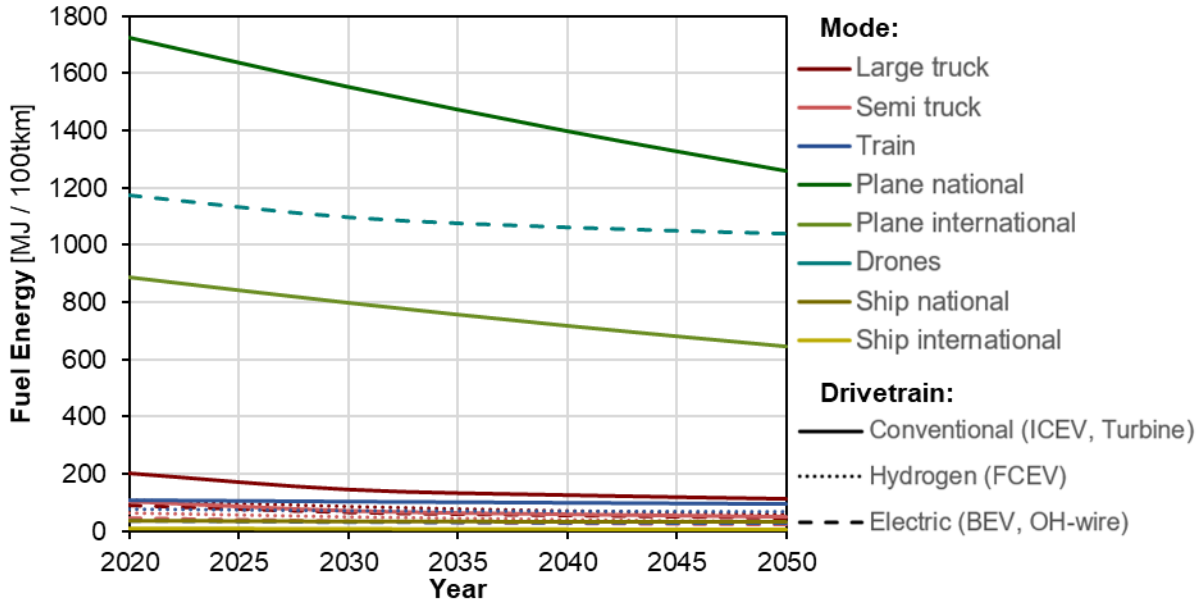

Figure 43: Future fuel energy requirements for all freight modes until 2050

As expected, Figure 43 shows that aviation modes remain the least energy-efficient modes of freight transport in the future. Drones show an improvement of only 11.5%, while airplanes show an improvement of 27.1% till 2050. It should be noted that for drones, only drivetrain improvements are considered. Other improvements, such as in aerodynamics and flight control surfaces, are not taken into account.

Figure 44 shows the same data without the aviation modes in order to distinguish the changes in energy demand for the other freight transport modes.

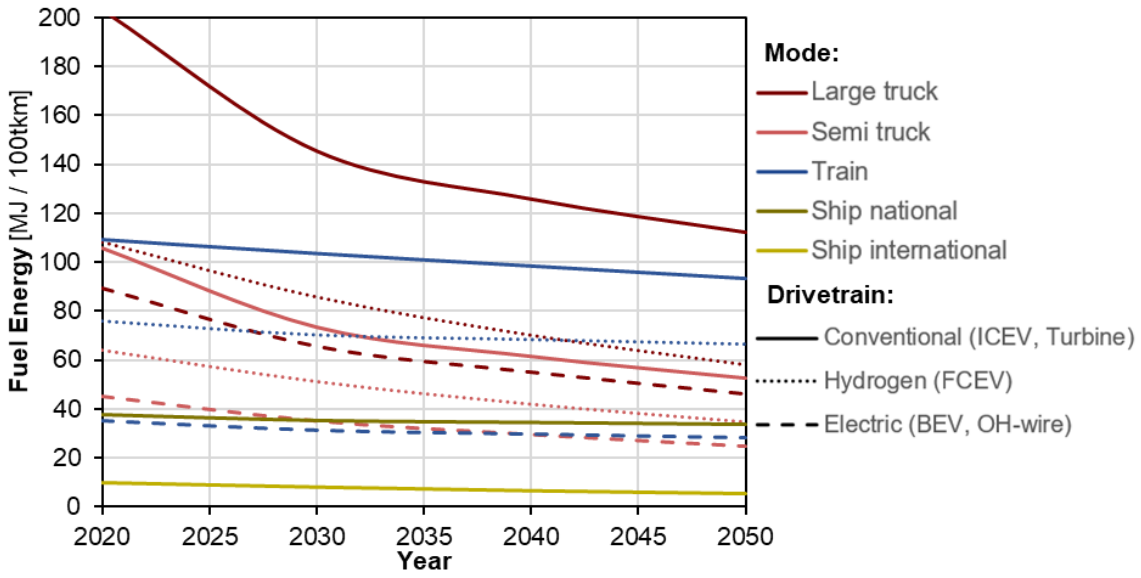

Figure 44: Future fuel energy requirements for freight modes until 2050, without aviation

Figure 44 shows that ICEV-d semi-trucks achieve the greatest energy efficiency improvement at 50.3% relative to 2020 values. In general, all the semi-truck and large truck modes show significant efficiency improvements. Despite showing the least improvement, national shipping remains one of the most efficient freight transport means. ICEV-d and FCEV trains show little improvement at 14.7% and 12.5%, respectively. With a 45.5% improvement, international shipping remains the most efficient freight transport mode by a large margin.

5.7.3. Comparison to other studies

This section compares the future energy trends estimated by the model with those predicted in the literature. Figure 45 compares the model results with fuel energy consumption reported in the literature for ICEV-g, FCEV, and BEV medium cars.

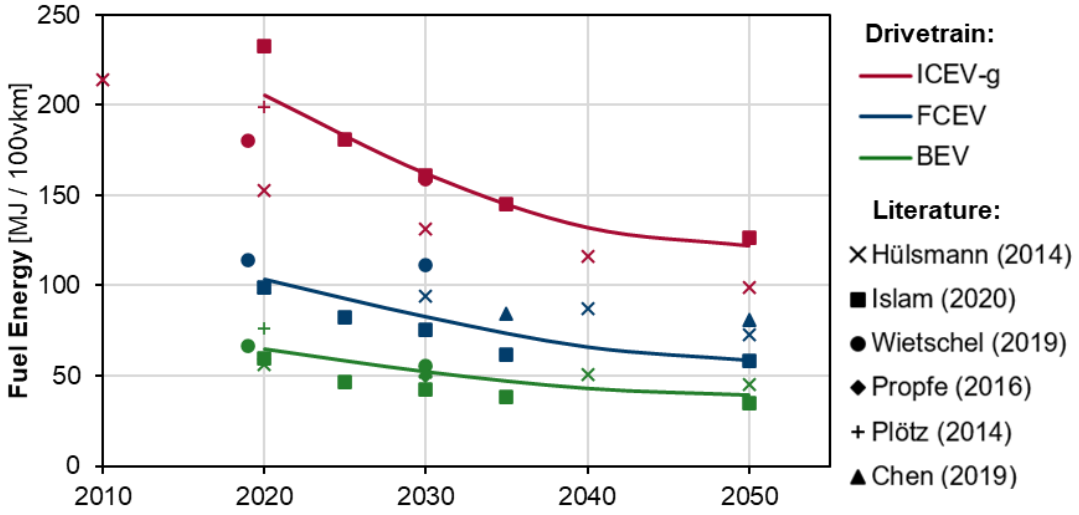

Figure 45: Future fuel energy requirements for medium car and literature data [71], [105], [107], [147], [148], [149]. *The solid lines represent model results.*

As can be seen from Figure 45, the literature values, for the most part, resemble the results from the model. ICEV-g data from Hülsmann et al. (2014) considers the effects of hybridization [105]. Thus the values are lower than the ones predicted by the model. The average of high and low technology progress values for ICEV-g from Islam et al. (2020) [71] equate almost perfectly with the model estimates for the years 2025 and onwards. FCEV values from Hülsmann et al. (2014) [105] are higher compared to model data for future scenarios, suggesting that the model assumes higher efficiency Improvement in the future. However, FCEV data from Islam et al. (2020) [71] matches well with the model data for 2050. BEV data for the future also agree with literature values.

Figure 46 compares the model results with fuel energy consumption reported in the literature for ICEV-d, FCEV, and BEV medium buses. The range of values represents occupancy rates between 0% and 100%.

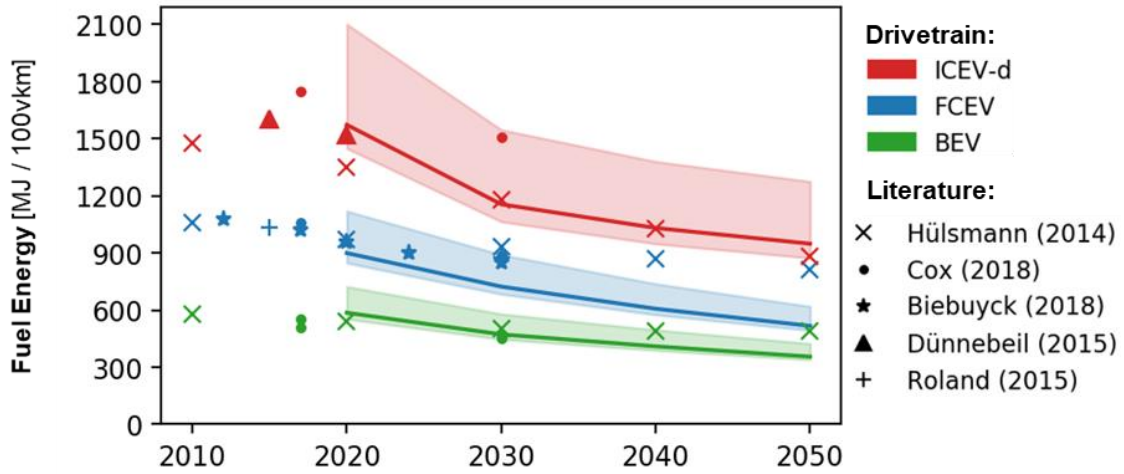

Figure 46: Future fuel energy requirements for medium bus and literature data [105], [72], [106]. *The solid lines represent the fuel energy demand for the average occupancy rate. The shaded area represents the energy demand for varying occupancy rates between 0% and 100%, according to the model.*

As is evident from Figure 46, the results match well with the data reported in the literature. As previously noted, FCEV's efficiency improvements in Hülsmann et al. (2014) are not very optimistic. Therefore, the values are higher than the model results for 2050 [105]. The model results for ICEV-d and BEV agree with the literature values.

Figure 47 compares the model results with fuel energy consumption reported in the literature for ICEV-d, FCEV, and BEV large trucks. The range of values represents occupancy rates between 0% and 100%.

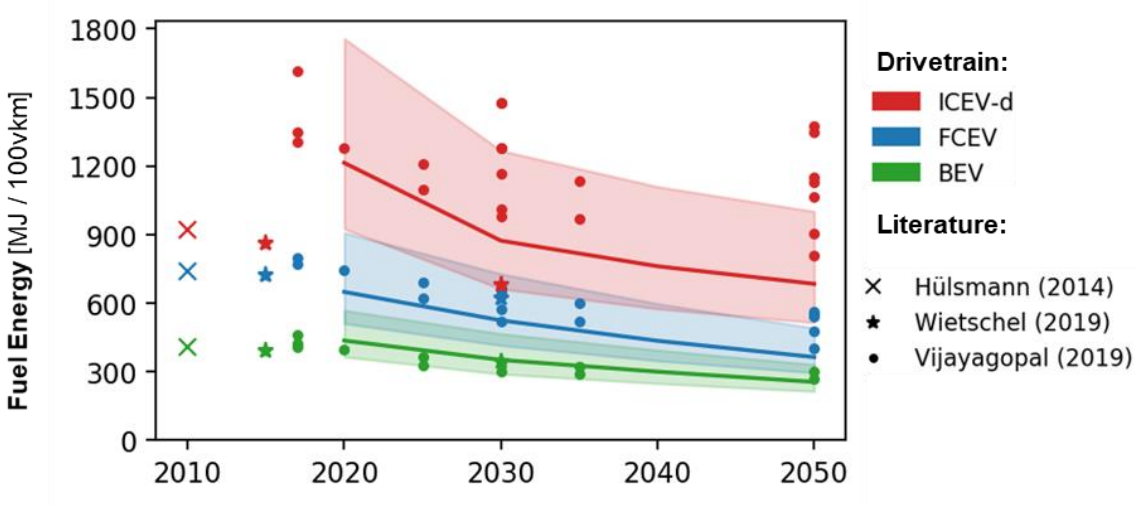

Figure 47: Future fuel energy requirements for large truck and literature data [105], [107], [108]. *The solid lines represent the fuel energy demand for the average occupancy rate. The shaded area represents the energy demand for varying occupancy rates between 0% and 100%, according to the model.*

Figure 47 shows that the model results compare well with literature values until 2050 for all drivetrains. Although the ICEV-d values reported by Vijayagopal et al. (2019) diverges from model results for later years, the results are still within the range. Vijayagopal et al. (2019) report the energy demand for various driving conditions, including different driving cycles and gradient profiles, which is why there are multiple data points for a given year [108]. Furthermore, fuel energy demand from the model for FCEV and BEV matches well with the literature values.

It can be summarized that the model results agree with the data predicted in the literature for future scenarios of cars, buses, and trucks.

5.8. Side Analysis: Last-mile delivery

A side analysis is carried out in this section. The analysis considers the energy required to carry out last-mile deliveries using a BEV drone versus using a battery electric LCV.

It is assumed that the average mass of a package is 2.3 kg. This is assumed based on the carrying capacity of an Amazon Prime Air Drone [40]. The energy demand for package delivery by drones is plotted against the distance flown to deliver one package. The results are shown on the upper axis of Figure 48.

Each parcel carrier delivers, on average, around 20 packages per hour [150]. This adds up to 160 packages per day, assuming an 8-hour workday. Therefore, it is assumed that the LCV will initially have 160 packages, each weighing 2.3kg. Since the LCV will travel door-to-door, dropping off packages, the average occupancy throughout the trip can be considered half of this, 80 packages. The additional mass of the cargo is then added to the vehicle mass. The energy required to deliver each package is plotted against the additional distance traveled for each package delivery. The results are plotted on the lower axis of Figure 48. The total distance traveled per day by the LCV for 160 packages delivered is also plotted.

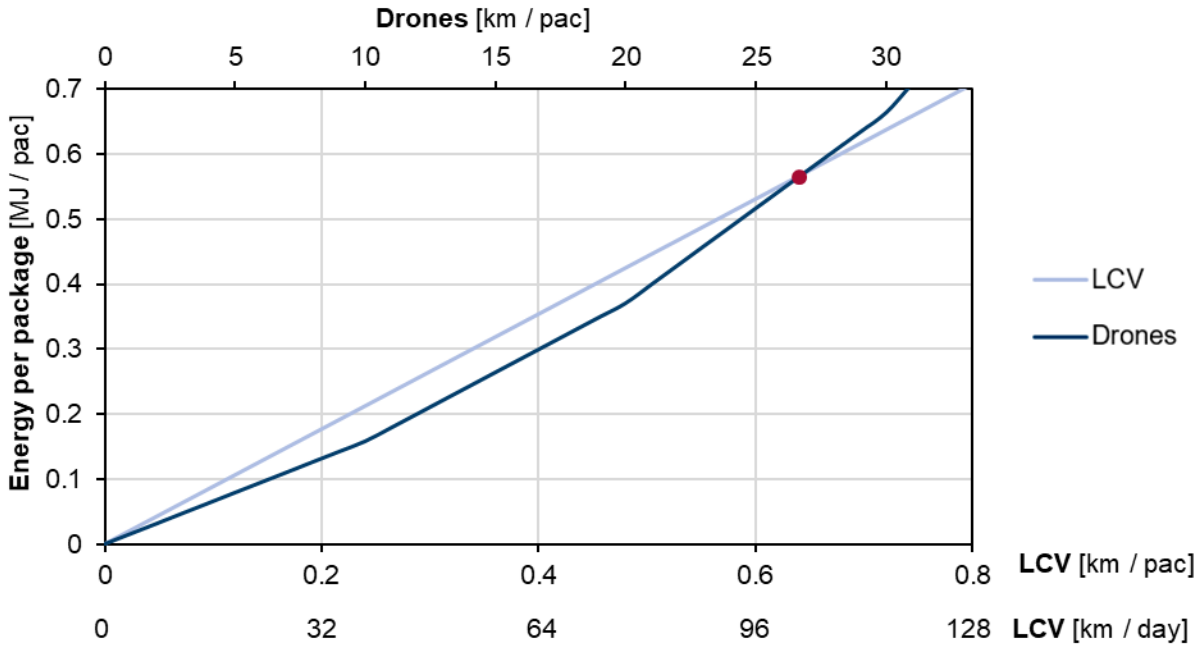

Figure 48: Energy required for last-mile delivery by drones and LCVs

Anderson (2020) reports that the additional distance traveled by delivery vehicles for each package delivered is 0.64km [151]. The energy required for this additional distance traveled by an LCV is equivalent to around 27km traveled by a drone. Therefore, if the drone travels less than 27km per package delivery, drone delivery would be more energy-efficient than a battery-electric LCV.

It must be noted that in order for drone deliveries to reach all parties, a larger number of fulfillment centers will be required than for LCV delivery, owing to the lower range of drones. The additional energy required to maintain these facilities is not considered in this analysis.

6. Conclusion

This thesis aimed to build an energy model for the major modes of transport in Germany. Furthermore, future efficiency improvements were also considered for the various modes. The results were found to be valid by comparison with real vehicles and data from the literature.

For urban use vehicles, the implementation of regenerative braking showed a large reduction in fuel consumption. The use of a realistic recuperation braking system with 45% efficiency reduced the mechanical energy demand for a vehicle by 27% for urban driving conditions. This is one of the reasons why vehicles with electric motors, which usually are used as recuperating devices, showed such low energy demands in urban driving conditions. This had the additional benefit of reducing air pollution, which often asphyxiates large metro areas.

Vehicles intended for use in urban areas do not need a high driving range. Therefore, these BEVs can be specially designed with lower battery capacity lowering the vehicle mass. Furthermore, urban vehicles could be designed to be smaller, thus lighter, as the luggage capacity requirement is lower than a vehicle used for longer routes. Reducing vehicle mass was shown to be the most effective way of lowering vehicle energy demand in urban use scenarios. A reduction of 10% in vehicle mass resulted in a reduction of 6.7% in the fuel energy demand. Aerodynamic improvements can be the last consideration for these vehicles.

For vehicles intended for highway use, priority should be given to improving the aerodynamics. A 10% improvement in vehicle aerodynamics reduced energy consumption by 5.5% for highway driving conditions. A BEV used for highway driving will require a higher driving range, thus a larger capacity battery pack, which will increase the vehicle mass. For vehicles intended for general use, the vehicle mass should be the first priority, followed by the aerodynamics and then the rolling resistance. These recommendations are made, taking into account the energy consumption values only and not considering any costs incurred for the improvement process.

Furthermore, electrification and regenerative braking showed a high energy saving potential in hilly areas as the regenerative braking can recuperate gravitation potential energy while going downhill. This, combined with the stop-and-go traffic in cities, means that large cities in hilly areas like San Fransisco, Seattle, Lisbon, and Barcelona can reap huge benefits from fleet electrification. These cities also have moderate climates, so the battery capacity will not face any detrimental effects due to extremes of temperatures.

For both short- and long-distance passenger transport, public transportation was often the most energy-efficient means. For short-distance journeys, battery-electric buses (33.9 MJ/100pkm) and trams (45.8 MJ/100pkm), and for long-distance journeys, battery-electric coaches (21.3 MJ/100pkm) and electric trains (31.8 MJ/100pkm) represented the best energy efficiencies. The use of these public modes of transport also has the additional benefit of reducing congestion.

The aviation modes considered in this model, airplanes, and drones, generally had the highest energy consumption values for passenger and freight transport. Of course, it is hard to argue against international aviation's importance; there is no viable alternative to airplanes for transatlantic passenger transport. However, national flights do not hold such a status. National flights (214.5 MJ/100pkm) were often the worst-performing member among the aviation modes. Combined with the fact that there are often viable alternatives in the form of high-speed trains and even car-sharing, it is hard to justify national flights' need in a world constantly facing energy concerns. Government policies intended to increase the adaption of coaches and high-speed trains might be one of the factors that can reduce the prevalence of national flights. Encouraging the use of carpooling and ridesharing can also reduce the energy consumption for passenger transportation. However, the effects of ridesharing on urban traffic, as well as exploitations by multinational ridesharing conglomerates, must be thoroughly assessed.

For freight transportation, international shipping (9.9 MJ/100tkm) proved to be the most energy-efficient mode of transport. For national freight transport, electric trains (35.2 MJ/100tkm), along with battery-electric (45.1 MJ/100tkm) and fuel-cell (64.2 MJ/100tkm) semi-trucks, were some of the best modes.

In future transport scenarios, the first aim should be to increase occupancy rates. It will be difficult to implement, but it is a free upgrade, as no additional investment in technology is required to decrease the energy intensity of transport. Furthermore, increased electrification of drivetrains will reduce the final energy demand for the transport sector.

Appendix

Appendix A: Thermal and mechanical energy for vehicle climate control in Grube (2014)

The next consideration is the energy demand for vehicle climate control. Grube (2014) states that the vehicle interior HVAC system is the most power-hungry auxiliary consumer. Along with providing a mixture of fresh and recirculated air for passenger comfort, the air-conditioning system is also responsible for maintaining the windows free from condensation and ice for driving safety.

For ICEVs, the engine waste heat is usually enough to cover the interior heating requirements and is not generated separately. In extreme conditions, an auxiliary heater can provide extra heat. The engine also provides the mechanical energy required to operate the cooling circuit for an ICEV.

For hybrid vehicles with an internal combustion engine, HVAC's power requirements can only be partly met by the engine. Moreover, for vehicles with fully electric drivetrains, this ratio is zero as there is no internal combustion engine, to begin with. In such cases, a positive temperature coefficient (PTC) heater can provide the heating energy demand. An electrically operated air-conditioning unit provides the cooling.

Ceramic PTC heaters with non-linear resistance curves are used in cars for heating due to its many advantages over other heating devices. Foremost among them is that PTCs can self-regulate their thermal output, thus preventing problems like overheated seats. Furthermore, they are efficient, have fast response times, and have high specific power consumption. Thus the heating module can be made small and reduce overall vehicle weight [152].

Grube uses historical weather data for Germany to determine that a summer day is one with a daily maximum temperature of greater than or equal to 25°C, and a winter day as one with a daily minimum of less than or equal to 0°C. The starting temperature of the cabin is set to 22°C.

The model also assumes that the solar radiation on a summer day is 1000W/m^2. The sun is taken to be at a specific point in space with respect to the vehicle, described by the sun's horizontal and vertical angles with reference to the vehicle. It is assumed that on a winter day, there is no solar radiation present.

A simplified thermal model of the cabin is then created. Different heat sinks and sources for a cabin with one occupant are considered. This model is shown in Figure 49 below.

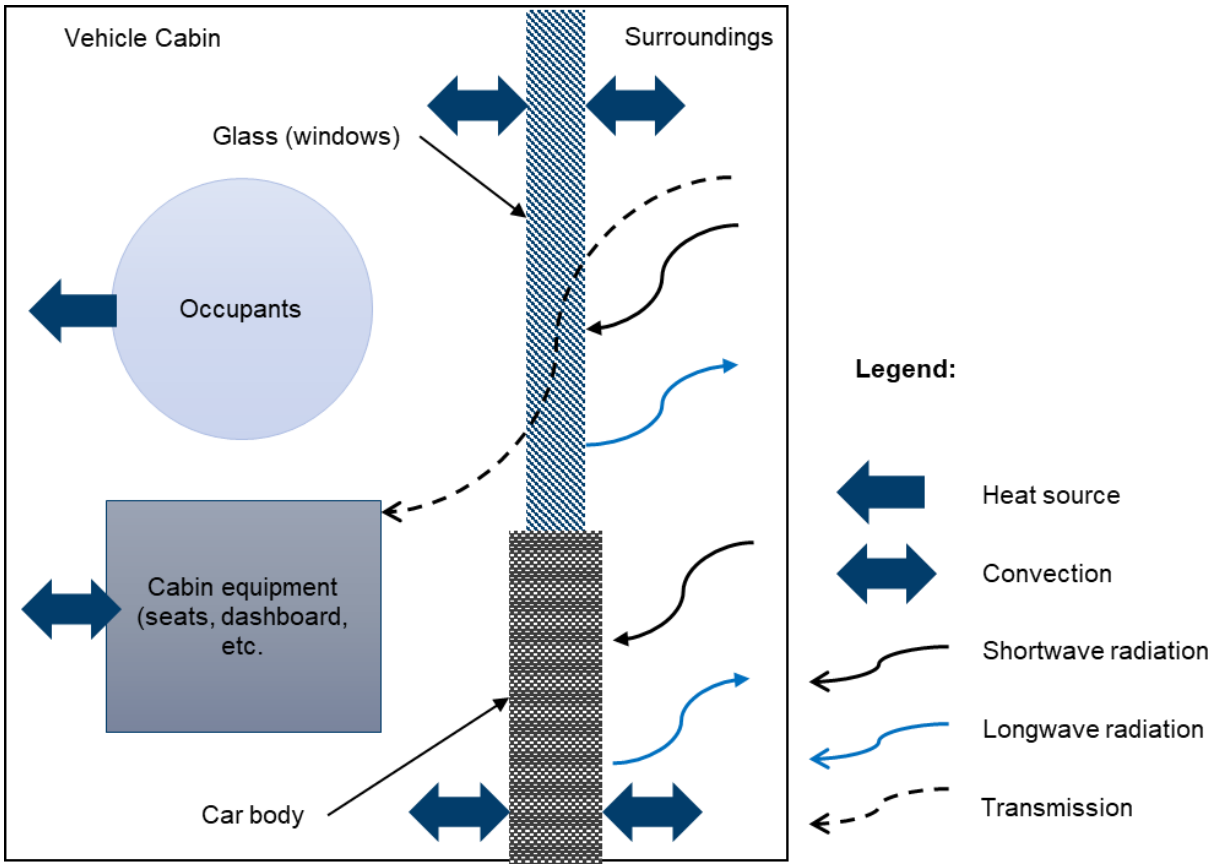

Figure 49: Thermal model of the vehicle cabin

Heat transfer modes of convection and radiation are considered in the model. Convective heat transfer is considered between the cabin equipment and cabin air, between the occupants and cabin air, and between the cabin's outer surfaces and cabin air. Radiant heat exchange is considered between the cabin equipment and the surroundings.

The cabin temperature is then calculated as the average of the inlet and outlet airflow temperatures.

The value of the inlet airflow temperature is the input to the system and can be controlled by the temperature regulating system. The value of the outlet airflow temperature is determined by solving the thermal model represented in Figure 49.

Certain simplifying assumptions are made when solving this model:

- The windows are assumed to be flat surfaces.

- The car's sides are assumed to be flat vertical surfaces, and the roof is considered a flat horizontal surface.
- Cabin equipment is assumed to have a uniform heat-capacity and absorption coefficients.
- Surface temperatures of the cabin equipment are assumed to be the same as the car body.
- The cabin equipment entirely absorbs radiation transmitted through the window.

Appendix B: Standard driving cycles

Some of the standard driving cycles not discussed in section 4.1.1 are discussed here.

Worldwide Harmonized Light Vehicles Test Cycle (WLTC) Class 3a and Class 2

WLTC Class 3a is developed for vehicles with a maximum speed of less than 120km/h. These correspond to average vehicles in European and Japanese markets. Table 16 shows some of the crucial parameters for Class 3b and Class 3a driving cycles [64].

Table 16: WLTC Class 3a and 3b parameters [64]

Phase	Duration (s)	Stop Duration (s)	Distance (m)	Max Speed (km/h)	Avg. Speed Without Stops (km/h)	Avg. Speed With Stops (km/h)	Min. Acceleration (m/s^2)	Max. Acceleration (m/s^2)
Class 3b								
Low	589	156	3095	56.5	25.7	18.9	-1.47	1.47
Medium	433	48	4756	76.6	44.5	39.5	-1.49	1.57
High	455	31	7162	97.4	60.8	56.7	-1.49	1.58
Extra-High	323	7	8254	131.3	94	92	-1.21	1.03
Total	1800	242	23266					
Class 3a								
Low	589	156	3095	56.5	25.7	18.9	-1.47	1.47
Medium	433	48	4721	76.6	44.1	39.3	-1.47	1.28
High	455	31	7124	97.4	60.5	56.4	-1.49	1.58
Extra-High	323	7	8254	131.3	94	92	-1.21	1.03
Total	1800	242	23194					

WLTC Class 2 is developed for vehicles with lower power to mass ratios.

Table 17 shows some of the important parameters of the Class 2 driving cycle [64].

Table 17: WLTC Class 2 parameters [64]

Phase	Duration (s)	Stop Duration (s)	Distance (m)	Max Speed (km/h)	Avg. Speed without stops (km/h)	Avg. Speed with stops (km/h)	Min. Acceleration (m/s^2)	Max. Acceleration (m/s^2)
Low	589	155	3101	51.4	25.7	19	-0.94	0.9
Medium	433	48	4737	74.7	44.3	39.4	-0.93	0.96
High	455	30	6792	85.2	57.5	53.7	-1.11	0.85
Extra-High	323	7	8019	123.1	91.4	89.4	-1.06	0.65
Total	1800	240	22649					

The driving cycle Class 3a is shown in Figure 50, below [64].

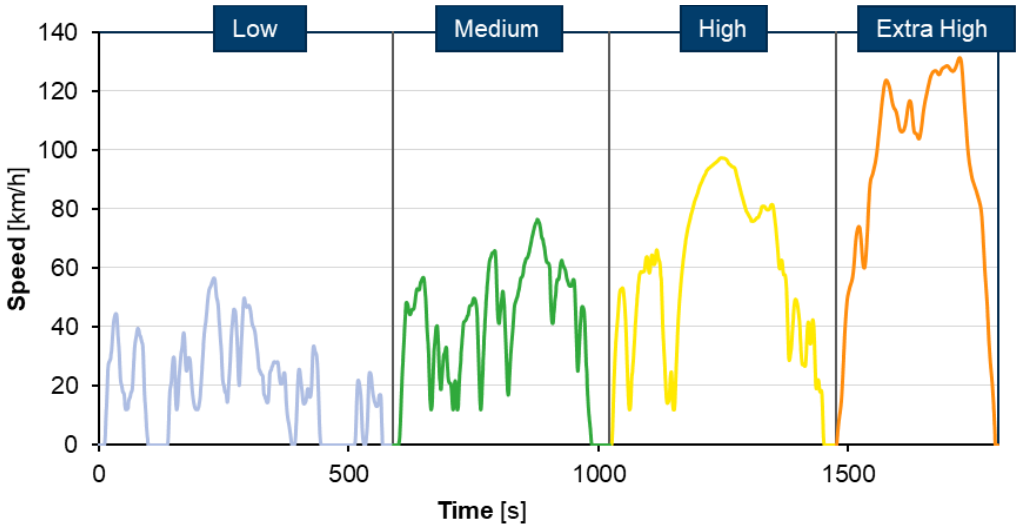

Figure 50: WLTC class 3a with different driving scenarios (Adapted from [64]*)*

The driving cycle Class 2 is shown in Figure 51, below [64].

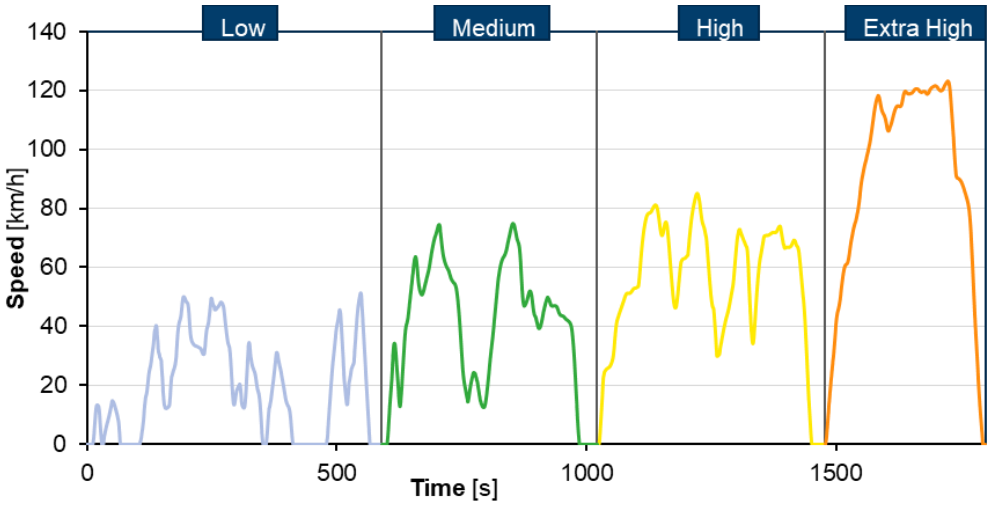

Figure 51: WLTC class 2 with different driving scenarios (Adapted from [64]*)*

As shown in Figure 50 and Figure 51, the WLTC class 3a and class 2 are divided into four distinct driving scenarios representing Urban, Suburban, Rural, and Highway driving.

Orange County Bus (OC BUS) Cycle

The orange county bus cycle is a chassis dynamometer test for heady duty vehicles developed by the West Virginia University. It is developed based on the transit buses' driving patterns in the urban area of Los Angeles, California. The driving cycle is shown in Figure 52, below [153].

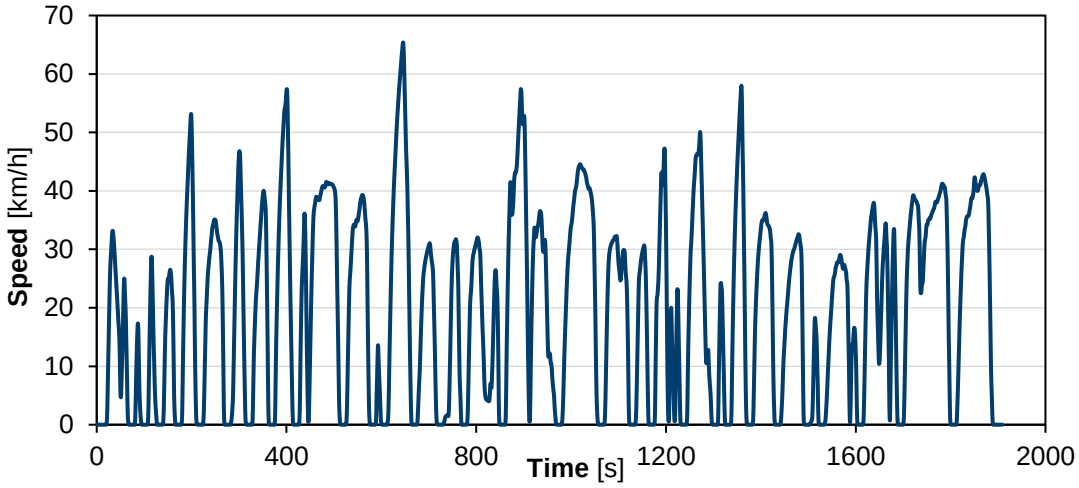

Figure 52: Orange County Bus (OC BUS) Cycle [153]

The OC Bus Cycle is characterized by constant acceleration and deceleration cycles characteristic of Urban stop-and-go traffic and the presence of frequent bus-stops in Urban areas.

Braunschweig City Driving Cycle

The Technical University of Braunschweig developed the Braunschweig City Driving Cycle. It simulates an urban bus driving cycle with frequent stops. Figure 53 below shows the driving cycle [154].

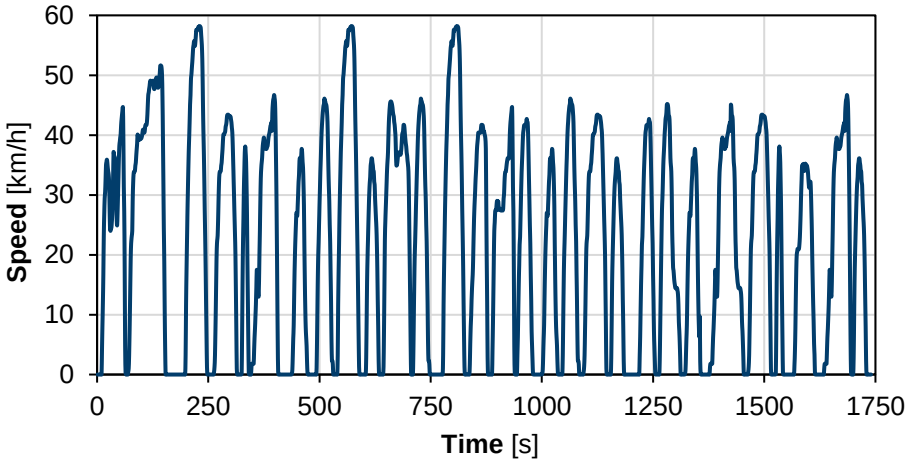

Figure 53: Braunschweig City Driving Cycle [154]

As shown in Figure 53, the driving cycle represents stop-and-go traffic and low maximum speeds prevalent in urban areas. Furthermore, it also incorporates frequent longer stops portraying periodic bus-stops. Braunschweig City Driving Cycle is used to simulate the urban driving part for small, medium, and large buses in the model.

City Suburban Heavy Vehicle Cycle

The West Virginia University developed the City Suburban Cycle (CSC). It simulates a heavy-duty vehicle driven in a suburban scenario. Figure 54 below shows the driving cycle [155].

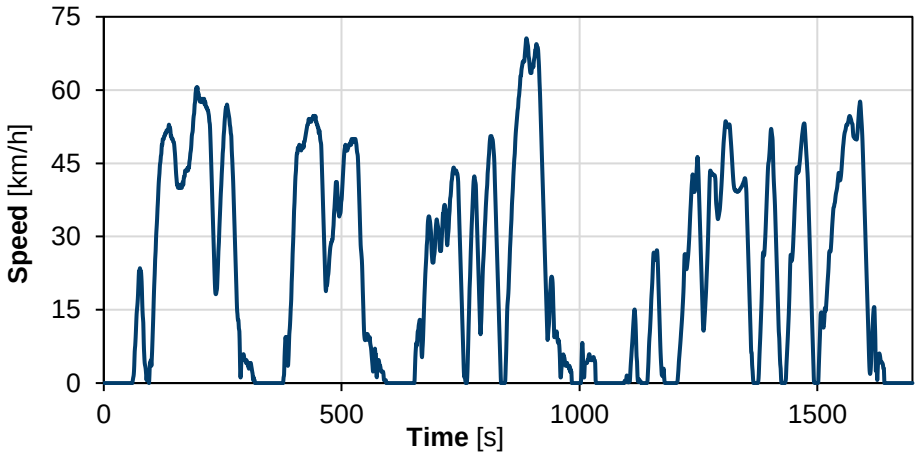

Figure 54: City Suburban Cycle (CSC) [155]

CSC is used to simulate the rural part for small, medium, and large buses in the model. As can be seen in Figure 54, vehicle speeds are higher than those for urban driving. Furthermore, there are longer periods of non-stop

driving, which can take place outside the urban area. The CSC, combined with the Braunschweig City driving cycle, is used to simulate the driving of small, medium, and large buses.

Standardized On-Road Tests Cycles (SORT)

The SORT cycles were developed by the SORT project based on statistical data from multiple European transport companies. SORT cycles were specifically developed for measuring the fuel consumption of buses in the European context. There are three cycles developed representing heavy urban (SORT 1), easy urban (SORT 2), and suburban (SORT 3) driving conditions. Each of the cycles consists of three regions of constant acceleration, three regions of constant speed, and three regions of constant deceleration. When plotted as a speed vs. time graph, this generates three trapezoids. Table 18 shows some of the characteristic parameters of the three cycles [156].

Table 18: SORT parameters [156]

	SORT 1	SORT 2	SORT 3
Average speed (km/h)	12.1	18	25.3
Stop/km	5.8	3.3	2.1
Trapeze 1: v-const. (km/h) / length (m)	20/100	20/100	30/200
Acceleration (m/s^2)	1.03	1.03	0.77
Trapeze 2: v-const. (km/h) / length (m)	30/200	40/220	50/600
Acceleration (m/s^2)	0.77	0.62	0.57
Trapeze 3: v-const. (km/h) / length (m)	40/220	50/600	60/650
Acceleration (m/s^2)	0.62	0.57	0.46
Length of stops (s)	20/20/20	20/20/20	20/10/10
Total length (m)	520	920	1450
Deceleration (m/s^2)	0.8	0.8	0.8

Figure 55, Figure 56, and Figure 57 show SORT 1. SORT 2, and SORT 3 cycles, respectively.

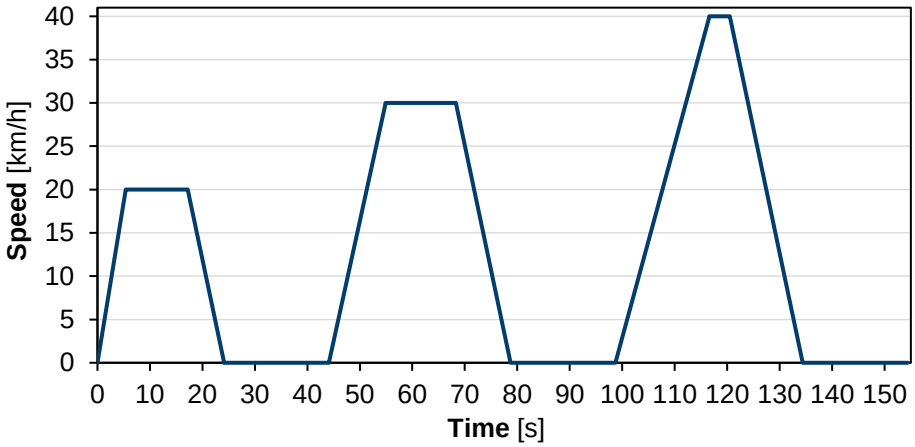

Figure 55: SORT 1: Heavy urban cycle (Adapted from [156]*)*

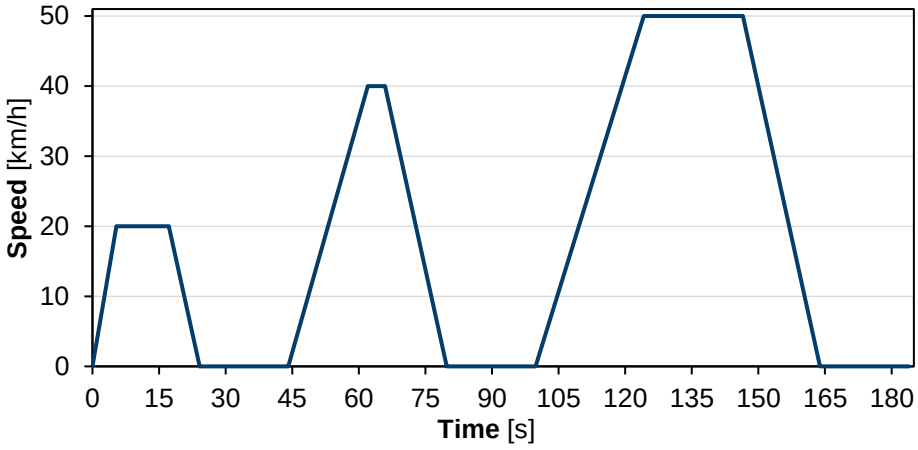

Figure 56: SORT 2: Easy urban cycle (Adapted from [156]*)*

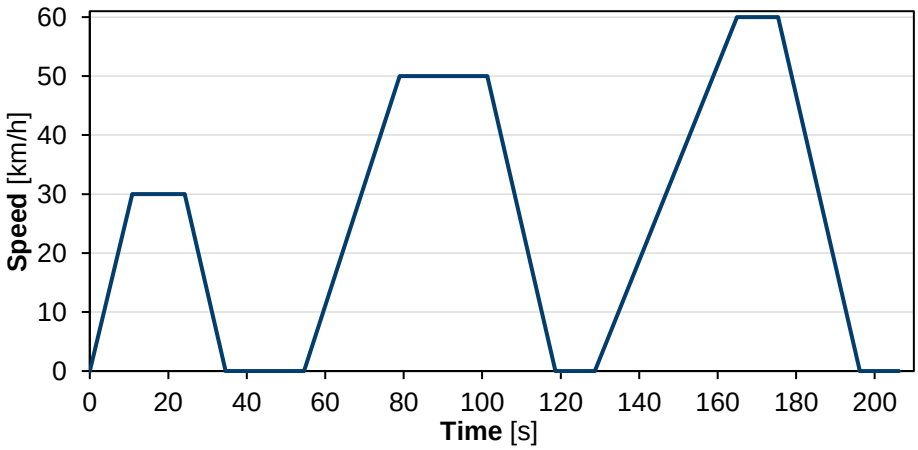

Figure 57: SORT 3: Suburban cycle (Adapted from [156]*)*

Neighborhood Refuse Truck Cycle

National Renewable Energy Laboratory developed the Neighborhood Refuse Truck Cycle (NRTC) for the US EPA Smartway program. It simulates a refuse truck's use-case with low-speed driving in residential neighborhoods, with frequent stops to collect the waste. It also includes a part representing travel to and from the collection route. Figure 58 below shows the driving cycle [157].

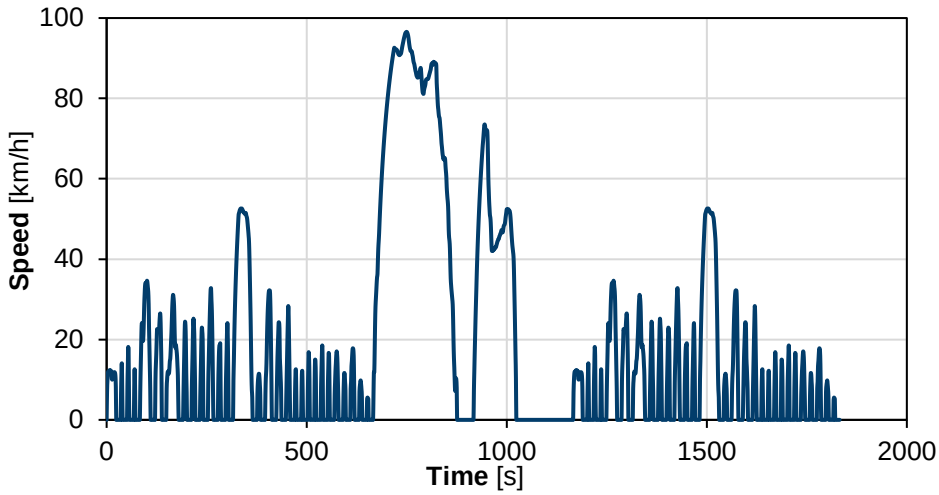

Figure 58: Neighborhood Refuse Truck Cycle (NRTC) [157]

In addition to simulating garbage trucks, the NRTC is also used to simulate last-mile package and mail delivery trucks' routes due to the similarity in their driving conditions.

Appendix C: Supplementary data

LDV data

Table 19 shows the top 30 bestselling cars in Germany for the year 2019.

Table 19: Bestselling car models in Germany for 2019 (Based on [69]*)*

Sold	Brand	Model	Mode	Sold	Brand	Model	Mode
204,550	VW	GOLF	Medium Car	44,189	Mercedes	A-Class	Medium Car
87,771	VW	TIGUAN	SUV	43,892	Opel	ASTRA	Medium Car
64,403	Mercedes	C-Class	Small Car	43,327	BMW	3 Series	Large Car
61,286	VW	POLO	Small Car	43,316	Ford	FIESTA	Small Car
59,322	VW	PASSAT	Large Car	42,609	Audi	A3, S3	Medium Car
58,898	VW	T-ROC	SUV	42,099	Skoda	FABIA	Small Car
58,261	Ford	FOCUS	Medium Car	39,637	SEAT	LEON	Medium Car
55,210	Skoda	OCTAVIA	Large Car	38,369	Mercedes	GLK, GLC	SUV
51,708	Opel	CORSA	Small Car	37,503	Fiat	500	Small Car
50,740	Audi	A4, S4	Large Car	36,109	BMW	X1	SUV
50,019	MINI	MINI	Small Car	33,037	BMW	2 Series	Medium Car
49,625	Ford	KUGA	SUV	31,901	BMW	1 Series	Medium Car

Airplane data

Table 20 shows the airplane models in Lufthansa Group’s fleet as of the end of 2019.

Table 20: Aircraft models in Lufthansa Group's fleet [117]

Manufacturer/type	Lufthansa German Airlines, including regional airlines	SWISS and Edelweiss	Austrian Airlines	Eurowings, Brussels Airlines and Germanwings
Airbus A320	95	29	25	76
Airbus A319	30	3	7	73
Airbus A321	68	9	6	5
Airbus A330	15	16		22
Airbus A340	34	9		
Embraer	26		17	
Bombardier CRJ	35			
Boeing 747	32			
Bombardier Q-Series			15	15
Airbus A220		29		
Boeing 777		12	6	
Airbus A350	15			
Airbus A380	14			
Boeing 777F				
Boeing MD-11F				
Boeing 767			6	
Total aircraft	364	107	82	191

Table 21 shows the seating and freight capacity for different airplane models used in the model to determine the airplane fuel energy demand.

Table 21: Seating and freight capacity for individual airplane models used to determine airplane fuel demand

Airplane Model	Seating Capacity [-]	Freight Capacity [kg]	Sources
AIRBUS A319-100	138	-	[158]
AIRBUS A320-200	168	17000	[158], [159]
AIRBUS A320NEO	180	-	[158]
AIRBUS A321-100/200	200	24000	[158]
AIRBUS A321NEO	215	-	[158] , [159]
AIRBUS A330-300	255	65000	[158], [160]
AIRBUS A340-300	283	-	[158]
AIRBUS A340-600	297	-	[158]
AIRBUS A350-900	293	-	[158]
AIRBUS A380-800	509	150000	[158] , [161]
BOEING 737-800	186	23900	[162], [163]
BOEING 747-400	371	128500	[158], [164]
BOEING 747-800	364	139000	[158], [165]
BOEING 777 300	-	102800	[166]
BOMBARDIER CRJ900	90	9600	[158], [167]
De Havilland Canada Dash 8 Q400	80	8163	[168], [169]
EMBRAER 190	100	3000	[158], [170]
EMBRAER 195	120	3750	[158] , [170]

Occupancy data

Table 22 shows the default occupancy rates for all transport modes used in the model.

Table 22: Default occupancy rates for the different modes [87], [99], [125], [138], [140]

Mode	Occupancy rate [%]	Sources
LDV	26	[87]
Bus	19	[99]
Coach	57	[99]
Small truck	32	[99]
Medium truck	32	[99]
Large truck	35	[99]
Semi-truck	45	[99]
Airplane	82	[125]
Drone	82	-
Tram	18	[140]
Short-distance train	21	[140]
Long-distance train	56	[138]
Freight train	38	[140]
National shipping	50	[99]
International shipping	80	-

Bibliography

[1] IPBES, "The global assessment report on summury on policymakers of the IPBES global asessment report on biodiversity and ecosystem services," 2019. [Online]. Available: https://ipbes.net/system/tdf/ipbes_global_assessment_report_summary_for_policymakers.pdf?file=1&type=node&id=35329.

[2] "Data & Statistics - IEA," *The Federal Minister for the Environment, Nature Conservation, and Nuclear Safety*, 2019. https://www.iea.org/data-and-statistics?country=WORLD&fuel=CO2 emissions&indicator=CO2 emissions by sector (accessed Jul. 04, 2020).

[3] T. Kuhnimhof, D. Zumkeller, and B. Chlond, "Who Made Peak Car, and How? A Breakdown of Trends over Four Decades in Four Countries," *Transp. Rev.*, vol. 33, no. 3, pp. 325–342, 2013, doi: 10.1080/01441647.2013.801928.

[4] D. Sperling and D. Gordon, *Two Billion Cars: Driving Towards Sustainability*, First Edit. Oxfor University Press, 2009.

[5] "Climate Action Plan 2050 – Germany's long-term emission development strategy | BMU," *The Federal Minister for the Environment, Nature Conservation, and Nuclear Safety*. https://www.bmu.de/en/topics/climate-energy/climate/national-climate-policy/greenhouse-gas-neutral-germany-2050/ (accessed Jul. 05, 2020).

[6] L. Cheng, J. De Vos, and F. Witlox, "Transport modes and sustainability," in *International Encyclopedia of Transportation*, no. January, Elsevier, 2021, pp. 0–10.

[7] P. Jardin, A. Esser, S. Givone, T. Eichenlaub, J.-E. Schleiffer, and S. Rinderknecht, "The Sensitivity in Consumption of Different Vehicle Drivetrain Concepts Under Varying Operating Conditions: A Simulative Data Driven Approach," *Vehicles*, vol. 1, no. 1, pp. 69–87, 2019, doi: 10.3390/vehicles1010005.

[8] R. Abousleiman and O. Rawashdeh, "Energy consumption model of an electric vehicle," *2015 IEEE Transp. Electrif. Conf. Expo, ITEC 2015*, no. 1, 2015, doi: 10.1109/ITEC.2015.7165773.

[9] W. Edwardes and H. Rakha, "Virginia tech comprehensive power-based fuel consumption model,"

Transp. Res. Rec., vol. 2428, no. 2428, pp. 1–9, 2014, doi: 10.3141/2428-01.

[10] W. Edwardes and H. Rakha, "Modeling diesel and hybrid bus fuel consumption with Virginia Tech comprehensive power-based fuel consumption model: Model enhancements and calibration issues," *Transp. Res. Rec.*, vol. 2533, no. 2533, pp. 100–108, 2015, doi: 10.3141/2533-11.

[11] M. Meradji, C. Cecati, G. Wang, and D. Xu, "Dynamic modeling and optimal control for hybrid electric vehicle drivetrain," *Proc. IEEE Int. Conf. Ind. Technol.*, vol. 2016-May, pp. 1424–1429, 2016, doi: 10.1109/ICIT.2016.7474967.

[12] J. Wang, I. Besselink, and H. Nijmeijer, "Battery electric vehicle energy consumption prediction for a trip based on route information," *Proc. Inst. Mech. Eng. Part D J. Automob. Eng.*, vol. 232, no. 11, pp. 1528–1542, 2018, doi: 10.1177/0954407017729938.

[13] C. Fiori, K. Ahn, and H. A. Rakha, "Power-based electric vehicle energy consumption model: Model development and validation," *Appl. Energy*, vol. 168, pp. 257–268, 2016, doi: 10.1016/j.apenergy.2016.01.097.

[14] T. Grube and D. Stolten, "The impact of drive cycles and auxiliary power on passenger car fuel economy," *Energies*, vol. 11, no. 4, 2018, doi: 10.3390/en11041010.

[15] X. Xu, H. M. A. Aziz, and R. Guensler, "A modal-based approach for estimating electric vehicle energy consumption in transportation networks," *Transp. Res. Part D Transp. Environ.*, vol. 75, no. September, pp. 249–264, 2019, doi: 10.1016/j.trd.2019.09.001.

[16] M. Ziyadi, H. Ozer, S. Kang, and I. L. Al-Qadi, "Vehicle energy consumption and an environmental impact calculation model for the transportation infrastructure systems," *J. Clean. Prod.*, vol. 174, pp. 424–436, 2018, doi: 10.1016/j.jclepro.2017.10.292.

[17] F. Ahmad, S. A. Mazlan, H. Zamzuri, H. Jamaluddin, K. Hudha, and M. Short, "MODELLING AND VALIDATION OF THE VEHICLE LONGITUDINAL MODEL," *Int. J. Automot. Mech. Eng.*, vol. 10, no. 12, pp. 2042–2056, Dec. 2014, doi: 10.15282/ijame.10.2014.21.0172.

[18] B. Luin, S. Petelin, and F. Al-Mansour, "Microsimulation of electric vehicle energy consumption," *Energy*, vol. 174, pp. 24–32, 2019, doi: 10.1016/j.energy.2019.02.034.

[19] D. W. Gao, C. Mi, and A. Emadi, "Modeling and Simulation of Electric and Hybrid Vehicles," *Proc. IEEE*, vol. 95, no. 4, pp. 729–745, Apr. 2007, doi: 10.1109/JPROC.2006.890127.

[20] L. Guzzella and A. Sciarretta, *Vehicle Propulsion Systems*, Second Edi. Zürich: Springer, 2007.

[21] C. Vagg, C. J. Brace, S. Akehurst, and L. Ash, "Minimizing battery stress during hybrid electric vehicle control design: Real world considerations for model-based control development," *2013 9th IEEE Veh. Power Propuls. Conf. IEEE VPPC 2013*, pp. 329–334, 2013, doi: 10.1109/VPPC.2013.6671713.

[22] S. A. Gadsden and S. R. Habibi, "Model-based fault detection of a battery system in a hybrid electric vehicle," *2011 IEEE Veh. Power Propuls. Conf. VPPC 2011*, 2011, doi: 10.1109/VPPC.2011.6043175.

[23] A. D. Hilshey, "A trip-purpose based model of Plug-in Electric Vehicle charging demand," *IEEE Power Energy Soc. Gen. Meet.*, vol. 2015-Septe, pp. 1–5, 2015, doi: 10.1109/PESGM.2015.7286370.

[24] J. G. Hayes and K. Davis, "Simplified electric vehicle powertrain model for range and energy consumption based on EPA Coast-down Parameters and Test Validation by Argonne national lab data on the Nissan leaf," *2014 IEEE Transp. Electrif. Conf. Expo Components, Syst. Power Electron. - From Technol. to Bus. Public Policy, ITEC 2014*, 2014, doi: 10.1109/itec.2014.6861831.

[25] K. Liu, J. Wang, T. Yamamoto, and T. Morikawa, "Exploring the interactive effects of ambient temperature and vehicle auxiliary loads on electric vehicle energy consumption," *Appl. Energy*, vol. 227, no. August, pp. 324–331, 2018, doi: 10.1016/j.apenergy.2017.08.074.

[26] X. Wu, D. Freese, A. Cabrera, and W. A. Kitch, "Electric vehicles' energy consumption measurement and estimation," *Transp. Res. Part D Transp. Environ.*, vol. 34, pp. 52–67, 2015, doi: 10.1016/j.trd.2014.10.007.

[27] T. Grube, "Potentiale des Strommanagements zur Reduzierung des spezifischen Energiebedarfs von Pkw," Berlin, Technische Universität, 2014.

[28] National Research Council of the National Academies, "Transitions to alternative vehicles and fuels," 2013. doi: 10.17226/18264.

[29] A. Brooker, J. Gonder, L. Wang, E. Wood, S. Lopp, and L. Ramroth, "FASTSim: A Model to Estimate Vehicle Efficiency, Cost and Performance," *SAE Tech. Pap.*, vol. 2015-April, no. April, pp. 21–23, 2015, doi: 10.4271/2015-01-0973.

[30] "VECTO - Overview 2018," *2018 VECTO Workshop*. European Commission's science and knowledge

service, 2018.
[31] “Vehicle Energy Consumption calculation TOol - VECTO | Climate Action.” https://ec.europa.eu/clima/policies/transport/vehicles/vecto_en (accessed Sep. 09, 2020).
[32] “Energy statistics-an overview Statistics Explained.” Accessed: Oct. 15, 2020. [Online]. Available: https://ec.europa.eu/eurostat/statisticsexplained/.
[33] “Energiewende Outlook: Transportation sector.” Accessed: Sep. 10, 2020. [Online]. Available: www.pwc.de/energy-transition.
[34] M. Burzlaff, “Aircraft Fuel Consumption - Estimation and Visualization,” *Fuel Consum.*, 2017, doi: 10.15488/2553.
[35] Y. Park and M. E. O’Kelly, “Fuel burn rates of commercial passenger aircraft: Variations by seat configuration and stage distance,” *J. Transp. Geogr.*, vol. 41, pp. 137–147, 2014, doi: 10.1016/j.jtrangeo.2014.08.017.
[36] P. Peeters, J. Middel, and A. Hoolhorts, “Fuel efficiency of commercial aircraft: An overview of historical and future trends,” Amsterdam, 2005. doi: http://www.transportenvironment.org/Publications/prep_hand_out/lid/398.
[37] A. Kharina and D. Rutherford, “Fuel efficiency trends for new commercial jet aircraft : 1960 to 2014,” Washington, 2015. [Online]. Available: https://theicct.org/publications/fuel-efficiency-trends-new-commercial-jet-aircraft-1960-2014.
[38] C. C. Chao and C. W. Hsu, “Cost analysis of air cargo transport and effects of fluctuations in fuel price,” *J. Air Transp. Manag.*, vol. 35, pp. 51–56, 2014, doi: 10.1016/j.jairtraman.2013.11.010.
[39] D. A. Senzig, G. G. Fleming, and R. J. Iovinelli, “Modeling of terminal-area airplane fuel consumption,” *J. Aircr.*, vol. 46, no. 4, pp. 1089–1093, 2009, doi: 10.2514/1.42025.
[40] J. Xu, “Design Perspectives on Delivery Drones,” RAND Corporation, 2017. doi: 10.7249/RR1718.2.
[41] “Electric VTOL Aircraft for Urban Air Mobility: Bauhaus Luftfahrt.” https://www.bauhaus-luftfahrt.net/en/research/systems-aircraft-technologies/electric-vtol-aircraft-for-urban-air-mobility/ (accessed Sep. 28, 2020).
[42] H. Zhang, L. Jia, L. Wang, and X. Xu, “Energy consumption optimization of train operation for railway systems: Algorithm development and real-world case study,” *J. Clean. Prod.*, vol. 214, pp. 1024–1037, Mar. 2019, doi: 10.1016/j.jclepro.2019.01.023.
[43] P. Salvador, P. Martínez, I. Villalba, and R. Insa, “Modelling energy consumption in diesel multiple units,” *Proc. Inst. Mech. Eng. Part F J. Rail Rapid Transit*, vol. 232, no. 5, pp. 1539–1548, May 2018, doi: 10.1177/0954409717737226.
[44] J. Wang and H. A. Rakha, “Electric train energy consumption modeling,” *Appl. Energy*, vol. 193, pp. 346–355, May 2017, doi: 10.1016/j.apenergy.2017.02.058.
[45] H. Zhou, J. Feng, J. Shen, L. Cheng, and Q. Wang, “Simulation of Train Energy Consumption Based on UAS,” *IOP Conf. Ser. Earth Environ. Sci.*, vol. 300, no. 4, p. 042129, Aug. 2019, doi: 10.1088/1755-1315/300/4/042129.
[46] S. ZHAO, Z. YANG, H. YUAN, and W. SHI, “Application of Energy Plus in High Speed Train Energy Consumption Analysis,” *DEStech Trans. Comput. Sci. Eng.*, no. cmsam, pp. 1–4, Nov. 2016, doi: 10.12783/dtcse/cmsam2016/3640.
[47] K.-K. Kee, B.-Y. Lau Simon, and K.-H. Yong Renco, “Prediction of Ship Fuel Consumption and Speed Curve by Using Statistical Method,” *J. Comput. Sci. Comput. Math.*, vol. 8, no. 2, pp. 19–24, Jun. 2018, doi: 10.20967/jcscm.2018.02.002.
[48] M. Jeon, Y. Noh, Y. Shin, O.-K. Lim, I. Lee, and D. Cho, “Prediction of ship fuel consumption by using an artificial neural network,” *J. Mech. Sci. Technol.*, vol. 32, no. 12, pp. 5785–5796, Dec. 2018, doi: 10.1007/s12206-018-1126-4.
[49] L. Yang, G. Chen, N. G. M. Rytter, J. Zhao, and D. Yang, “A genetic algorithm-based grey-box model for ship fuel consumption prediction towards sustainable shipping,” *Ann. Oper. Res.*, Mar. 2019, doi: 10.1007/s10479-019-03183-5.
[50] “Germany - Countries & Regions - IEA.” https://www.iea.org/countries/germany (accessed Jul. 09, 2020).
[51] V. A. Petrushov, “Improvement in vehicle aerodynamic drag and rolling resistance determination from coast-down tests,” *Proc. Inst. Mech. Eng. Part D J. Automob. Eng.*, vol. 212, no. 5, pp. 369–380, 1998, doi: 10.1243/0954407981526037.
[52] C. E. I. Byrne, “Aerodynamics of Road Vehicles — 4th edition. Edited by W-H. Hucho. SAE International,

Warrendale, PA, USA. Materials Park, OH 44073-0002, USA 1998. 918 pp. Illustrated. £78.," *Aeronaut. J.*, 1999, doi: 10.1017/s0001924000064642.
[53] J. Kühlwein, "Driving Resistances of Light-Duty Vehicles in Europe: Present Situation, Trends and Scenarios for 2025," *Int. Counc. Clean Transp.*, no. December, pp. 1–46, 2016.
[54] S. Das and B. Redrouthu, "Tyre modelling for rolling resistance," Chalmers University of Technology, 2014.
[55] J. C. Páscoa, F. P. Brójo, F. C. Santos, and P. O. Fael, "An innovative experimental on-road testing method and its demonstration on a prototype vehicle," *J. Mech. Sci. Technol.*, vol. 26, no. 6, pp. 1663–1670, 2012, doi: 10.1007/s12206-012-0413-8.
[56] "Rolling Resistance." https://www.engineeringtoolbox.com/rolling-friction-resistance-d_1303.html (accessed Jul. 07, 2020).
[57] P. Fajri, R. Ahmadi, and M. Ferdowsi, "Equivalent vehicle rotational inertia used for electric vehicle test bench dynamic studies," *IECON Proc. (Industrial Electron. Conf.*, no. 2, pp. 4115–4120, 2012, doi: 10.1109/IECON.2012.6389231.
[58] R. Rajamani, *Vehicle dynamics and control*, First Edit., no. 12. Minnesota: Springer US, 2006.
[59] "Forward and Backward Euler Methods." https://web.mit.edu/10.001/Web/Course_Notes/Differential_Equations_Notes/node3.html (accessed Sep. 16, 2020).
[60] H. Burchard and L. Umlauf, "Finite difference schemes," in *Numerical methods for conservation laws*, 2018, pp. 18–29.
[61] T. J. Barlow, S. Latham, I. S. Mccrae, and P. G. Boulter, "A reference book of driving cycles for use in the measurement of road vehicle emissions," Berkshire, 2009.
[62] "Vehicle Emissions Testing for WLTP & RDE emissions| TÜV SÜD." https://www.tuvsud.com/en/industries/mobility-and-automotive/automotive-and-oem/automotive-testing-solutions/emissions-and-fuel-efficiency-testing (accessed Sep. 16, 2020).
[63] "RDE: What is the real driving emissions test? | Car Emissions Testing Facts." https://www.caremissionstestingfacts.eu/rde-real-driving-emissions-test/ (accessed Sep. 16, 2020).
[64] "Emission Test Cycles: WLTC." https://dieselnet.com/standards/cycles/wltp.php (accessed Jul. 10, 2020).
[65] "Emission Test Cycles: World Harmonized Vehicle Cycle (WHVC)." https://dieselnet.com/standards/cycles/whvc.php (accessed Jul. 10, 2020).
[66] "Emission Test Cycles: World Harmonized Transient Cycle (WHTC)." https://dieselnet.com/standards/cycles/whtc.php (accessed Jul. 10, 2020).
[67] "Euro NCAP | How To Read The Stars." https://www.euroncap.com/en/about-euro-ncap/ (accessed Sep. 17, 2020).
[68] Office for Official Publications of the European Communities L-2985 Luxembourg, "REGULATION (EEC) No 4064/89 MERGER PROCEDURE Article 6(1)(b)," Brussels, 1999.
[69] "2019 (Full Year) Germany: Best-Selling Car Models - Car Sales Statistics." https://www.best-selling-cars.com/germany/2019-full-year-germany-best-selling-car-models/ (accessed Sep. 17, 2020).
[70] "• Best-selling light-commercial vehicle models in EU-28: 2016 | Statista." https://www.statista.com/statistics/260027/best-selling-light-commercial-vehicle-models-eu-27/ (accessed Sep. 17, 2020).
[71] E. S. Islam, A. Moawad, N. Kim, and A. Rousseau, "Energy Consumption and Cost Reduction of Future Light-Duty Vehicles through Advanced Vehicle Technologies : A Modeling Simulation Study Through 2050," Illinois, 2020. [Online]. Available: http://www.osti.gov/.
[72] B. Cox, "Mobility and the Energy Transition: A Life Cycle Assessment of Swiss Passenger Transport Technologies including Developments until 2050," 2018, [Online]. Available: https://doi.org/10.3929/ethz-b-000276298 Rights.
[73] K. Li and K. J. Tseng, "Energy efficiency of lithium-ion battery used as energy storage devices in micro-grid," in *IECON 2015 - 41st Annual Conference of the IEEE Industrial Electronics Society*, 2015, pp. 5235–5240, doi: 10.1109/IECON.2015.7392923.
[74] M. Schimpe *et al.*, "Energy efficiency evaluation of a stationary lithium-ion battery container storage system via electro-thermal modeling and detailed component analysis," *Appl. Energy*, vol. 210, pp. 211–229, Jan. 2018, doi: 10.1016/j.apenergy.2017.10.129.
[75] A. Eftekhari, "Energy efficiency: A critically important but neglected factor in battery research," *Sustain.*

Energy Fuels, vol. 1, no. 10, pp. 2053–2060, Nov. 2017, doi: 10.1039/c7se00350a.
[76] *Cost, effectiveness, and deployment of fuel economy technologies for light-duty vehicles*. National Academies Press, 2015.
[77] A. Irimescu, L. Mihon, and G. Pãdure, "AUTOMOTIVE TRANSMISSION EFFICIENCY MEASUREMENT USING A CHASSIS DYNAMOMETER," *Int. J. Automot. Technol.*, vol. 12, no. 4, pp. 555–559, 2011, doi: 10.1007/s12239−011−0065−1.
[78] P. Spanoudakis, N. Tsourveloudis, L. Doitsidis, and E. Karapidakis, "Experimental Research of Transmissions on Electric Vehicles' Energy Consumption," *Energies*, vol. 12, no. 3, p. 388, Jan. 2019, doi: 10.3390/en12030388.
[79] "Drivetrain losses (efficiency) – x-engineer.org." https://x-engineer.org/automotive-engineering/drivetrain/transmissions/drivetrain-losses-efficiency/ (accessed Sep. 17, 2020).
[80] "Electric Car Myth Buster — Efficiency." https://cleantechnica.com/2018/03/10/electric-car-myth-buster-efficiency/ (accessed Sep. 17, 2020).
[81] A. Al-Samari, "Study of emissions and fuel economy for parallel hybrid versus conventional vehicles on real world and standard driving cycles," *Alexandria Eng. J.*, vol. 56, no. 4, pp. 721–726, 2017, doi: 10.1016/j.aej.2017.04.010.
[82] T. Ott, F. Zurbriggen, C. Onder, and L. Guzzella, "Cycle-averaged efficiency of hybrid electric vehicles," *Proc. Inst. Mech. Eng. Part D J. Automob. Eng.*, vol. 227, no. 1, pp. 78–86, Jan. 2013, doi: 10.1177/0954407012447508.
[83] X. Hu, N. Murgovski, L. Johannesson, and B. Egardt, "Energy efficiency analysis of a series plug-in hybrid electric bus with different energy management strategies and battery sizes," *Appl. Energy*, vol. 111, pp. 1001–1009, Nov. 2013, doi: 10.1016/j.apenergy.2013.06.056.
[84] G. Xu, W. Li, K. Xu, and Z. Song, "An intelligent regenerative braking strategy for electric vehicles," *Energies*, vol. 4, no. 9, pp. 1461–1477, 2011, doi: 10.3390/en4091461.
[85] T. Trost, *Erneuerbare Mobilität im motorisierten Individualverkehr*. Kassel, 2016.
[86] P. Plötz, C. Moll, G. Bieker, P. Mock, and Y. Li, "REAL-WORLD USAGE OF PLUG-IN HYBRID ELECTRIC VEHICLES FUEL CONSUMPTION, ELECTRIC DRIVING, AND CO 2 EMISSIONS," 2020. Accessed: Oct. 27, 2020. [Online]. Available: www.theicct.orgcommunications@theicct.org.
[87] "Occupancy rates — European Environment Agency." https://www.eea.europa.eu/publications/ENVISSUENo12/page029.html (accessed Oct. 15, 2020).
[88] "Air - Density, Specific Weight and Thermal Expansion Coefficient at Varying Temperature and Constant Pressures." https://www.engineeringtoolbox.com/air-density-specific-weight-d_600.html?vA=15&units=C# (accessed Sep. 17, 2020).
[89] "Survey on standard weights of passengers and baggage Final report."
[90] "Heavy-duty vehicle efficiency | International Council on Clean Transportation." https://theicct.org/heavy-duty-vehicle-efficiency (accessed Sep. 22, 2020).
[91] L. Xu, J. Li, J. Hua, X. Li, and M. Ouyang, "Optimal vehicle control strategy of a fuel cell/battery hybrid city bus," *Int. J. Hydrogen Energy*, vol. 34, no. 17, pp. 7323–7333, Sep. 2009, doi: 10.1016/j.ijhydene.2009.06.021.
[92] S. Kanekar, P. Thakre, and E. Rajkumar, "Aerodynamic study of state transport bus using computational fluid dynamics," in *IOP Conference Series: Materials Science and Engineering*, Dec. 2017, vol. 263, no. 6, p. 062052, doi: 10.1088/1757-899X/263/6/062052.
[93] C.-H. KIM, "A Streamlined Design of a High-Speed Coach for Fuel Savings and Reduction of Carbon Dioxide," *Int. J. Automot. Eng.*, vol. 2, no. 4, pp. 101–107, 2011, doi: 10.20485/jsaeijae.2.4_101.
[94] "Record Run Buses 2012 started today: unique efficiency test for Euro VI-certified Mercedes-Benz Citaro and Setra ComfortClass 500 - Daimler Global Media Site." https://media.daimler.com/marsMediaSite/en/instance/ko/Record-Run-Buses-2012-started-today-unique-efficiency-test-for-Euro-VI-certified-Mercedes-Benz-Citaro-and-Setra-ComfortClass-500.xhtml?oid=9903865 (accessed Sep. 18, 2020).
[95] Siemens AG - Mobility Division, Technische Universität Dresden, and Deutsches Zentrum für Luft- und Raumfahrt e.V., "FuE-Programm 'Förderung von Forschung und Entwicklung im Bereich der Elektromobilität' des Bundesministeriums für Umwelt, Naturschutz, Bau und Reaktorsicherheit (BMUB) Gemeinsamer Abschlussbericht ENUBA 2-Elektromobilität bei schweren Nutzfahrzeugen zur U."
[96] "EUR-Lex - 32020R0740 - EN - EUR-Lex." https://eur-lex.europa.eu/legal-

content/EN/TXT/?uri=CELEX:32020R0740 (accessed Sep. 20, 2020).
[97] T. Knote, B. Haufe, and L. Saroch, “Gefördert durch das Bundesministerium für Umwelt, Naturschutz, Bau und Reaktorsicherheit E-Bus-Standard »Ansätze zur Standardisierung und Zielkosten für Elektrobusse«,” 2017.
[98] Truck Techology, “Truck technology | Inconvenient Trucks,” 2018. https://inconvenienttruck.eu/trucks-options-fuel-consumption/ (accessed Sep. 21, 2020).
[99] M. Allekotte *et al.*, “Ökologische Bewertung von Verkehrsarten,” 2019. Accessed: Sep. 22, 2020. [Online]. Available: http://www.umweltbundesamt.de/publikationen.
[100] L. Hjelm and B. Bergqvist, “European truck aerodynamics - A comparison between conventional and coe truck aerodynamics and a look into future trends and possibilities,” *Lect. Notes Appl. Comput. Mech.*, vol. 41, pp. 469–477, 2009, doi: 10.1007/978-3-540-85070-0-45.
[101] National Research Council, *Review of the 21st century truck partnership, second report*. Washington, DC: The National Academies Press, 2012.
[102] A. Hariram, T. Koch, B. Mårdberg, and J. Kyncl, “A study in options to improve aerodynamic profile of heavy-duty vehicles in Europe,” *Sustain.*, vol. 11, no. 19, 2019, doi: 10.3390/su11195519.
[103] T. Hendricks and M. O’Keefe, “Heavy vehicle auxiliary load electrification for the Essential Power System Program: Benefits, tradeoffs, and remaining challenges,” *SAE Tech. Pap.*, vol. 111, pp. 841–851, 2002, doi: 10.4271/2002-01-3135.
[104] “Emissions measurement in cars - VDA.” https://www.vda.de/en/topics/environment-and-climate/exhaust-emissions/emissions-measurement.html (accessed Oct. 16, 2020).
[105] F. Hülsmann, M. Mottschall, F. Hacker, and P. Kasten, “Konventionelle und alternative Fahrzeugtechnologien bei Pkw und schweren Nutzfahrzeugen – Potenziale zur Minderung des Energieverbrauchs bis 2050,” Freiburg, 2014. [Online]. Available: https://www.oeko.de/oekodoc/2105/2014-662-de.pdf.
[106] F. Dünnebeil and H. Keller, “Monitoring emission savings from low rolling resistance tire labelling and phase-out schemes,” Heidelberg, 2015. [Online]. Available: http://transferproject.org/wp-content/uploads/2014/10/TRANSfer_MRV-Blueprint_lower-tires_EU.pdf.
[107] M. Wietschel *et al.*, “Klimabilanz , Kosten und Potenziale verschiedener Kraftstoffarten und Antriebssysteme für Pkw und Lkw,” Karlsruhe, 2019. [Online]. Available: https://www.isi.fraunhofer.de/content/dam/isi/dokumente/cce/2019/klimabilanz-kosten-potenziale-antriebe-pkw-lkw.pdf.
[108] R. Vijayagopal, D. N. Prada, and A. Rousseau, “Fuel Economy and Cost Estimates for Medium- and Heavy-Duty Trucks,” Illinois, 2019. [Online]. Available: http://www.osti.gov/.
[109] M. LEE, L. K. B. LI, and W. SONG, “Analysis of direct operating cost of wide-body passenger aircraft: A parametric study based on Hong Kong,” *Chinese J. Aeronaut.*, vol. 32, no. 5, pp. 1222–1243, May 2019, doi: 10.1016/j.cja.2019.03.011.
[110] Air Transport Action Group, “Beginner ’ s Guide to Aviation Efficiency,” Geneva, 2010. [Online]. Available: http://large.stanford.edu/courses/2016/ph240/eenkemavandijk2/docs/atag_aviation_efficiency_2010.pdf.
[111] K. Rypdal, N. Kilde, S. Steve, and T. Karen, “Aircraft emissions,” *Energy Sect.*, vol. 7, no. 10, pp. 93–102, 2000, doi: 10.1021/es60082a602.
[112] “Freight transport statistics - Statistics Explained.” https://ec.europa.eu/eurostat/statistics-explained/index.php/Freight_transport_statistics#Modal_split (accessed Sep. 13, 2020).
[113] “Demand For Air Cargo Capacity Is Urgent — Who Will Fill It?” https://www.forbes.com/sites/tedreed/2020/04/18/demand-for-air-cargo-capacity-is-urgent-and-huge---who-will-step-in-to-fill-it/#3a426cbf7c51 (accessed Oct. 15, 2020).
[114] “IATA - Air Cargo Capacity Crunch: Demand Plummets but Capacity Disappears Even Faster.” https://www.iata.org/en/pressroom/pr/2020-06-02-01/ (accessed Oct. 15, 2020).
[115] “Germany: state of the market | Routesonline.” https://www.routesonline.com/news/29/breaking-news/283754/germany-state-of-the-market-/ (accessed Sep. 13, 2020).
[116] “Study on air traffic: Lufthansa dominates the skies over Germany.” https://ga.de/ga-english/news/lufthansa-dominates-the-skies-over-germany_aid-43675911 (accessed Sep. 13, 2020).
[117] “Fleet - Lufthansa Group Investor Relations.” https://investor-relations.lufthansagroup.com/en/corporate-facts/fleet.html (accessed Sep. 13, 2020).

[118] “1.A.3.a Aviation 2 LTO emissions calculator 2019 — European Environment Agency.” https://www.eea.europa.eu/publications/emep-eea-guidebook-2019/part-b-sectoral-guidance-chapters/1-energy/1-a-combustion/1-a-3-a-aviation-1-annex5-LTO/view (accessed Sep. 13, 2020).
[119] Air BP, “Handbook of Products,” *Air BP Ltd.*, pp. 6–9, 2000, [Online]. Available: http://www.bp.com/liveassets/bp_internet/aviation/air_bp/STAGING/local_assets/downloads_pdfs/a/air_bp_products_handbook_04004_1.pdf.
[120] M. Winther *et al.*, “1.A.3.a Aviation 2019,” pp. 1–51, 2019, [Online]. Available: www.eea.europa.eu/publications/emep-eea-guidebook-2019/part-b-sectoral-guidance-chapters/1-energy/1-a-combustion/1-a-3-a-aviation.
[121] “Why Germans are flying less - BBC Worklife.” https://www.bbc.com/worklife/article/20200128-why-germans-are-flying-less (accessed Sep. 14, 2020).
[122] E. Brennan, “Environmental Protection is both a challenge and an opportunity for European aviation,” *Skyway - Spring/Summer 2020*, pp. 5–7, 2020.
[123] “Sustainable Aviation Fuel (SAF) | SkyNRG.” https://skynrg.com/sustainable-aviation-fuel/saf/ (accessed Oct. 15, 2020).
[124] “Coronavirus havoc forces airlines to retire iconic planes sooner - Business Insider.” https://www.businessinsider.com/coronavirus-havoc-forces-airlines-to-retire-iconic-planes-sooner-2020-3?r=DE&IR=T (accessed Sep. 02, 2020).
[125] “Facts & figures.” https://www.atag.org/facts-figures.html (accessed Oct. 02, 2020).
[126] Deutsche Flugsicherung, “Air traffic in Germany Mobility Report 2016,” Langen, 2016. Accessed: Oct. 19, 2020. [Online]. Available: https://www.dfs.de/dfs_homepage/en/Press/Publications/Mobilitaetsbericht2016_EN_web.pdf.
[127] G. Aerospace Center, “Analyses of the European air transport market UPDATED VERSION.” Accessed: Oct. 19, 2020. [Online]. Available: http://www.dlr.de/fw.
[128] “Where’s Your Flying Car? Still Years From Reality - The New York Times.” https://www.nytimes.com/2020/01/07/business/hyundai-uber-flying-car.html (accessed Sep. 24, 2020).
[129] “Japan wants flying cars in its skies in three years. Here’s how they plan to pull it off - ABC News.” https://www.abc.net.au/news/2020-08-29/flying-cars-could-be-a-reality-in-japan-in-three-years/12599544 (accessed Sep. 24, 2020).
[130] J. K. Stolaroff, C. Samaras, E. R. O’Neill, A. Lubers, A. S. Mitchell, and D. Ceperley, “Energy use and life cycle greenhouse gas emissions of drones for commercial package delivery,” *Nat. Commun.*, vol. 9, no. 1, p. 409, Dec. 2018, doi: 10.1038/s41467-017-02411-5.
[131] “Amazon Prime Air delivery drones get FAA approval.” https://www.fastcompany.com/90545556/amazon-is-now-one-step-closer-to-drone-delivery (accessed Sep. 24, 2020).
[132] Morgan Stanley Research, “Are Flying Cars Preparing for Takeoff?,” 2019. https://www.morganstanley.com/ideas/autonomous-aircraft.
[133] “Rail – Analysis - IEA.” https://www.iea.org/reports/rail (accessed Sep. 20, 2020).
[134] “Train Travel in Germany | The German Way & More.” https://www.german-way.com/travel-and-tourism/train-travel-europe/train-travel-in-germany/ (accessed Sep. 20, 2020).
[135] T. Kuminek, “Energy consumption in tram transport,” *Logist. Transp.*, vol. 18, no. 2, pp. 93–100, 2013.
[136] “GEMIS Database - IINAS.” http://iinas.org/database.html (accessed Sep. 30, 2020).
[137] W. Klebsch, N. Guckes, and P. Heininger, “Bewertung klimaneutraler Alternativen zu Dieseltriebzügen,” Frankfurt am Main, 2020. [Online]. Available: https://www.vde.com/resource/blob/1979350/a41e9c3559af76fee9c91befbc1e9216/studie-klimaneutrale-alternative-zu-dieseltriebzuegen-data.pdf.
[138] Deutsche Bahn AG, “Deutsche Bahn 2018 Integrated Report On track towards a better railway,” Berlin, 2019. Accessed: Sep. 30, 2020. [Online]. Available: https://ib.deutschebahn.com/ib2018/fileadmin/PDF/IB18_e_web.pdf.
[139] T. Bründlinger *et al.*, “dena-Leitstudie Integrierte Energiewende. Impulse für die Gestaltung des Energiesystems bis 2050,” 2018. [Online]. Available: https://shop.dena.de/fileadmin/denashop/media/Downloads_Dateien/esd/9261_dena-Leitstudie_Integrierte_Energiewende_lang.pdf.
[140] W. Zimmer *et al.*, “Endbericht Renewbility III,” Berlin, 2016. [Online]. Available:

http://www.renewbility.de/wp-content/uploads/Renewbility_III_Endbericht.pdf.
[141] “International Shipping – Analysis - IEA.” https://www.iea.org/reports/international-shipping (accessed Oct. 15, 2020).
[142] Central Commission for the Navigation of the Rhine, “Inland Navigation in Europe Market Observation,” 2017. Accessed: Oct. 16, 2020. [Online]. Available: https://www.ccr-zkr.org/files/documents/om/om17_II_en.pdf.
[143] “IMO2020 For greener shipping.” Accessed: Oct. 15, 2020. [Online]. Available: www.hapag-lloyd.com.
[144] Hapag-Lloyd, “For greener shipping,” 2020. Accessed: Oct. 15, 2020. [Online]. Available: https://www.hapag-lloyd.com/content/dam/website/downloads/press_and_media/publications/Hapag-Lloyd_Presentation_IMO2020_For_greener_shipping.pdf.
[145] “LNG as an alternative fuel for the operation of ships and heavy-duty vehicles Short study in the context of the scientific supervision, support and guidance of the BMVI in the sec-tors Transport and Mobility with a specific focus on fuels and pro-pulsion .”
[146] “BU-502: Discharging at High and Low Temperatures – Battery University.” https://batteryuniversity.com/learn/article/discharging_at_high_and_low_temperatures (accessed Oct. 28, 2020).
[147] B. Propfe, “Marktpotentiale elektrifizierter Fahrzeugkonzepte unter Berücksichtigung von technischen, politischen und ökonomischen Randbedingungen,” 2016, doi: http://dx.doi.org/10.18419/opus-6897.
[148] M. Wietschel, P. Plötz, T. Gnann, and A. Kühn, “Markthochlaufszenarien für Elektrofahrzeuge,” *Fraunhofer ISI*, vol. 2013, no. September 2013, 2014.
[149] Y. Chen and M. Melaina, “Model-based techno-economic evaluation of fuel cell vehicles considering technology uncertainties,” *Transp. Res. Part D Transp. Environ.*, vol. 74, no. August, pp. 234–244, 2019, doi: 10.1016/j.trd.2019.08.002.
[150] “DHL, Hermes & Co.: Darum klingeln Postboten immer seltener | Karriere.” https://www.tz.de/leben/karriere/darum-klingeln-paketboten-dhl-hermes-immer-seltener-zr-10043419.html (accessed Oct. 28, 2020).
[151] D. Anderson, “SMART Webinar #1 Systems-Level Transportation Simulation - Creating the SMART Mobility Modeling Workflow,” 2020.
[152] R. Musat and E. Helerea, “Characteristics of the PTC heater used in automotive HVAC systems,” *IFIP Adv. Inf. Commun. Technol.*, vol. 314, pp. 461–468, 2010, doi: 10.1007/978-3-642-11628-5_51.
[153] “Emission Test Cycles: Orange County Bus (OC BUS) Cycle.” https://dieselnet.com/standards/cycles/ocbus.php (accessed Sep. 16, 2020).
[154] “Emission Test Cycles: Braunschweig City Driving Cycle.” https://dieselnet.com/standards/cycles/braunschweig.php (accessed Sep. 20, 2020).
[155] “Emission Test Cycles: City Suburban Cycle and Route.” https://dieselnet.com/standards/cycles/csc.php (accessed Sep. 20, 2020).
[156] S. Mišanović and V. Spasojević, “MEASUREMENT THE FUEL CONSUMPTION OF BUSES FOR PUBLIC TRANSPORT BY THE METHODOLOGY ‘“SORT”’ (STANDARDISED ON-ROAD TESTS CYCLES),” 2015.
[157] “Emission Test Cycles: Neighborhood Refuse Truck Cycle.” https://dieselnet.com/standards/cycles/neigh_refuse_truck.php (accessed Sep. 26, 2020).
[158] Lufthansa, “Lufthansa Group: Lufthansa and regional partners,” *Lufthansagroup.com*. https://www.lufthansagroup.com/en/company/fleet/lufthansa-and-regional-partners.html (accessed Nov. 23, 2020).
[159] D. Brett, “Chapman Freeborn and Avion team up on A320 and A321 freight flights,” *Aircargo news*, Apr. 23, 2020. https://www.aircargonews.net/airlines/bellyhold-airline/chapman-freeborn-and-avion-team-up-on-a320-and-a321-freight-flights/ (accessed Nov. 23, 2020).
[160] AIRBUS, “A330-200F - Freighter - Airbus,” *AIRBUS*. https://www.airbus.com/aircraft/freighter/a330-200f.html (accessed Nov. 24, 2020).
[161] A. Hess, “Airbus A380-800, high-capacity airliner,” *Skytamer*. https://www.skytamer.com/Airbus_A380.html (accessed Nov. 24, 2020).
[162] Boeing, “Boeing Next-Generation 737,” *Boeing*, 2019. https://www.boeing.com/commercial/737ng/ (accessed Nov. 23, 2020).
[163] Aerospace Technology, “737-800 Boeing Converted Freighter (BCF), United States of America.”

https://www.aerospace-technology.com/projects/737-800-boeing-converted-freighter-bcf/ (accessed Nov. 24, 2020).
[164] AirBridgeCargo, "AirBridgeCargo Airlines - Boeing 747-400F." https://www.airbridgecargo.com/en/page/38/boeing-747-400f (accessed Nov. 24, 2020).
[165] AirBridgeCargo, "AirBridgeCargo Airlines - Boeing 747-8F." https://www.airbridgecargo.com/en/page/37/boeing-747-8f (accessed Nov. 24, 2020).
[166] J. Clark and K. Kirwan, "777 FREIGHTER : Greater Efficiency for Long-Haul Operators," *Boeing*. https://www.boeing.com/commercial/aeromagazine/articles/qtr_02_09/article_02_1.html (accessed Nov. 24, 2020).
[167] SAS, "CRJ900 - SAS," *SAS*. https://www.sasgroup.net/about-sas/the-fleet/crj900/ (accessed Nov. 24, 2020).
[168] Transport Canada, "NICO: Certificate Detail." https://wwwapps.tc.gc.ca/saf-sec-sur/2/nico-celn/c_d.aspx?lang=eng&amp%3Baprv_num=A-142&amp%3BISU_NUM=41&amp%3BSTART_DATE=2019-06-01&amp%3BAUTH_DESC=&amp%3BDESC=&amp%3BFRGN_NUM=&amp%3Baprv_type=TA&amp%3BPARTS_NUM=&amp%3Bid_num=1146 (accessed Nov. 23, 2020).
[169] D. Grover, "De Havilland freighter conversions approved through mid-2021," *Cargo Newswire - International Cargo Wire News*. https://www.cargonewswire.com/de-havilland-freighter-conversions-approved-through-mid-2021/ (accessed Nov. 24, 2020).
[170] A. Gavine, "Embraer enhances cargo capability across range," *Aircraft Interiors International*. https://www.aircraftinteriorsinternational.com/news/cabin-design/embraer-enhances-cargo-capability-across-range.html (accessed Nov. 24, 2020).